RENEWAL OF WATER IN MONOPILES FOR OFFSHORE WIND

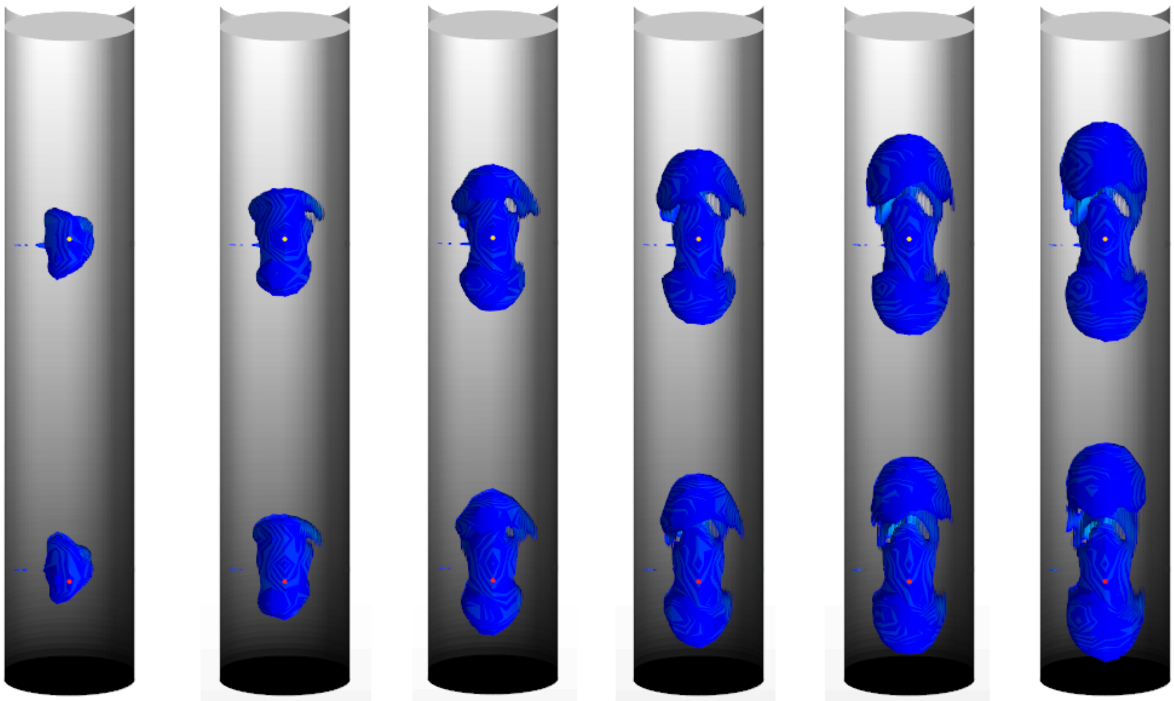

Structural and Civil Engineering
Aalborg University

Master thesis
Lasse Drejer Andersen

AALBORG UNIVERSITY
STUDENT REPORT

School of Engineering and Science
Study Board of Civil Engineering
Thomas Manns Vej 23, 9220 Aalborg Ø
Phone 99 40 84 84
http://www.ses.aau.dk/studienaevn/byggeri/

Title:
Renewal of water in monopiles for offshore wind

Project:
Master thesis

Project period:
September 1^{st} 2016 - June 8^{th} 2017

Project author:
Lasse Drejer Andersen

Participant:

____

Lasse Drejer Andersen

Supervisors:
Thomas Lykke Andersen

Morten Mejlhede Kramer

Editions: 4
Report pages: 89
15 pages appendix + 6 drawings
Completed 08-06-2017

Synopsis:

This thesis investigates a passive exchange system of the enclosed water inside a monopile, with the sea water . This increases the pH-value of the water inside and decrease the corrosion of the anodes.
The exchange system is investigated through numerical CFD simulation of the flow inside the monopile, in both two- and three-dimensional models. The exchange is through one or more holes drilled in the monopile.
The models are simplified by a comparison between the simulation and the energy equation. The internal flow is validated through laboratory experiments, which are compared with simulated CFD models.
It is found that hardly no exchange occurred from current, but a complete exchange might be possible from both tides and waves. The most promising results are from the wave conditions, as this introduce a higher velocity in the flow thought the holes.
The results of this thesis suggest that a exchange system, such as this, could result in a reduction of up to 80 % of the anode material needed for the corrosion.

Resume

Der er i dag stor fokus på miljøet, samt besparelse af konstruktions materialer, og derfor også fokus på besparelse i offshore sektoren. Dette projekt omhandler en metode for at reducere materiale forbruget ved konstruktionen af monopæls fundamenter for offshore brug. Materiale forbruget reduceres ved at sænke korrosionen af konstruktions materialerne. Reduktionen af korrosionen fungere ved at neutralisere pH-værdien af det indelukket vand inde i monopælene. Det indelukket vands pH-værdi sænkes ved at korrosionen frigiver hydrogen ioner til vandet. Den sænket pH-værdi resulter i en øget korrosion. Dette projekt undersøger muligheden for at udskifte det indelukket vand med hav vandet omkring, hvor pH-værdien er 8.

Udskiftningen forgår ved at et eller flere huller er boret i monopælen, hvor vandet kan strømme ind og ud gennem. Strømningen gennem hullerne bliver drevet af tryk forskelle mellem det indelukke vand og havvandet. Systemet er lavet passivt ved at strømningen kun drive af trykforskelle skabt af havforholdende . Der er i denne rapport undersøgt for tre forskellige havforhold; tidevand, bølger og strøm.

Målet er at opnå en total udskiftning af det indelukket vand for at øge pH-værdien i hele monopælen. Udskiftningen af vandet er undersøgt gennem CFD modeller i både to og tre-dimensioner. Initialt er lavet en simplificering af modellerne for at undgå at simulere havet omkring monopælen. Denne simplificering viser at havet kan reduceres til at lille område udenfor hullet, og randbetingelserne kan bestemme ved hjælp af energi ligningen.

Alle tre havforhold er først undersøgt for at bedømme om en fuld udskiftning er mulig. Denne undersøgelse er lavet i to-dimensionselle modeller. Simplificeringen fra tre-dimensioner til to-dimensioner resulter i store konsekvenser grundet geometrien af monopælen og hullerne. Der er derfor reduceret på tidevands og bølge perioden for at fastholde den samme procentmæssige udskiftning af det indelukket vand. Undersøgelsen af de tre havforhold, viser at ved en konstant strøm, opnås en meget lille udskiftning. I modsætning viser både bølger og tidevand at resultere i en mulighed for at udskiftet alt vandet. Reduktionen af perioden viser sig at have stor effekt på bølge simuleringerne, grundet den allerede korter periode for en bølge i modsætning til tidevandet. Grundet dette er der kun fortsat med tidevandet i to-dimensioner.

En videre undersøgelse af tidevandet viser at udskiftning er meget påvirket af temperatur variationen mellem det indelukke vand og hav vandet. Grundet tidevandet lange periode er hastigheden umiddelbart for langsom til at undgå lagdeling grundet densitet og temperatur forskellene. De to-dimensionelle model viser derfor at en højere hastighed er nødvendig. For at øge hastigheden gennem hullerne er den tre-dimensionelle undersøgelse fokuseret på bølger.

Før der er lavet analyser af de tre-dimensionelle modeller er strømningen undersøgt ved hjælp af eksperimentelle forsøg. Disse eksperimenter er sammenlignede med simulerings modeller. Det er er gjort for at validere $k-\varepsilon$ turbulens modellen brugt for simuleringerne.

Tre-dimensions modellerne er kun udført for bølger, da den har vist at give mulighed for høj udskiftning ved høj strømningshastighed. De tre-dimensionelle modelle viser udskiftningen er mulig ved brug af flere huller placeret modsat af hinanden.

Resultatet bliver derfor at en fuld udskiftning er mulig, og pH-værdien kan komme op og ligge næsten stabilt med det omkring liggende hav. Denne neutralisering af pH-værdien betyder at op imod 80 % af det nuværende anode materiale kan spares væk grundet den reduceret korrosion.

Preface

This master thesis analysis a passive exchange system to decrease the corrosion inside monopiles. The project is written by Lasse Drejer Andersen on the 4$^{\text{th}}$ semester of the MSc in Structural and Civil Engineering. The thesis is written in the project period from September 1st 2016 to June 8th 2017. The thesis includes CFD models and experiments for calculating the exchange system.

I would like to send a thanks to the project supervisors, Thomas Lykke Andersen and Morten Mejlhede Kramer, for help and guidance throughout the project period. As well a thanks directed to Nikolaj Holk for helping with the experiments.

Reading guide

This thesis is divided into five parts

- Validation
- 2-D models
- Experimental
- 3-D models
- Conclusion

The first parts states the foundation for the thesis. The second parts contains initial evaluation and numerical analysis in two-dimensions, which lay the foundation for the three-dimensional models in the fourth part. The third part validates the three-dimensional models. The fifth parts concludes the thesis, and the thesis is recommended to be read chronologically.

Appendix A shows a list of the item placed on the digital appendix and the folder structure.
Appendix B shows a list of the drawings included in this project.

On the digital appendix, the final CFD model for the two-dimensional evaluation, the experimental evaluation and the three-dimensional evaluation is included. For other specific models, a request can be send to the author. One the digital appendix is the used video files for the experiment placed, together with the simulation videos used as comparison.

Sources

Through the thesis the sources are referred to using Harvard referencing. This reference states the author and the year of publication.

Table of contents

1 | Introduction

The development of sustainable energy is of high interest all over the world, where Denmark has been one of the top advocates for sustainable energy for multiple years. One of the main reasons for Denmark's large amount of sustainable energy is the development of wind energy, which has expanded in the last 10 years. The development of electric energy in Denmark generated by wind power is shown in Fig. 1.1.

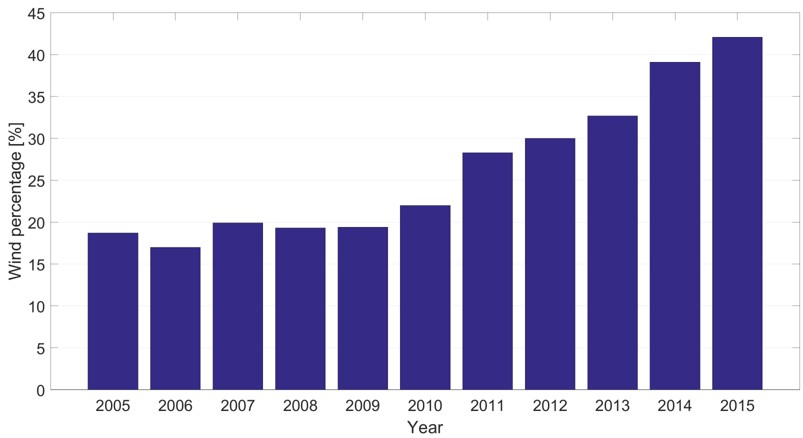

Fig. 1.1: Percentage of the electric energy produced by wind power over a 10 year period in Denmark. [Energinet, 2016]

Of the wind power generated in Denmark around 35 - 40 % is generated by offshore wind turbines located along the shore lines and in wind farms [Vindmølleforening, 2016]. The foundation of offshore wind turbines are in approximately 90 % of the cases monopile foundations [Ramboll, 2016]. The design lifetime for monopile foundations is typically designed to between 20 - 25 years, and is limited due to the internal corrosion of the monopile. [Hilbert et al., 2011] For unprotected steel immersed in sea water, the uniformed corrosion is expected to be 0.1 - 0.15 mm/yr. [Hilbert et al., 2011] The inside of the monopile is normally not corrosion protected, as the corrosion is depending on the oxygen concentration in the water. In a complete airtight monopile the corrosion from oxidation will decrease over time as the media turns more anaerobic. However, a completely airtight monopile has shown problematic to achieve. In a study by Hilbert et al. [2011], the oxygen concentration in 36 monopile foundations at an age of 5 - 10 years were measured. The monopiles were all constructed to be airtight. These measurements showed that only 8% could be categorised as oxygen free, therefore fully closed, where 70% had an oxygen concentration above 15%. The reason for the oxygen ingress was unknown, as the airtight seals were intact, but were expected to be due to cracks or leaks at the J-tube.

As there is an oxygen ingress in most cases, another form of internal corrosion protection is needed. To reduce the internal corrosion, a possible solution is to apply anodes to protect against corrosion. These anodes could, for example, be made of zinc or aluminium. The anodes are to act as a sacrificial material, to shift the corrosion of the steel to the anodes instead.

1.1 Project foundation

The use of an anode greatly reduces the corrosion compared to having unprotected steel. In offshore conditions a zinc anode will reduce the corrosion by 6 to 12 times [zinc association, 2017]. The corrosion of the anodes affects the pH balance, as the corrosion releases hydrogen ions. With the internal corrosion there is no exchange of the water, and the extra hydrogen results in a decrease of the pH-value. This project will evaluate the effect from applying anodes inside the monopile and a possible solution for reducing the negative effect that occur, as a result of the change in the internal pH-value.

1.1.1 pH effect

As anodes are placed inside the monopile, the corrosion shifts to the anodes rather than the monopile steel. This is caused, because the anode material is of a lower noble metal, than the carbon steel. The corrosion reactions depends on the material of the anodes, but the general reactions using either zinc or aluminium anodes are similar. Using zinc anodes, the following reaction occurs on the anode surface:

$$Zn \rightarrow Zn^{2+} + 2e^{-}$$

The Zn^{2+} then reacts further with the water and releases hydrogen ions and zinc hydroxide:

$$Zn^{2+} + 2H_2O \rightarrow Zn(OH)_2 + 2H^{+}$$

At the steel surface the released electrons react with the water:

$$2H_2O + 2e^{-} \rightarrow H_2 + 2OH^{-}$$

The hydrogen ions are released from the reaction between zinc and water, and the increased amount of hydrogen ions results in an acidification of the sea water. The hydroxide freed at the steel surface results in an alkalinity of the sea water, which neutralises the acidification. This results in an unchanged pH balance. On the steel surface the freed hydroxide reacts with the bicarbonate and calcium in the water, creating solid calcium carbonate. During this reaction, the hydroxide is not being used to neutralize the acidification of the sea water. This results in a slow acidification of the enclosed water from the application of zinc anodes. [Briskeby et al., 2015]

If the anodes are made of aluminium instead, the reactions are similar to the zinc anodes. At the anode surface the following reaction occurs:

$$Al \rightarrow Al^{3+} + 3e^{-}$$

The Al^{3+} then reacts further with the water to release hydrogen ions and aluminium hydroxide:

$$Al^{3+} + 3H_2O \rightarrow AL(OH)_3 + 3H^{+}$$

At the steel surface the water reacts with the released electrons, similar to the use of zinc anodes. As for the zinc anodes, the aluminium anodes results in a slow acidification, when some of the freed hydroxide creates solid calcium carbonate. The main difference on the pH balance between the use of zinc and aluminium anodes is that the aluminium hydroxide reacts with the water, and releases additional hydrogen ions. This reaction is as followed:

$$Al(OH)_3 + H_2O \rightarrow Al(OH)_4 + H^{+}$$

This reaction releases hydrogen ions, without releasing any additional electrons. Therefore, no additional hydroxide is created at the steel surface to neutralize the increase in the acidification. The acidification with aluminium anodes are therefore accelerated and the pH change is more drastic, compared to the used of zinc anodes. [Briskeby et al., 2015]

An experimental study performed by Briskeby et al. [2015] has evaluated the acidification over time for enclosed water, when zinc or aluminium anodes are used as the sacrificial material. In the study was studied the pH change at seabed, where the mud affected the pH change, and higher, where there was no influence from the mud. The anode surface was 7/100 of the monopile surface, which is a typical ratio between the anode and monopile surface areas. The initial pH-values of the sea water was 8. The pH-value of the enclosed water was measured on a regular basis. At every minute in the beginning of the experiment and then every hour later on, plus some spot check 1-2 times a week. The change in pH-value over time with the zinc and aluminium anode are shown in Fig. 1.2. The figure shows the spot check for both anodes with and without mud and a linear regression is determined based on these. The initial effects are estimated based on the regular measurements performed at the beginning of the experiment.

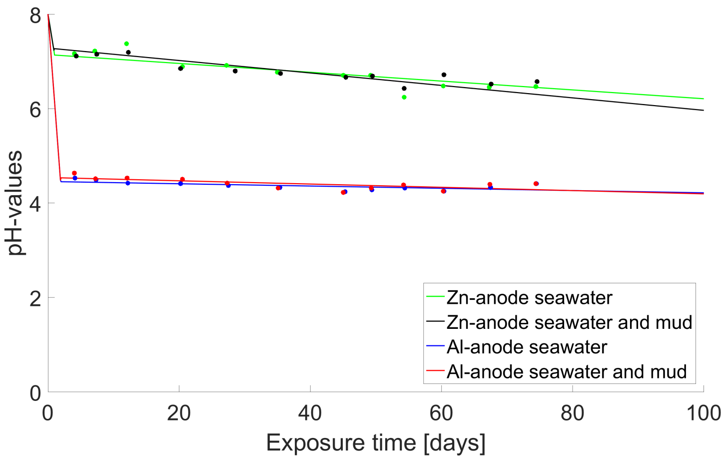

Fig. 1.2: Change in pH-value over time with a zinc or aluminium anode, and tests both with and without mud. [Briskeby et al., 2015]

For the aluminium anode the pH-value drops drastic over the first 2 days from a pH of 8 to 4.3, where it stabilises and stays constant. With zinc the initial drop is only down to 7.2 over the first 2 days, and then continues a slow decrease, rather than stabilising as the aluminium does. The pH-value continues to decrease with 1 pH per 107 days without the influence of the mud and per 75 days with the influence from the mud. Since the reactions that creates the acidification with both anode materials are similar, it is expected that the acidification with zinc will as well stabilise at a pH-value of 4.3. The drastic drop with the aluminium anode is due to the aluminium hydroxide reacting once more with the water. For the whole monopile a mean value for the pH change is introduced, and the change is shown in Fig. 1.3.

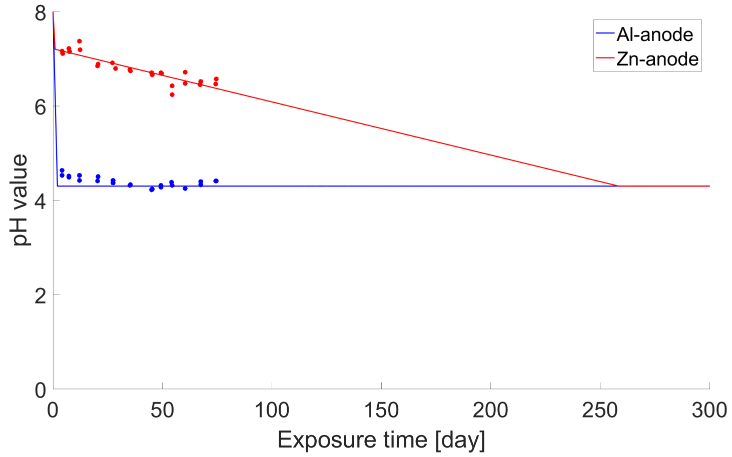

Fig. 1.3: The mean change of pH over time with the use of a zinc or aluminium anode.

With the use of zinc anodes, it takes approximately 250 days before stabilising at the pH-value of 4.3 rather than the 2 days, as the case with aluminium anodes showed. For the aluminium anode case the enclosed water exchange needs to result in a full exchange once ever second day. In the case with the zinc anode, the needed time for the exchange is extended significantly with approximately 125 times. This gives a time period where the pH-value can be affected by an exchange. Due to the close to instantaneously drop with the aluminium anode, only the use of zinc anodes and its effect on the pH change is analysed in the present thesis. The change in the pH-value is calculated with Eq. (1.1).

$$pH = \begin{cases} 8 - 4.057\dfrac{1}{days}\,t & \text{for } t < 2 \text{ days} \\ 7.211 - 1.127 \cdot 10^{-2}\dfrac{1}{days}\,t & \text{for } t >= 2 \text{ days and time} < 258.5 \text{ days} \\ 4.3 & \text{for } t >= 258.5 \text{ days} \end{cases} \tag{1.1}$$

The corrosion rate of the zinc is highly depending on the pH-value of the water, as shown in Fig. 1.4. The figure shows the sensitivity to pH-change relative to the corrosion at a pH-value of 8, meaning the corrosion rate is normalized to a corrosion rate at 1 for a pH-value of 8.

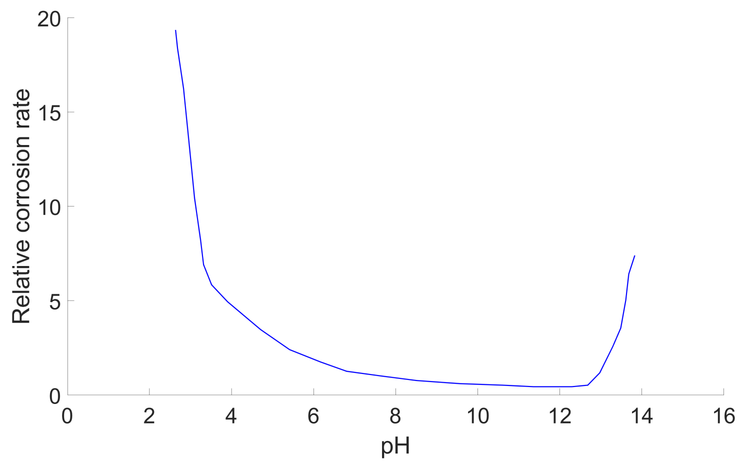

Fig. 1.4: The relative corrosion rate of zinc depending on the pH-value of the sea water. [Assosiation, 2017]

As the pH drops, the corrosion rate increases. This increases the amount of zinc anodes needed to achieving the same lifetime for the monopile. By knowing the rate of change of the pH-value inside the monopile, and the relative corrosion rate depending on the pH-value, the relative internal corrosion of the monopile over time can be found, if no water exchange occur. The normalized corrosion is shown in Fig. 1.5.

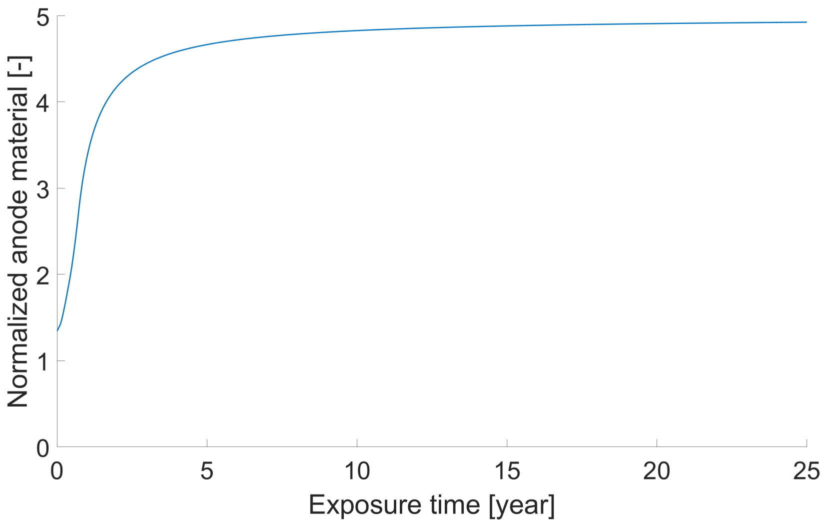

Fig. 1.5: Normalized corrosion rate over exposure time inside a monopile.

Fig. 1.5 is depends on the ratio between the surface area of the anodes and the monopile being 7/100.

For a case with an average corrosion of the anode material on 100 kg/year at a constant pH-value of 8, the needed anode material over the lifetime is shown in Fig. 1.6. Fig. 1.6 also shows the needed anode material, if the pH-value drops equal to Eq. (1.1) and no water exchange occur.

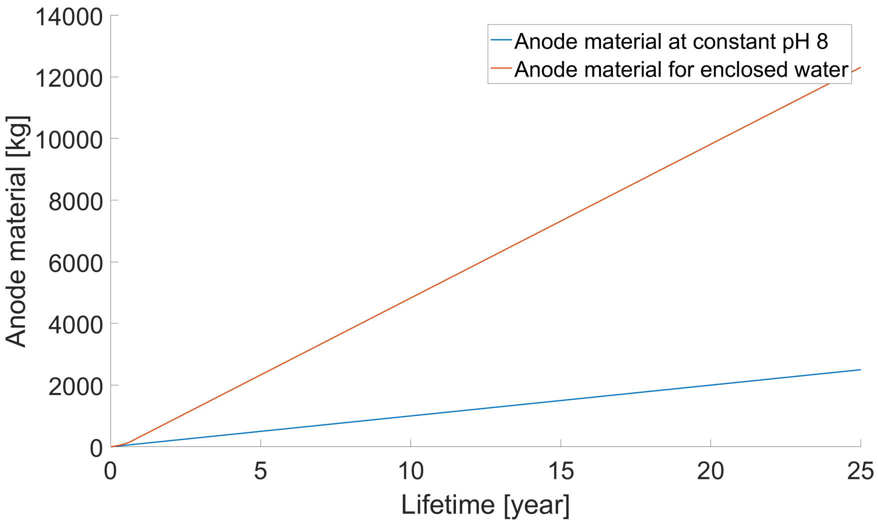

Fig. 1.6: Needed anode material at constant pH of 8 compared with needed material in enclosed water.

As shown in Fig 1.5 and Fig. 1.6 a large amount of additional anode material is needed, as a result of the decreasing pH-value of the enclosed water. This states that there is a great incentive to increase the internal pH-value and reduce the extra anode material needed for the structures lifetime.

2 | Project description

By applying the anodes, the enclosed water is acidified, which decreases the efficiency of the anodes. The acidification takes place as the enclosed water is stationary inside the monopile, and unable to exchange with the neutral sea water outside the monopile. An exchange between the enclosed water and the outside sea water would raise the pH-value inside the monopile and thereby reduce the internal corrosion. This project evaluates the effect of exchanging the water by drilling one or multiple small holes in the monopile surface to allow the water to flow through. The flow is generated by the changing pressure conditions outside the monopile. The pressure changes are due to the influence from the tides, waves and currents. The change in pressure creates a pressure difference between the inside and outside of the monopile, and thereby creating a flow from high to low pressure, through the holes, to equalise the pressure. By using the pressure change developed, the exchange system is a passive system, as no external influence is required. No external influence is only the case if the holes stay free of marine fouling. This project initially evaluates the possibilities of exchanging the enclosed water by each of the three conditions. In the initial evaluations the internal and external water are with an equal density. Furthermore, the best solutions are investigated further to optimise the solution. In the optimisation the difference in temperature and density in the water is introduce.

The exchange of the enclosed water from the monopile can be based on two factors. These two factors describes the rate of exchange and the amount exchanged:

- The first factor describes how rapid the exchange of the enclosed water occur, and is called the remaining coefficient, R. The remaining coefficient describes how many percentage of the enclosed water remains after a period of time. In this case the period is the tidal or wave period. The lower the remaining coefficient is faster the enclosed water is exchanges, as less enclosed water remains within the monopile after each cycle.
- The other factor describes the percentage of enclosed water, which are not being exchanged in the simulation, it is shorted to A_e. An optimal solution is that A_e is equal to zero, as that means all the enclosed water is exchanged over time.

To evaluate the cases and determine the two factors, The modelling of the models depends on multiple factors. The different factors and how they are implemented in this thesis are described in the following sections. The described factors are as follows:

- Monopile design
- Hole criteria
- Tidal conditions
- Wave conditions
- Current conditions
- Density conditions, including temperature and salinity

2.1 Monopile design

The design of a monopile varies depending on the usage and construction depth. For wind turbines, monopiles are the preferred foundation in water depths up to 30 m. For deeper water tripod and jacket foundations are highly used as well. For this project one monopile design is investigated. This monopile is at a water depth of 30 m at mean water level, and located off the west coast of Jutland. For a monopile at this depth, the diameter commonly range between 5-7 m. This project is therefore based on a monopile with the specifications shown in Fig. 2.1.

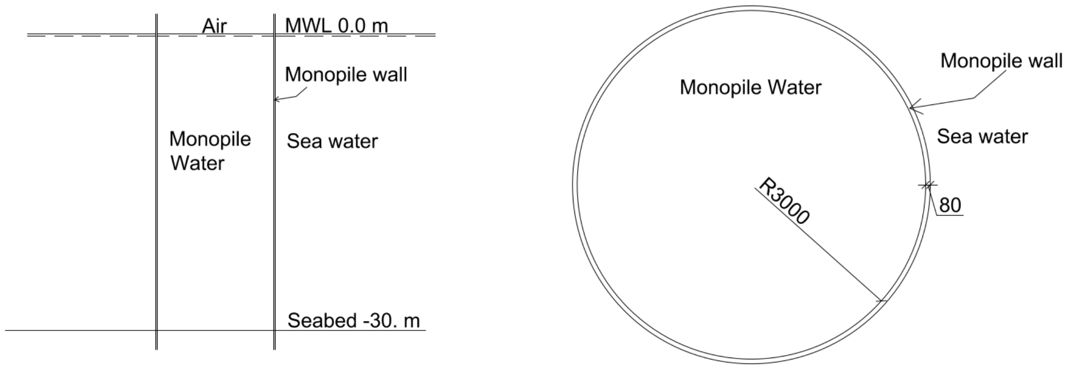

Fig. 2.1: Dimensions of the monopile. Datum is based on DVR90 and measurements are in mm, unless otherwise written.

2.2 Hole criteria

The size, number and location of the holes influence velocity of the flow through them. These criteria are determined after discussion with COWI. For the holes to keep the flow through, they need to be kept free of marine fouling, sand and mud from the seabed and the J-tubes. The location of the holes needs as well to be below the max wave trough, to avoid oxygen ingress through the holes. In this project the criteria for the location of the holes are stated as:

- Minimum 10 m below MWL.
- Minimum 5 m above seabed.

The holes needs a certain size to achieve a flow through. The maximum size is as well limited to avoid large effects on the load bearing capacity of the monopile. The maximum and minimum diameter of the holes are stated as followed:

- Maximum diameter of 0.2 m.
- Minimum diameter of 0.05 m.

The number of holes can highly influence the flow rate through each inlet, as a doubling in the numbers of inlets result in twice the inlet area. With a larger inlet area the internal and external water level difference is smaller, resulting in lower pressure difference. This results in lower velocity due to smaller pressure difference. It is expected that with a too low velocity, the mixing is insufficient and thus the sea water flowing in to a large degree be the same flowing out again. Therefore, the number of holes is, in combination with the hole size, a goal to gain a large internal water change, along with a high velocity, to achieve the completely and fast exchange of the enclosed water. To reduce the influence from the holes on the load bearing capacity, a criterion for the maximum allowed area of the holes is stated.

- The maximum hole area is 0.5 % of the surface area of the monopile.

2.3 Tidal conditions

The tides is the ocean being affected by the gravitational force of other astronomical bodies, primarily the moon and the sun. The tides multiple component, where the most dominating are the semi-diurnal effect. Beside the semi-diurnal component, both shorter and longer components effect the tide. The size as well varies depending the location. In the Danish waters the variations is between 0.2 - 2 m. The largest tidal waves are located along the west coast of Jutland, where multiple wind farms are located as well. The surface elevations at low and high tide at Esbjerg during 2016 were measured and are shown in Fig. 2.2. In the measured data a clear semi-diurnal and annual effect is visible, besides the remaining variation is due to the remaining components. The mean tidal wave at Esbjerg for 2016 was at 1.57 m. For this thesis only the semi-diurnal is included and a constant height of the tidal wave at 1.5 m is used. The actual surface elevation at low and high tide, and the simplified are compared in Fig. 2.2.

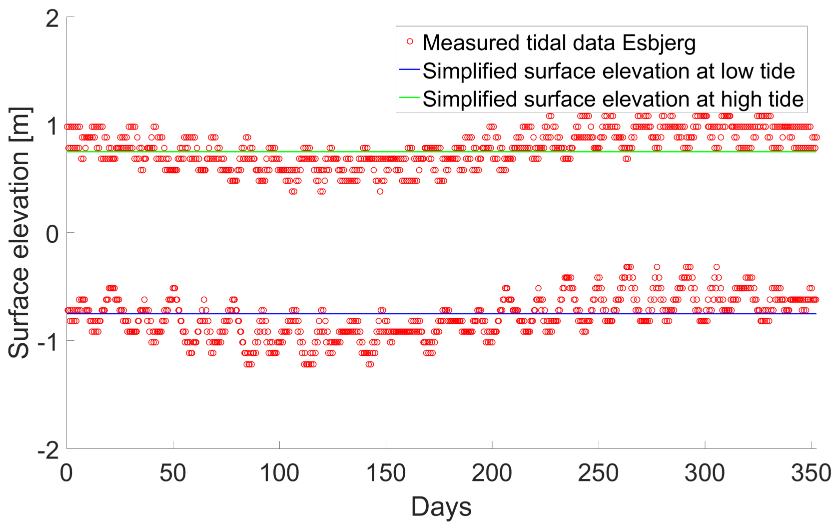

Fig. 2.2: The surface elevation at high and low tide measured in Esbjerg, and a simplified surface elevation for high and low tide, with a tidal amplitude of 0.75 m. [DMI, 2017]

The variation of the surface elevation over a tidal period is simplified to a cosine function. The cosine function has an amplitude of 0.75 m and tidal period of 12 h. The MWL is located at 0.0 m. The function for the tidal waves are given in Eq. (2.1).

$$h_A(t) = \cos\left(\frac{2\,\pi\,t}{T_p} + \pi\right)\,T_A + h_{MWL} \tag{2.1}$$

Where:

h_A	Water level
t	Time
T_p	Tidal period
T_A	Tidal Amplitude
h_{MWL}	Mean water level

A comparison between the simplified tidal period and a measured tidal wave at Esbjerg is shown at Fig. 2.3.

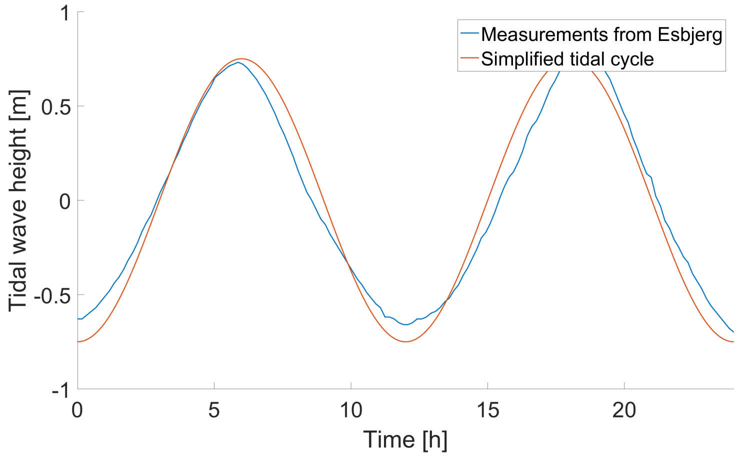

Fig. 2.3: Surface elevation measured at Esbjerg, the 22/01-17, and the surface elevation generated by the simplified tidal wave over a 24 hour period.

The overall tendencies between the simplified and measured tidal cycles are the same, ignoring than the 12 h component, but the steepness of the curves are alike. As a result, the simplified is used as the general tide for this project.

2.4 Wave conditions

The wave conditions varies depending on the location and are estimated in the North Sea based on DNV [2007, Appendix C]. DNV [2007, Appendix C] has estimated the parameters for a Weibull distribution of wave height and the parameters for a Log-Normal distribution for the wave period. The parameters are shown in Tab. 2.1 and the cumulative distribution functions for the wave height and wave period are shown in Fig. 2.4 and Fig. 2.5.

Significant wave height [H_s]		Peak wave period [T_p]	
α	β	a	b
2.19	1.26	0.935	0.1386

Tab. 2.1: Parameters for the Weibull and Log-Normal distribution functions for the calculation of the wave height and wave period in the North Sea.

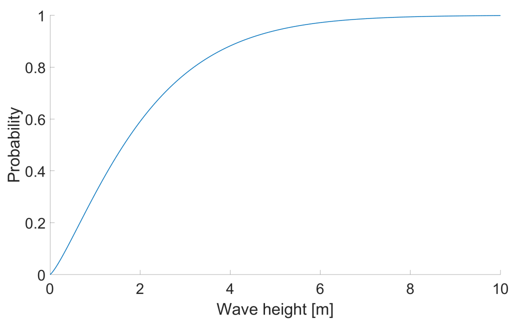

Fig. 2.4: Cumulative distribution of significant wave height.

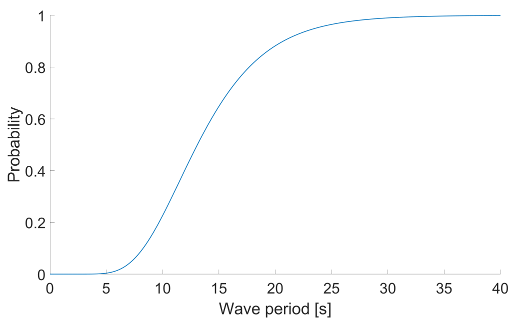

Fig. 2.5: Cumulative distribution of peak wave period.

As the waves are dependent on the weather conditions, a 50 % probability wave is chosen. This means that 50 % of the time, it is expected that the waves are larger. With a larger wave, the pressure difference is bigger, which results in higher velocity through the inlets. This is expected to result in a larger exchange of the enclosed water. The remaining 50 % the wave size will be smaller, which will expectantly result in less exchange. Therefore the waves are not a stable condition as the tide, and the exchange will variate. The 50 % probability wave is therefore chosen to estimate the mean exchange. The wave height and period used in this thesis are given in Tab. 2.2.

Significant wave Height	1.64 m
Peak wave period	13.0 s

Tab. 2.2: Significant wave height and peak period used for the calculations of the waves.

The water level is determined with linear wave theory and calculated with Eq. (2.2) and a wave period is shown in Fig. 2.6.

$$\eta = a \sin(\omega t + k x) \tag{2.2}$$

Where:

η	Water level
a	Wave amplitude, $H/2$
ω	Angular frequency, $2\pi/T$
k	Angular wave number, $2\pi/L$
x	Coordinate on x-axis

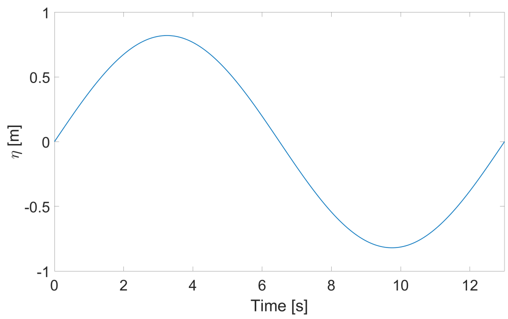

Fig. 2.6: Water level over a wave period.

2.5 Current conditions

The current is primarily created by the tides, and is therefore a semi-diurnal periodic changing velocity. The current conditions are measured at Horns Reef, west of the west coast of Jutland, by Nielsen [2000, Fig. 7.1]. The observations were taken over a period of a year, and showed peak current velocities of up to 1-1.5 m/s. The observations showed frequent current velocities of 0.5 m/s, when the data were averaged over a 24-hour period. For the evaluation of the current in this project it is chosen to use a constant velocity rather than a periodic. Therefore, the current velocity used is:

Current velocity, $U = 0.5\,\text{m/s}$

2.6 Density conditions

As the density of sea water depends on its temperature and salinity, the temperature change and salinity level are studied. The temperature of the sea is depending on the surface temperature and the depth. The temperature change for the first 30 m is below one degree, and thus dominated by the surface temperature. The low change is due to the first 30 m being within the mixing layer, where the sun, waves and current still affects the temperature. The largest temperature change occurs in the themocline zone, which is located at depth of 40 - 200 m. The sea temperature variates from a minimum temperature of 6 °C during winter, to 18 °C during summer. [Skjoldal, 2007] The salinity of the ocean is between 28 and 36 ‰. In the North Sea, at the western coast of Jutland, the salinity is determined by the mixing of the German Bight water (GBW), South North Sea water (SNSW) and Atlantic Ocean water (AW). These three waters have different salinities. The flow of the waters are shown in Fig. 2.7.

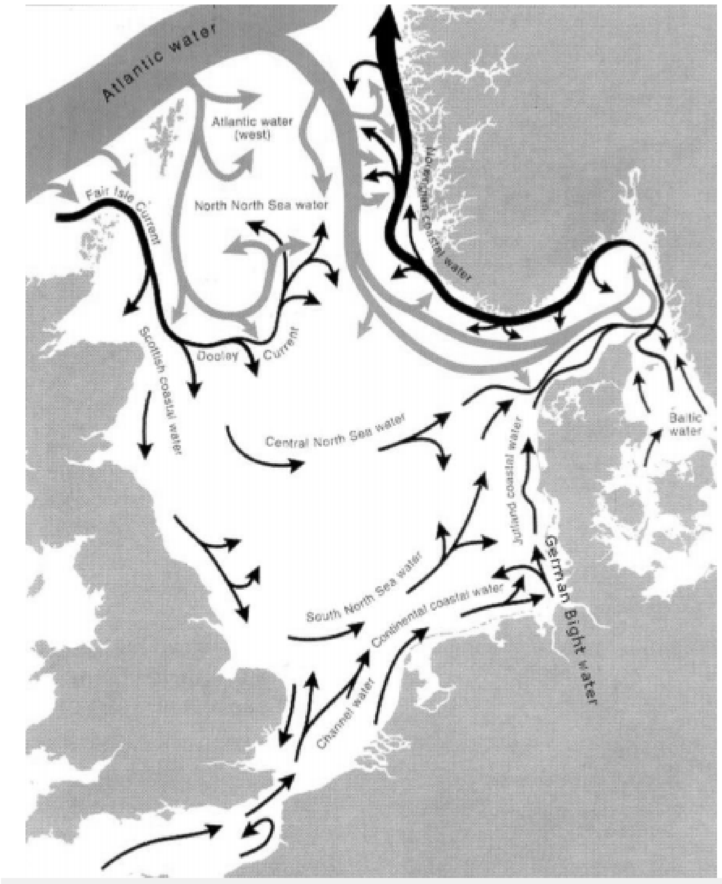

Fig. 2.7: Flow of the different water in the North Sea. [Nielsen, 2000]

The salinity of the GBW, SNSW and AW water is shown in Tab. 2.3.

	German Bight water (GBW)	South North Sea water (SNSW)	Atlantic Ocean water (AW)
Salinity	30.0 ‰	34.5 ‰	35.3 ‰

Tab. 2.3: Salinity of GBW, SNSW and AW flowing into the North Sea. [Nielsen, 2000]

At the southern part of Jutland's coast, the water is dominated by the salinity in the German bights, but the influences by the ocean waters raises the further north, as the percentage of GBW decreases. The percentage raises from a yearly mean of 32 ‰ at Blaavand, [Nielsen, 2000, app. D5, BLAA] to 34 ‰ at Hirtshals [Nielsen, 2000, app. D5, HIST]. As a result of the different salinities, the three waters have different densities, but only a small difference between SNSW and AW. Due to the higher density of SNSW and AW, the GBW has a tendency to flow above the others, when they encounter each other, and not creating a complete mix of the waters. As a result of this there is a change in the salinity of 1 ‰ over a 30 m depth. [Nielsen, 2000, app. E.5] To compare with the used tide, wave and current used in this project, salinity at Blaavand are used. This means the salinity changes from 32 ‰ at the surface to 33 ‰ at the seabed. Knowing the temperatures and salinity of the sea water, the density is calculated based on Millero and Poissont [1981]. The densities are shown in Tab. 2.4.

Season	Temperature [°C]	Sea surface density [kg/m^3]	Seabed density [kg/m^3]
Winter	6	1024.7	1025.5
Spring/fall	11	1024.0	1024.7
Summer	18	1022.5	1023.2

Tab. 2.4: Sea water temperature and density around the monopile.

For sea water enclosed in a monopile over a longer duration, the sun is unable to heat the water and current is unable to mix the water. This results in an altering temperature inside the monopile. The temperature becomes dependent on depth and time of the year. A study of the temperature inside the monopile in the inner waters of Denmark were carried out by Mathiesen et al. [2016]. The study shows the seabed temperature is fairly constant over the year, roughly 2-3 °C below the yearly mean temperature. The surface temperature showed to be within one degree of the sea water surface temperature. This meaning one degree higher during winter and one degree lower during summer. Adopting this to the North Sea, the temperature and density profile inside the monopile are given in Fig. 2.8 and Fig. 2.9. The salinity in the enclosed water is expected to variate as outside the monopile.

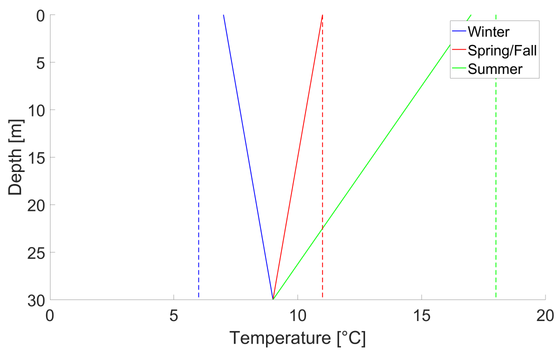

Fig. 2.8: Temperature profile for the enclosed water inside the monopile with no mixing. The temperature of the external sea water is shown with dashed lines.

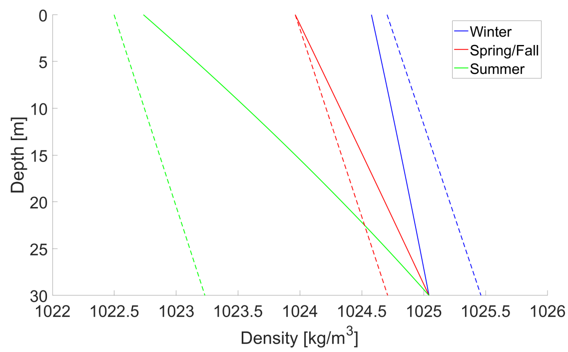

Fig. 2.9: Density profile for the enclosed water inside the monopile with no mixing. The density of the external sea water is shown with dashed lines.

During the winter the density is least dependent on the depth, as the colder water at the surface counteracts the lower salinity. During summer and spring the temperature decreases with depth, resulting in an increasing density, assisted by the increasing density from the increasing salinity.

Due to the density effects some stratification are expected to occur, but in limited extent as the density changes at a maximum of 2.5 kg/m^3 over a 30 m span. Looking at the sea water flowing into the monopile during winter, it is expected to flow downwards inside the monopile, due to a higher density of the external sea water. The opposite is expected during summer and spring, as the densities at this time are lower outside the monopile. The highest effect will occur during summer and be more drastic the lower the holes are located on the monopile.

The purpose of this project is to determine the exchange rate of the enclosed water in order to determine the pH-value and the needed increase in anodes. The exchange and flows in the monopile are estimated by the energy equation, two and three dimensional CFD-simulations. Experimental tests are used for validation of the three dimensional flow tendencies. An initial analysis are performed for tides, waves and currents in two-dimensions

Part I

Validation

In this part the monopile flow is analysed by the energy equation and compared with numerical CFD models from STAR-CCM+ as a validation of the inlet flow. Further the energy equation is used to calculate the flow velocity through the inlets. The external pressure conditions for the three cases of tide, wave and current are calculated, to used in determining the velocity through the inlets by the energy equation.

3 | Validation

Before analysing the exchange of the enclosed water, the simulation models are simplified, to avoid calculating large part of the ocean around the monopile. The simplifications are performed by validating two-dimensional CFD models against the energy equation. The energy equation is then used to calculate the flow rate through each hole, which is used as the flow rate in the simulations. The validation is based on the flow in the inlet, including the velocity and loss coefficients.

3.1 Energy equation

The energy equation is based on the pressure differential between two or more cross sections, here the sea water level, the inlet and the water level inside the monopile. The aim of the energy equation is to gain the average velocity and mass flow through the inlets in the monopile. The energy equation is based on the set-up in Fig. 3.1. The flow rate is calculated from a constant water level at section A and an increasing water level over time in section C. The energy level at the 3 section cuts are stated as:

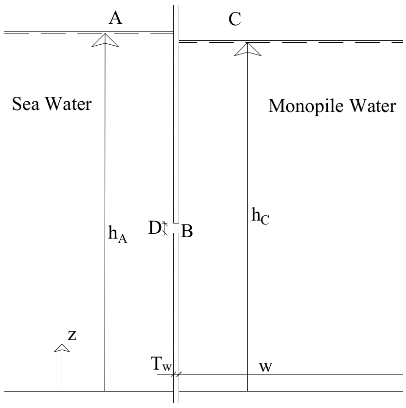

Fig. 3.1: Set-up of monopile with one hole.

$$H_A = \left(z + \frac{p}{\gamma}\right)_A + \frac{\alpha V_A^2}{2g} \approx h_A \qquad V_A \simeq 0$$

$$H_B = \left(z + \frac{p}{\gamma}\right)_B + \frac{\alpha V_B^2}{2g}$$

$$H_C = \left(z + \frac{p}{\gamma}\right)_C + \frac{\alpha V_C^2}{2g} \approx h_C \qquad V_C \simeq 0$$

Section A and C is located with a free water surface, and section B is located in the center of the hole. At section A and C the water change is very slow, therefore a velocity of 0 m/s is estimated as a simplification. The pressure loss between inside and outside the monopile is created by the major and minor loss. The major loss is simplified to 0 Pa due to an inlet length of 0.08 m. The minor loss is based on the entrance and exit of the inlet. These are sharp edged, which commonly has loss coefficients of: [Brorsen and Larsen, 2009]

$$K_{L,entrance} = 0.5 \qquad K_{L,exit} = 1.1$$

This gives the energy equation between the section cuts:

$$H_A = H_B + \Delta H_{AB} \qquad H_B = H_C + \Delta H_{BC}$$

$$h_a = H_B + \Delta H_{AB} \qquad H_B = h_C + \Delta H_{BC}$$

$$h_a = h_C + \Delta H_{AB} + \Delta H_{BC}$$

The pressure loss is depending on the velocity in the inlet, V_B, giving:

$$\Delta H = K_L \frac{V_B^2}{2g}$$

The water level inside the monopile is then defined and the velocity is determined by:

$$h_C = h_A - (K_{L,entrance} + K_{L,exit}) \frac{V_B^2}{2g} \Rightarrow \qquad V_B = \sqrt{\frac{(h_A - h_C)\,2g}{K_{L,entrance} + K_{L,exit}}} \tag{3.1}$$

Based on the continuity equation, the change in water level is calculated based on the velocity through the inlet. The water level change is based on the surface area in the monopile, the area of the inlet and the velocity through the inlet.

$$Q_B = Q_C \Rightarrow \qquad V_B\,A_B = V_C\,A_C \Rightarrow \qquad V_C = V_B\,\frac{A_B}{A_C} \Rightarrow$$
$$\frac{\Delta h_c}{\Delta t} = V_B\,\frac{A_B}{A_C} \Rightarrow \qquad \Delta h_c = V_B\,\frac{A_B}{A_C}\,\Delta t$$

Where:

A_B Vertical cross area of inlet
A_C horizontal cross area of monopile

The validation is performed in two-dimensions to compare the energy equation with the simulated results. The set-up for the validation is with a constant water level outside, and an initial water level difference of a half meter. Half a meter as the water level difference is chosen, as it result in a variation of the velocity from 2.5 m/s to 0 m/s, as seen in Fig. 3.4. The 2.5 m/s is slightly above the maximum velocity through the inlet as will occur in this thesis from the tides, waves or current. The water level outside the monopile is kept constant, and the height inside changes based on the continuity equation. The validation is done in two-dimension with one crack at an height of 0.1 m and a chamber width of 6 m, as seen on Fig. 3.2. Later, the effect from multiple holes, and different sizes of the inlet is looked into.

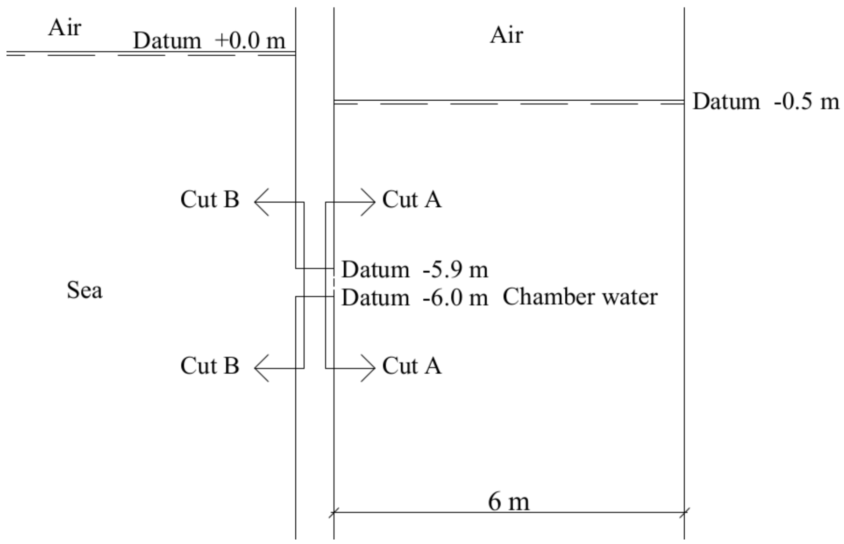

Fig. 3.2: The initial state used for calculation of the energy equation.

With the stated initial conditions, the velocity depending on time and the water level difference between the chamber water level and the sea water level is found. The energy equation is calculated with a total loss coefficient of 1.6. This gives the water level as a function of time, shown in Fig. 3.3 and the velocity shown in Fig. 3.4.

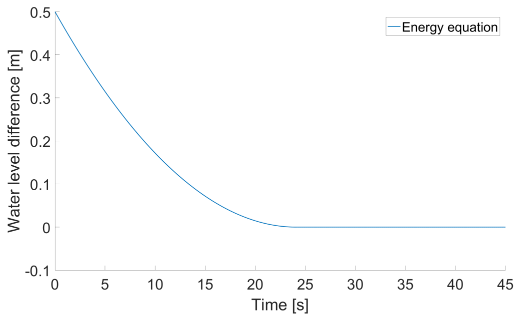

Fig. 3.3: Water level difference between external and internal water level.

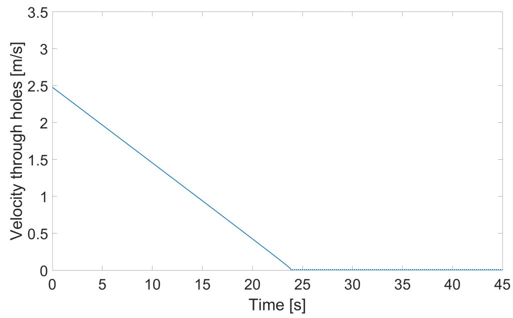

Fig. 3.4: Velocity in the inlet.

3.2 Comparison of velocity and loss coefficient at inlet

The energy equation results are compared to results from the STAR-CCM+ two-dimensional model. The simulation is made based on the boundary conditions and initial conditions shown in Fig. 3.5. The boundaries marked with black on Fig. 3.5, are simulated as walls.

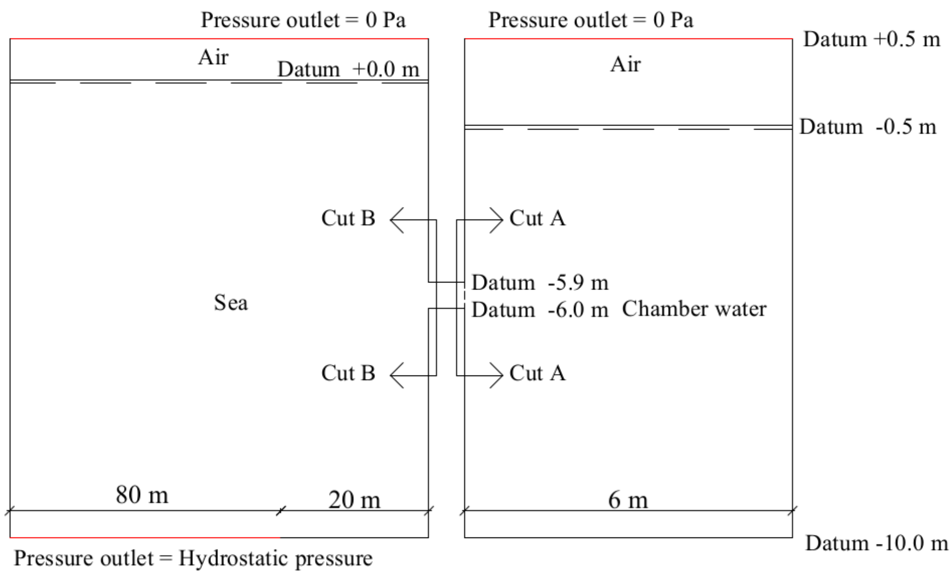

Fig. 3.5: The initial state and boundary conditions used for simulation in STAR-CCM+.

To keep the water level stable outside the monopile, part of the seabed is given a boundary condition, as a pressure outlet, with a constant pressure equal to the hydrostatic pressure at a depth of 10 m. As the model is a limited size compared to the sea, the flow into the chamber can be effected by the flow through the seabed. To limit the influence of the flow through the seabed, the model is created with a sea length of 100 m and the pressure outlet is only modelled over the 80 m furthest from the monopile. The water levels are estimated based on the volume fraction of chamber water, sea water and air inside and outside the chamber compared to the size and coordinates of the model. The volume fraction is measured as a percentage of each phase occurring in each element multiplied with the elements area/volume depending on two or three dimensions. The volume fraction of the 3 phases are measured independent inside and outside the chamber. The water levels are calculated with Eq. (3.2), which compare the volume of water with the total volume and gives the percentage of water inside the chamber. Knowing the total hight of the model and the datum for the seabed, the water level is calculated. The water level difference until stable water is obtained, is shown in Fig. 3.6. Cut A, see Fig. 3.5, is located at the exit of the inlet, to estimate the velocity profile and mean velocity through the inlet and the mean velocity through the inlet is shown on Fig. 3.7.

$$h(t) = h_m \frac{V_{F,sea}(t) + V_{F,chamber}(t)}{V_{F,sea}(t) + V_{F,chamber}(t) + V_{F,air}(t)} + b_{datum} \tag{3.2}$$

Where:

h	Water level
t	Time
h_m	Total height of model
$V_{F,}$	Fraction of the phase present either in- or outside of the chamber
b_{datum}	Datum for the bottom of the model

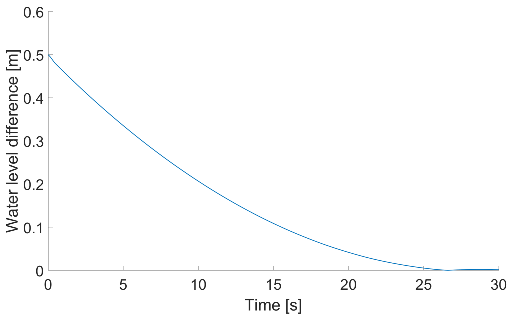

Fig. 3.6: Water difference between water level at sea and in chamber in simulation.

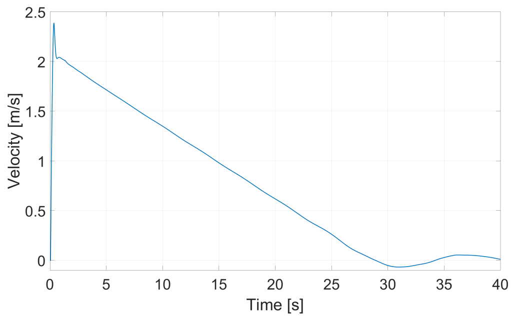

Fig. 3.7: Mean velocity through the inlet.

On Fig. 3.7 the velocity starts at 0 m/s due to the initial state, and first stabilises to a steady velocity after approximately one second. The acceleration from 0 m/s to stable velocity results in the peak on the velocity seen in Fig. 3.7. The loss coefficient through the exit of the inlet is estimated to compare with the energy equation. The loss coefficient is estimated by the mean velocity and the water difference, as shown in Eq. (3.3).

$$K_L(t) = \frac{2\,\Delta h(t)\,g}{u_{mean}(t)^2} \tag{3.3}$$

Where:

K_L	Loss coefficient
t	Time
Δh	Water level difference
u_{mean}	Mean velocity at inlet

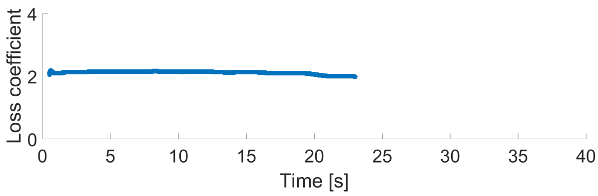

Fig. 3.8: Total loss coefficient calculated from the simulation.

The loss coefficient is stable in the first 20 second as shown in Fig. 3.8 and then varies in the last seconds. The large variation at the end is due to the velocity being close to 0, and practically no water level difference, where small variations results in large changes. The K_L value is averaged over the first 20 second, resulting in a total loss coefficient of:

$$K_L = 2.1$$

The total loss coefficient calculated within the energy equation and the one estimated from the STAR-CCM+ model are not identical, resulting in a variation of the time it takes for the external and internal water level to stabilise. The loss coefficient at the exit of the inlet is dependent on the velocity profile, where a velocity distribution coefficient of α=1.1 is assigned in the energy equation calculation. The velocity profile and velocity distribution coefficient in the STAR-CCM+ can be estimated. As the velocity is decreasing over time, the velocity is normalised against the mean velocity at Cut A at the time step. The velocity profile is then averaged over time as shown in Eq. (3.4). The normalised velocity profile is shown in Fig. 3.9. The velocity is measured in 20 probes across Cut A with a distance between them of 5 mm.

$$u_{normprof}(z) = \frac{1}{m}\sum_{t=1}^{m}\frac{u_{probe}(z,t)}{u_{mean}(t)} \tag{3.4}$$

Where:

$u_{normprof}$	Normalised velocity profile
z	Location across the inlet
m	Numbers of time steps
t	Time
u_{probe}	Velocity measured in the probes at the inlet

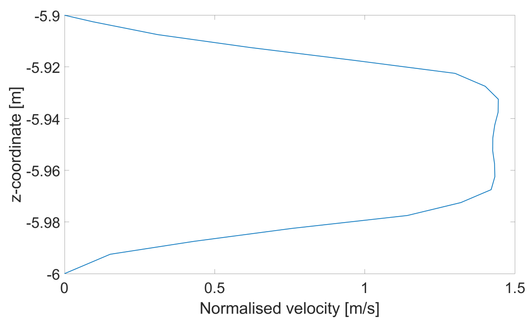

Fig. 3.9: Velocity profile at cut A estimated from the simulation.

With the velocity profile from the simulation known at the exit of the inlet, the velocity distribution coefficient can be calculated by Eq. (3.5).

$$\alpha = \frac{\int_{c_h} u_{normprof}^3 \, dc_h}{\left(\frac{1}{n}\sum_{z=1}^{n} u_{normprof}(z)\right)^3 \; c_h} = 1.6 \tag{3.5}$$

Where:

α	Velocity distribution coefficient
n	Numbers of measurements probes across cut A

As the value for the velocity distribution coefficient is different from the original expected value of 1.1, the loss coefficient at the exit of the inlet changes. With a new velocity distribution coefficient the energy equation can be recalculated. The water level difference for the two energy equations and the STAR-CCM+ model is compared in Fig. 3.10. The total loss coefficients for the energy equations and for the simulations are given in Tab. 3.1.

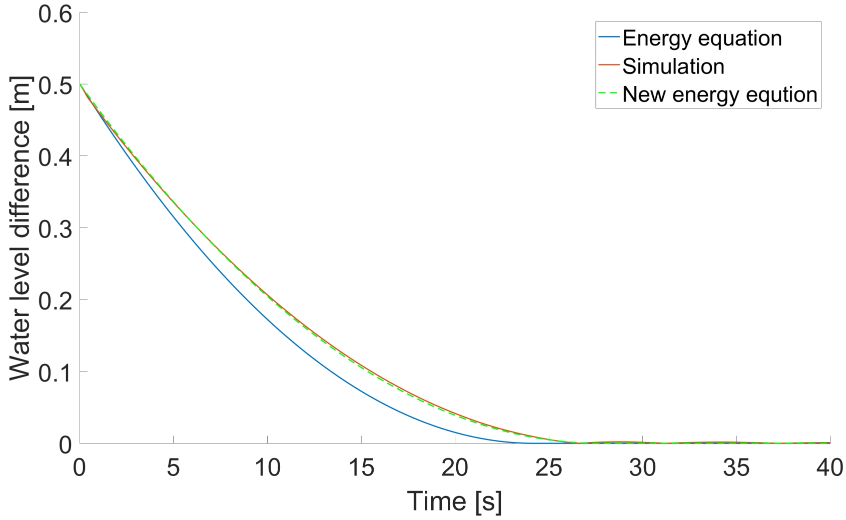

Fig. 3.10: Comparison between the two energy equations and the STAR-CCM+ model.

	K_L
Energy equation	1.6
STAR-CCM+ model	2.1
New energy equation	2.1

Tab. 3.1: Total loss coefficient for the 3 models.

The energy equation gives a faster stability of the water level, as the total loss coefficient is lower than from the model. The difference between the STAR-CCM+ model and the New energy equation is low, as the loss coefficients are the same. With am energy equation matching the STAR-CCM+ model, the model can be compared to achieve some simplifications of the models, to reduce the simulation time. The simplifications will be based on reducing the around laying ocean.

3.2.1 Without sea

To avoid calculating the sea in the later models, The STAR-CCM+ model with the sea is compared with models with reduced, or without, the sea. First a model is created, where the entire sea is removed, and the model only includes the chamber and the inlet. In this case the inlet is simulated as a velocity inlet, with the velocity calculated from the New energy equation. The model is shown in Fig. 3.11. The mean velocity used for the velocity inlet in the simulation, is shown in Fig. 3.12.

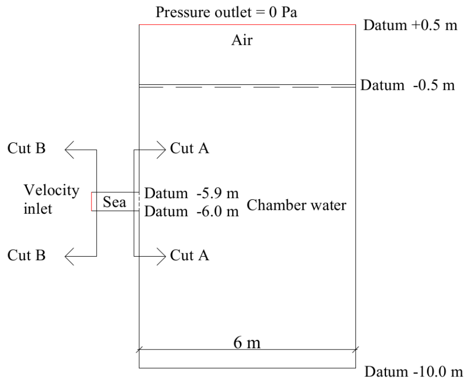

Fig. 3.11: Model of the monopile without the sea, including the boundary conditions and initial state.

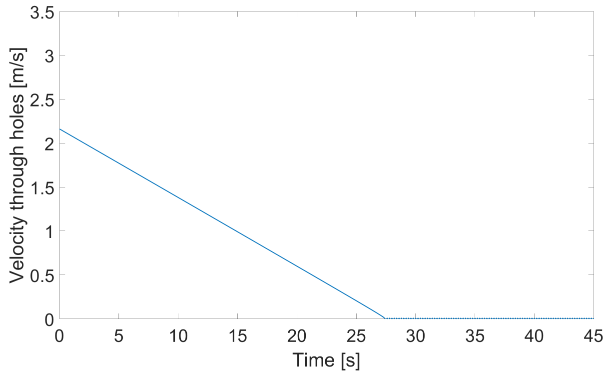

Fig. 3.12: Velocity at the inlet over time based on new energy equation.

To estimate the error without the sea, the different water levels are compared together with the velocity profile in cut A. The water level differences are compared on Fig. 3.13 and the two velocity profiles are shown in Fig. 3.14.

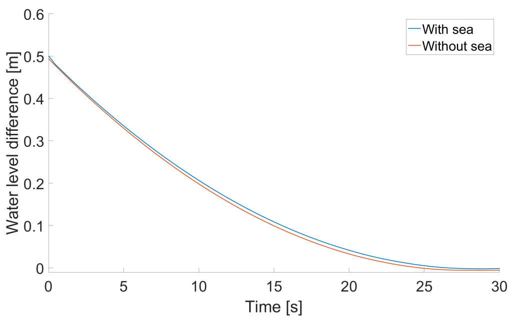

Fig. 3.13: Water level difference between sea and chamber water level.

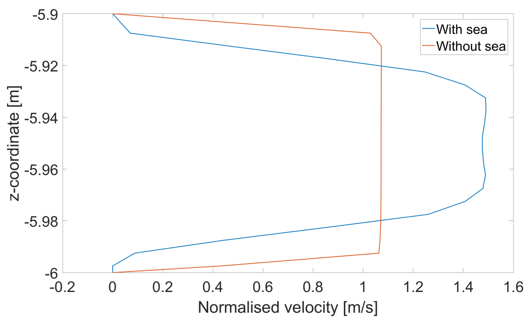

Fig. 3.14: Normalised velocity profile in cut A.

In Fig. 3.13 the water levels are similar, but without sea it stabilises slightly faster. This is because without the sea, the accelerating flow through the inlet in the first second, is removed. In the velocity profile there is a great difference, as seen on Fig. 3.14. The great difference is due to the flow through the velocity inlet being uniform. When the sea is included, the velocity profile is uniform at the entrance of the inlet, but influence from the sharp edged entrance, results in a non-uniform velocity profile inside the inlet. Without the sea included, the influence of the sharp edged entrance is removed, resulting in a uniformed flow inside the inlet, as seen on Fig. 3.14. The flow shown in Fig. 3.15, shows how the water streams from all around the inlet and flows through. Due to the corners of the inlet, eddies are created along top and bottom of the crack. These eddies are as long as the inlet itself, which results in the flow not reaching a fully developed state, before reaching the end of the inlet. The eddies are not created in the model without the sea, so to include this effect, the edges needs to remain in the model.

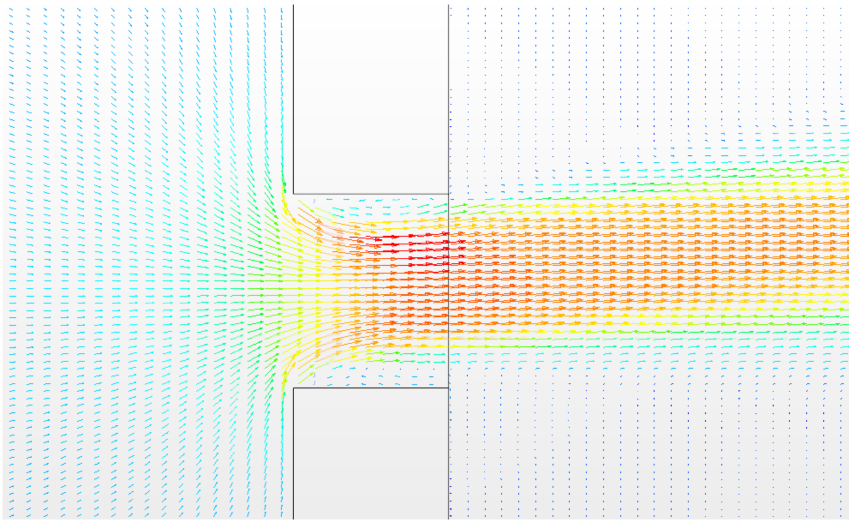

Fig. 3.15: The flow into the chamber through the inlet.

To keep the sharp edges, a small part of the ocean needs to be included in the model just outside of the inlet. This miniature sea is modelled in four different ways to define the best design. The four designs are shown in Fig. 3.16.

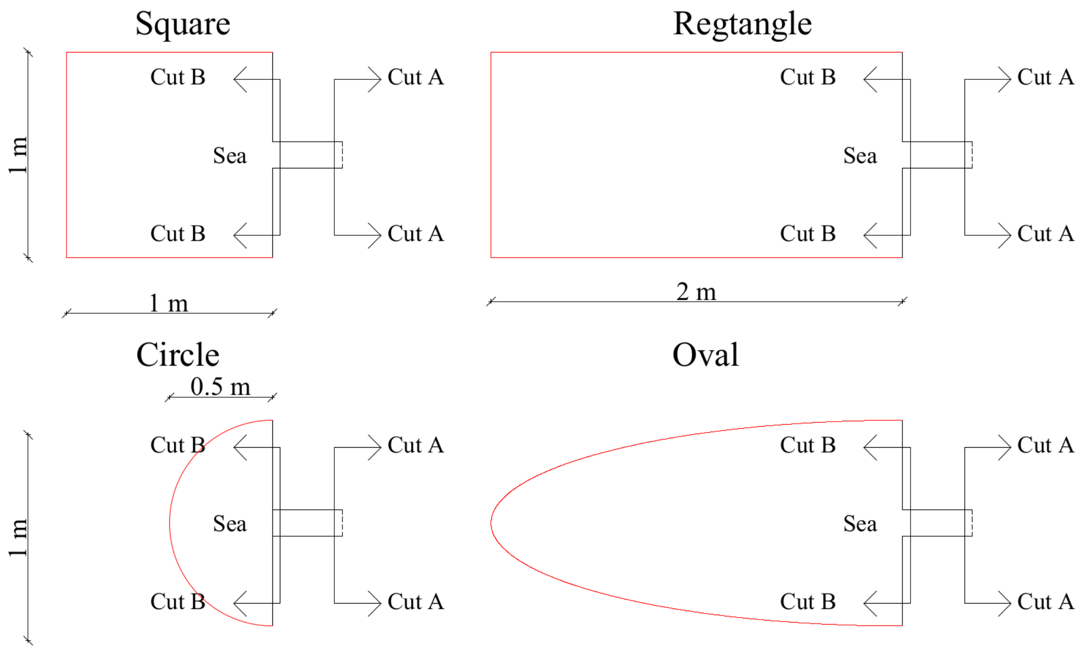

Fig. 3.16: The designs of the four miniature sea design outside the inlet of the monopile. The mass flow inlet boundary condition is marked with red on the designs.

The Square design is the simplest. The symmetrical design allows the water to flow to the inlet equally from the three outer sides. The Rectangle extends further back from the inlet to compensate for the jet created as the flow exits the monopile. The Circle is tested to avoid any complications at the corners in the Square and Rectangle. With the Circle the flow avoids perpendicular stream lines in the flow at the corners. The Oval is a combination of the Rectangle and Circle by extending to compensate for the exiting jet and smooth to avoid corner effects. In all four designs the inlet boundary condition is a mass flow inlet. The mass flow is calculated based on the mean velocity in Fig. 3.12, the density and the inlet area, as shown in Eq. (3.6).

$$Q = u_{mean}(t)\, A\, \rho \tag{3.6}$$

Where:

n	Number of measurement probes across inlet
i	Identifier for individual measurement probe
Q	Mass flow at inlet
A	Inlet cross area

The four designs are simulated to determine the velocity profile at Cut A to be compared to the correct simulation. The comparison is shown in Fig. 3.17 and to estimate the best solution the Mean Absolute Error (MAE) is calculated for each design. The MAE is calculated with Eq. (3.7).

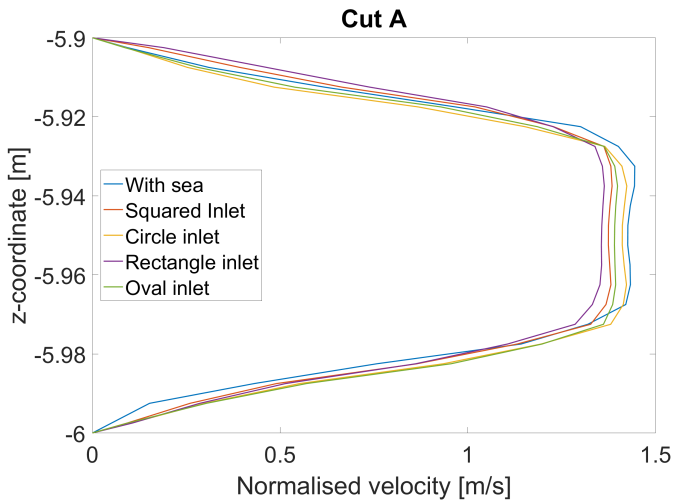

Fig. 3.17: The velocity profile at Cut A for the model with sea compared with the 4 different designs.

$$MAE = \frac{\sum_{i=1}^{n} |u_{normprof,c}(z) - u_{normprof,d}(z)|}{n} \tag{3.7}$$

Where:

MAE	Mean Absolute Error
$u_{normprof,c}$	Normalised velocity profile for design with sea
$u_{normprof,d}$	Normalised velocity profile for the designs

The MAE of the four designs is calculated for both a flow into and out of the monopile. For the out going flow the MAE is calculated in Cut B. The out going flow is calculated with the same parameters as the ingoing flow, meaning the initial internal water level is 0.5 m higher than the external water level. The external water level is still kept constant. The MAE's are given in Tab. 3.2.

MAE	Ingoing	Outgoing
Square	5.1	4.7
Rectangle	5.6	5.0
Circle	7.6	11.4
Oval	5.7	10.4

Tab. 3.2: MAE for the four different designs for in- and outgoing flow.

Based on the MAE the optimal design is the Square, where the smallest error in both in- and outgoing flow is calculated. The Square is therefore used in the simulations. The interesting is still mainly the flow tendencies inside the monopile. The flow of the sea water inside the chamber is compared between the original model with sea, and the Square design model, to see if they are similar. The two are compared based on the sea water's location inside the chamber after 20 s. Fig. 3.18 and Fig. 3.19 shows the volume fraction of the sea water and chamber water inside the chamber.

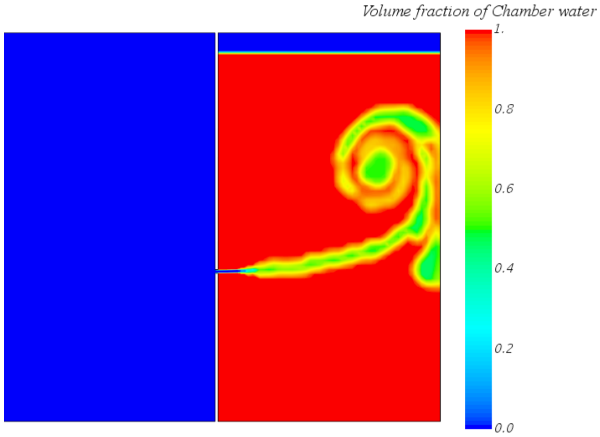

Fig. 3.18: The location of the sea water after 20 s in the original model with sea.

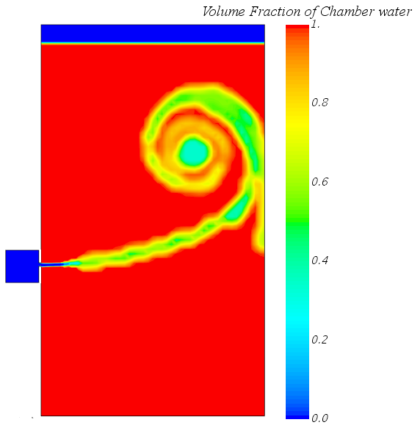

Fig. 3.19: The location of the sea water after 20 s in Square design model.

The two figures shows similar tendency with both having a dominance of an upwards going flow, as the flow is influenced by the back wall. The upwards going tendency is due to the water being in a closed cylinder and therefore flows to where there is less resistance, which is at the water surface. The Square design shows a slightly steeper climb than on Fig. 3.18. This variation is a result of the time the original model uses to initiate the velocity through the inlet, as can be seen during the first second on Fig. 3.7. The error is chosen to be acceptable to avoid the simulation with the sea.

The miniature sea results in some errors in small wave periods, as the boundary is not located right at the hole. This can be a problem with the wave condition, as the volume of sea water from each period is less than the miniature sea volume. Therefore the flow tendencies with a velocity inlet is compared to the original. These are shown in Fig. 3.20 and Fig. 3.21.

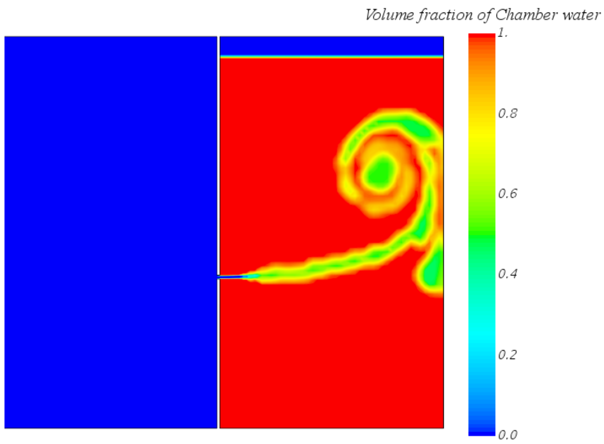

Fig. 3.20: The location of the sea water after 20 s in the original model with the sea.

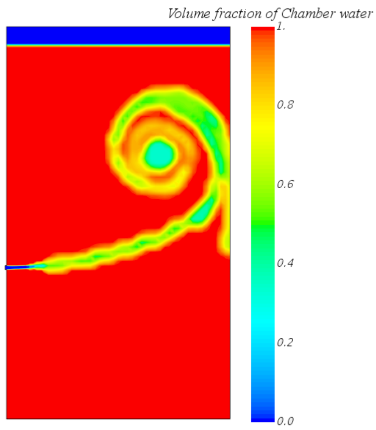

Fig. 3.21: The location of the sea water after 20 s without the sea.

The flow from the velocity inlet shows a flow equal to the Square design. The low effect on the flow tendencies is due to the flow still being symmetric in the inlet of the original, just not completely uniformed, and the mean velocity is equal to each other. The effect from the velocity profile therefore shows to be limited, but the flow is instead dominated by the mean velocity at the inlet. As this only investigates a short period of the flow, the effect could raise over longer durations and multiple wave/tide periods. For the tides the flow volume through the inlet for each period is large compared to the miniature sea due to the period of 12 h, thus the effect of the miniature sea volume is limited and is used for the calculations with tides. For the waves the miniature sea is removed, as the flow volume through the inlet is small for each period, and the effect of the miniature sea volume is large.

3.3 Multiple inlets

If multiple inlets are located along the monopile, then based on the energy equation, an equal flow through each inlet is obtained. Then the pressure difference at each inlet is equal, when only the hydrostatic pressure is introduced. To validate this claim, a model with two inlets, including the sea, is simulated, based on the boundary conditions shown in Fig. 3.22.

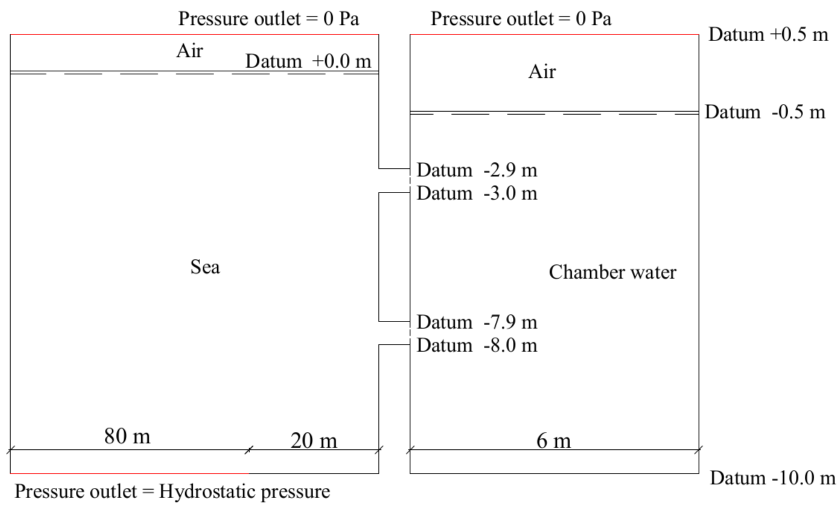

Fig. 3.22: Boundary conditions for the model of 2 inlets.

The mean velocity through the inlets is measured and shown in Fig. 3.23. Based on this, the flows through the inlets are shown to be similar, only with small variations, due to some instability in the flow. This is expected to be from the pressure boundary condition at the seabed.

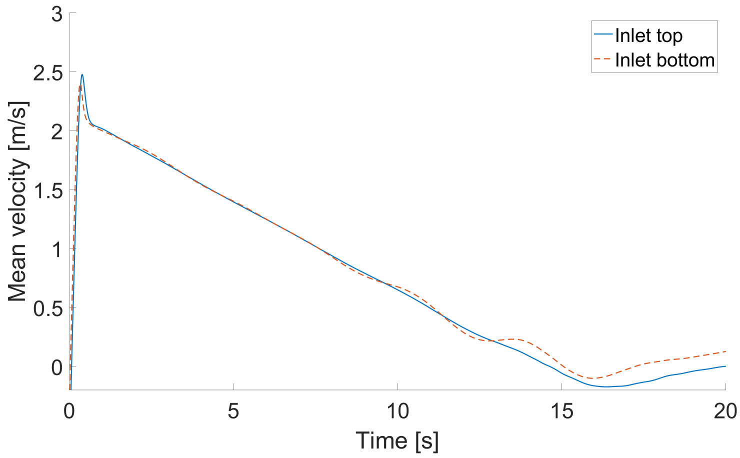

Fig. 3.23: Velocity through each of the two inlet.

As the mean velocity of the two inlets is equal to each other, the location of the inlet has no influence on the flow through them, when the flow is only influenced by hydrostatic pressure. For the waves, the pressure is not only influenced by the hydrostatic pressure, so the velocity varies depending on its location. This location dependence is calculated in Chap. 4.

3.4 Inlet size

The size of the inlet affects the flow through the holes, both by the cross area and the loss coefficients. As it was described in Sec. 3.1 the inlet is too short for the flow to fully develop before exiting the inlet. This resulted in the loss coefficient for the exit being different from the standard. The simulation shows the loss coefficient at the exit with a hole diameter of 0.1 m is 1.6, as calculated in Eq. (3.5). To determine the effect of the hole diameter on the loss coefficient, simulations are performed with different hole diameters. The tested inlet diameters and the resulting total loss coefficients are shown in Tab. 3.3.

Inlet diameter	Loss coefficient at exit	Total loss coefficient
0.05 m	1.5	2.0
0.1 m	1.6	2.1
0.2 m	1.7	2.2

Tab. 3.3: Loss coefficient for the inlet depending on its size.

The results show a lower loss coefficient, with a smaller inlet. This is due to the flow being more influenced by the sides, as the ratio between the inlet size and length is smaller. This results in a more developed flow in the inlet. These loss coefficients are used further in this project for the different inlet sizes.

4 Pressure generated by the sea conditions

The flow generated by the three sea conditions, tides, waves and currents, is based on the difference between the internal and external pressure at the inlets. With the energy equation, validated in Chap. 3, the velocity of the flow through the inlets is calculated. The pressure for the three sea conditions is calculated in this chapter.

4.1 Tide pressure

The tide is a slow changing process with two domination periods during 24 h. The tide is based on the simplified water level change, defined in Sec. 2.3 on page 9, and only include the semi-diurnal waves. Due to the slow change in the surface elevation, the particle velocity and particle acceleration of the tidal waves are approximated to 0 m/s^2, and therefore induces no added force from drag or inertia on the structure. The flow is instead driven only by the pressure difference occurring due to difference in external and internal water level. The pressure is calculated as the hydrostatic pressure. For a short wave period, the pressure generated by the changing surface elevation would, depend on the depth. For the tidal wave, the wave period are 12 h, with which the wave pressure can develop over the full depth, and the pressure is merely the hydrostatic pressure at the current water level, as shown i Eq. (4.1).

$$p_0 = -\gamma\,(\eta + z) \tag{4.1}$$

Where:

p_0	Hydrostatic pressure
γ	Specific weight
η	Surface elevation
z	Vertical coordinate, with zero at MWL.

The hydrostatic pressure is shown at depth -5 m over a tidal period in Fig. 4.1. In Fig. 4.2 the pressure is shown over depth with surface elevation at $\eta = 0$ m.

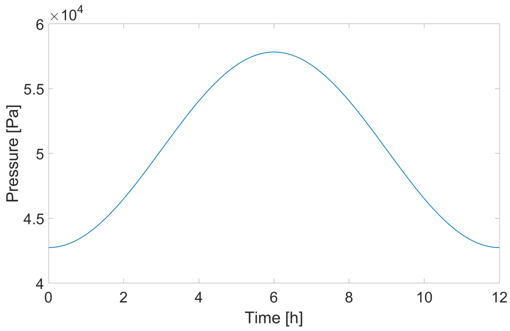

Fig. 4.1: Pressure at depth -5 m over a tidal period.

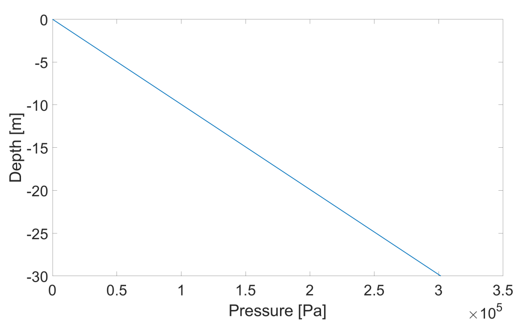

Fig. 4.2: Pressure over the depth, with the surface elevation at $\eta = 0$ m.

The tide pressure can then be compared with the internal pressure to calculate the mean velocity through the holes.

4.2 Wave pressure

The pressure generated by the waves is a combination of the hydrostatic pressure, the wave pressure and the disturbance pressure by the monopile located in the flow. The hydrostatic pressure is calculated with Eq. (4.2).

$$p_{hyd} = -\gamma z \tag{4.2}$$

Where:

p_{hyd} Hydrostatic pressure

The wave and disturbance pressure is calculated together by the use of potential theory for flow around a cylinder. The theory is based on combining the undisturbed flow with a scatted flow, which occurs from the monopile. The undisturbed and scattered flow results in a velocity potential given as:

$$\varphi_0 = \frac{a\,g}{\omega}\,\frac{\cosh(k\,(z+h))}{\cosh(k\,d)}\,\cos(\omega\,t-k\,x) \;=\; g_0\,\cos(\omega\,t-k\,x) \tag{4.3}$$

$$\varphi_d = \frac{R^2}{r^2}\,(\phi_0 - g_0\,\cos(\omega\,t)) \tag{4.4}$$

Where:

φ_0 Velocity potential for undisturbed flow
φ_d Velocity potential for disturbed flow
a Wave amplitude
g Gravity
ω Angular frequency, $2\pi/T$
k Angular wave number, $2\pi/L$
x Horizontal coordinate
R Radius of monopile.

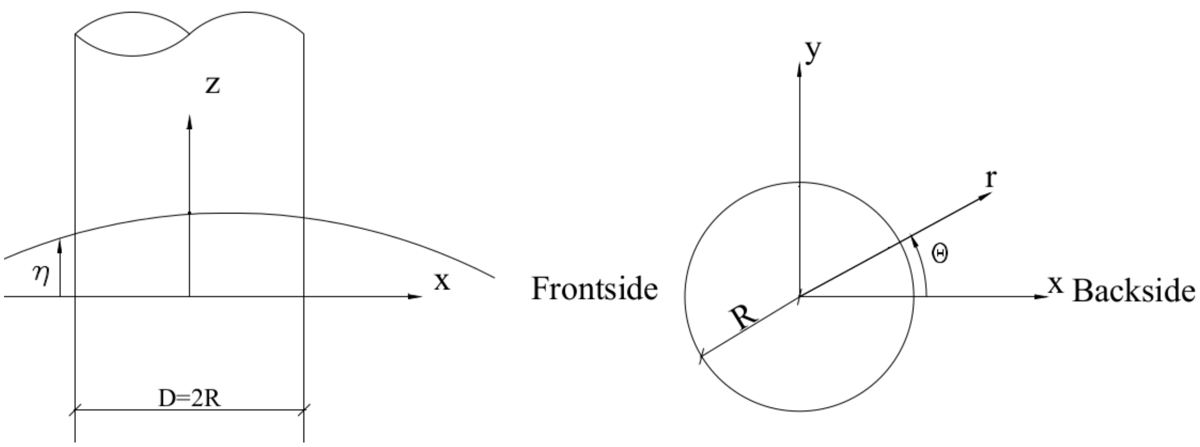

Fig. 4.3: Factors for the wave and the monopile.

The complete velocity potential is a sum of the undisturbed and disturbed potential, resulting in:

$$\varphi = \varphi_0 + \varphi_d = g_0\,\cos(\omega\,t-k\,x) + \frac{R^2}{r^2}\,g_0\,(\cos(\omega\,t-k\,x) - \cos(\omega\,t)) \tag{4.5}$$

The velocity potential can be simplified by determining the size of the cylinder as being small relative to the wave length, and that only the pressure on the monopile surface is of interest. The simplification is shown in App. C. The simplified velocity potential results in Eq. (4.6).

$$\varphi = g_0 \left(\cos(\omega\, t) + \sin(\omega\, t)\, k\, r\, \cos(\theta) \left(1 + \frac{R^2}{r^2}\right)\right) \tag{4.6}$$

This equation can be verified by the Laplace partial differential equation. The boundary conditions states no disturbance far away from the monopile and no flow through the monopile itself. These and the Laplace equation are verified in App. C. With the equation for the velocity potential, the pressure around the monopile is found by the linearised Bernoulli equation:

$$p_w = -\rho \frac{\partial\, \varphi}{\partial\, t} = -\rho\, g_0 \left(-\omega\, \sin(\omega\, t) + \omega\, \cos(\omega\, t)\, k\, r\, \cos(\theta) \left(1 + \frac{R^2}{r^2}\right)\right) \tag{4.7}$$

Where:

p_w Wave pressure, depending on depth, location and time

The interest is at the surface of the monopile, where $r = R$, resulting in the pressure only depending on the depth, angle and time step of the waves, as shown in Eq. (4.8).

$$p_w(z,t,\theta) = -\rho \frac{\partial\, \varphi}{\partial\, t} = -\rho\, g_0\, (-\omega\, \sin(\omega\, t) + \omega\, \cos(\omega\, t)\, 2\, k\, r\, \cos(\theta))) \tag{4.8}$$

The total pressure is found by adding the hydrostatic pressure to the wave pressure as in Eq. (4.9).

$$p(z,t,\theta) = p_{hyd}(z) + p_w(z,t,\theta) \tag{4.9}$$

Where:

p Total pressure at depth, depending on location and time.

The total pressure around the monopile at depth -5 m for 4 time instances is shown in Fig. 4.5.

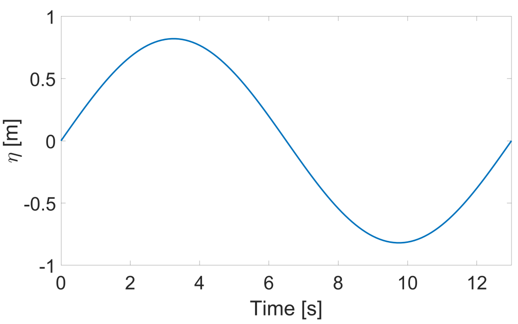

Fig. 4.4: Surface elevation relative to time.

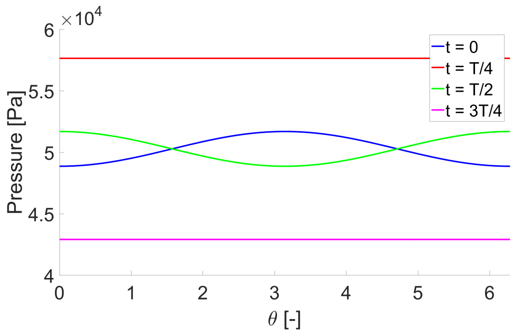

Fig. 4.5: Wave and hydrostatic pressure summarized around the monopile at depth -5 m. T equal to 13 s.

The pressure is dominated by the hydrostatic pressure, as this raises linearly with the depth. Conversely the wave pressure, induced from the inertia force, decreases with depth, due to lower acceleration of the particles at larger depths. The flow is calculated with potential theory, therefore no drag forces are included. The effect of the wave pressure relative to the depth is shown in Fig. 4.6. The wave pressure is shown at time, $t = 0$ s for both the front and rear.

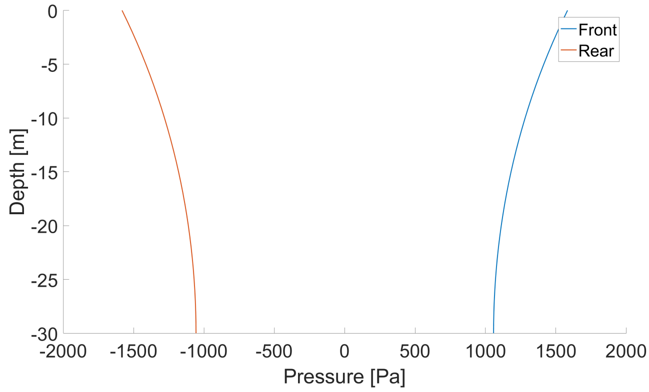

Fig. 4.6: The wave induced pressure on the front and rear of the monopile at t = 0 s.

The wave pressure is calculated at t = 0 s, as the surface elevation at this time is equal to the mean water level, and the acceleration of the flow is directly horizontal. thus only the inertia forces acts on the pile surface. The inertia forces are created by the acceleration of the particles towards or from the monopile. As the particles accelerates towards the monopile, the added pressure is created, as it is seen on the front, and negative on the rear, as the acceleration is away from the rear surface at t = 0 s. On the sides of the monopile the acceleration is tangent with the surface, resulting in no increase or decrease in the pressure. At Fig. 4.5 the pressure is constant around the monopile at $t = T/2$ and $t = 3\,T/2$. This is due to the acceleration of the particles only being in the z-direction at wave crest and trough. Due to a low maximum particle velocity, the Keulengan-Carpenter number is below 5. This results in the flow around the cylinder is not separating from the monopile and creating a wake behind it.This also explains the pressure in Fig. 4.6 being opposites of each other. The Keulengan-Carpenter number is defined as:

$$KC = \frac{U_m\,T}{D} \tag{4.10}$$

Where:

KC	Keulengan-Carpenter number
U_m	Maximum particle velocity
T	Wave period
D	Monopile diameter

The total pressure calculated can then be used for the pressure calculation, when defining the flow velocity through the holes in the monopile.

4.3 Current pressure

The pressure generated by current is from the drag on the structure. The current velocity variates close to the bottom due to friction along the bottom, which creates a boundary layer and varies at the surface, due to surface distortion. As the holes are only located away from both bottom and surface, due to the limitations in Sec. 2.2 on page 8, the change in depth is insignificantly small and the current velocity is calculated constant. The pressure is calculated based on potential theory, but including the D'Alembert Paradox to define the pressure on the rear. For the current, a steady uniformed flow is estimated, resulting in no acceleration. The velocity potential for the undisturbed and disturbed flow is shown in respectively Eq. (4.11) and (4.12).

$$\varphi_0 = U\,r\,\cos(\theta) \tag{4.11}$$

$$\varphi_d = U \, \frac{R^2}{r} \, \cos(\theta) \tag{4.12}$$

Where:

U Current velocity

The combined velocity potential for the flow results in:

$$\varphi = \varphi_0 + \varphi_d = U \, \cos(\theta) \, \left(r + \frac{R^2}{r}\right) \tag{4.13}$$

The velocity potential can, as the wave, be validated by the Laplace equation and the boundary conditions by showing that φ is equal to φ_0 far from the cylinder and that no flow is going through the cylinder. This is shown in App. C. The surface pressure is calculated based on the Bernoulli equation, given in Eq. (4.14). As the flow is independent of the time, it can be reduced to:

$$\frac{p_d}{\rho} + \frac{1}{2} \, u_\theta^2 + \frac{\partial \, \varphi}{\partial \, t} = \text{Constant} \;\Rightarrow\; \frac{p_d}{\rho} + \frac{1}{2} \, u_\theta^2 = \text{Constant} \tag{4.14}$$

Where:

p_d Pressure from disturbance
ρ Density of the water
u_θ Velocity tangent with the surface

To calculate Bernoulli's equation the velocity, u_θ, is needed, which is found from the velocity potential. The interesting part is the pressure at the surface, therefore the velocity tangent to the surface can be reduced to:

$$u_\theta = \frac{1}{r} \, \frac{\partial \, \varphi}{\partial \, \theta} \;\Rightarrow\; u_\theta = -U \, \sin(\theta) \, \left(1 + \frac{R^2}{r^2}\right) \;\Rightarrow\; u_\theta(r = R) = -2 \, U \, \sin(\theta) \tag{4.15}$$

As there is no disturbance far from the surface, meaning p_d = 0, the constant in Eq. (4.14) can be defined as:

$$\text{Constant} = \frac{1}{2} \, U^2$$

The pressure at the surface can then be defined as:

$$p_d(r = R) = \frac{1}{2} \, \rho \, U^2 \, \left(1 - 4 \, \sin^2(\theta)\right) \tag{4.16}$$

This results in a pressure distribution around the monopile as shown on Fig. 4.7.

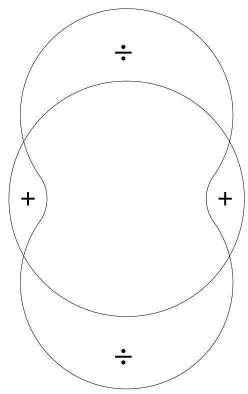

Fig. 4.7: Pressure around the monopile from current based on potential theory.

The total force on the monopile equals to 0, as the pressure on the front and rear is equal each other. This means the cylinder is unaffected by the steady current, which doesn't correspond to reality. In reality a suction is created on the rear of the cylinder due to creation of a wake behind, as the flow separates from the cylinder. The separation is created due to viscosity effects in real fluids. The evaluation of the pressure on the front half of the cylinder is assumed to be correct, as the separation occurs at $\theta = \pm\pi$. On the rear a constant pressure is estimated, based on the velocity at the separation points. The correct pressure is shown in Fig. 4.8 and given in Eq. (4.17).

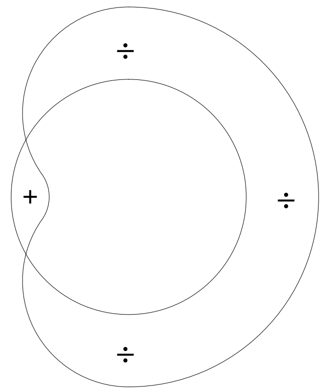

Fig. 4.8: Correct pressure from current including suction on the rear.

$$p_d = \begin{cases} -\frac{3}{2} U^2 \rho & \text{If } \theta < \pm\pi \\ \frac{1}{2} \rho U^2 \left(1 - 4 \sin^2(\theta)\right) & \text{Otherwise} \end{cases} \tag{4.17}$$

The current pressure is, as well as with tide and wave, used to calculate the mean velocity through the holes in the monopile.

Part II

2-D models

In this part the monopile is analysed in two-dimensional models. The analyses includes mesh convergence analyse and an initial analysis of the three cases, tides, waves and currents. The analysis looks on the effects of the inlet, in form of number, size and location and the effects from the seasons on the water density. The part ends with a conclusion of the effects and the work forward in three-dimensional models.

5 | Initial evaluation

As a simplification the monopile is first analysed in two-dimensional simulations. The two-dimensional analysis is used to determine the effect of numbers, location and size of inlets, as well as the density variation of the water, to improve the solution. Simplifying the model from three to two-dimensions requires some significant simplifications. The simplification reduces the cylinder to a chamber and the hole to a crack, as seen on Fig. 5.1. This simplification result in a different ratio between the hole area and cylinder volume in three-dimensions, compared with the ratio between the crack height and the area of the monopile chamber in two-dimensions. To compensate for the different ratios, some different simplifications can be done on:

- Water level change
- Crack height
- Wave period
- Mass flow
- Monopile width

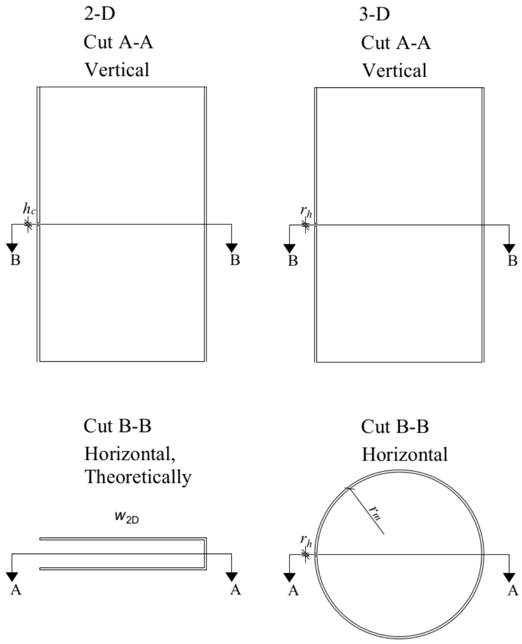

Fig. 5.1: The difference between a two- and three dimensional model.

As the exchange rate is the interesting factor, the water level change is Required to be equal in both two- and three-dimensions. This results in the same percentage of sea water is induced at each cycle. For the sea water percent to remain equal, the monopile height is kept equal in both dimensions. To keep a similar flow profile at the inlets, the crack height is kept equal to the diameter of the hole. For the flow profile to remain similar, the same velocity variation is required, including the same maximum and minimums velocity. If the same mass flow is kept between two and three-dimension, the water level change is larger in two-dimension due to the different ratio. To compensate for the different ratio, the wave period can be reduced, or the width of the monopile can be increased. The relationship between two and three-dimension is based on ratio between the volume in the monopile, the inlet area and the period:

$$\frac{\text{Surface length}}{\text{Crack height} \cdot \text{2D period}} = \frac{\text{Surface area}}{\text{Hole area} \cdot \text{3D period}} \quad \Rightarrow \quad \frac{w_{2D}}{h_c\, n\, T_{2D}} = \frac{r_m^2\, \pi}{r_h^2\, \pi\, n\, T_{3D}} \quad \Rightarrow$$

$$\frac{w_{2D}}{T_{2D}} = \frac{r_m^2\, h_c\, n}{r_h^2\, n\, T_{3D}}$$

This results in the width and wave period is depending on the radius/height of the hole/crack and the radius/width of the monopile/chamber. The width and wave period in two-dimensions is, as an example, calculated for a hole diameter and crack height of 0.1 m and a monopile diameter of 6 m. It is calculated here for the tidal case, which is used for a convergence analysis later. The simplification can either be a change of the chamber width in two-dimensions, in this calculation the wave period is kept constant at 12 h. Else a change of the wave period can be used, where instead the width of the chamber is kept unchanged at 6 meter in two-dimensions. These two simplifications are calculated in Eq. (5.1).

$$w_{2D} = \frac{r_m^2\, h_c\, T_{p2D}}{r_h^2\, T_{p3D}} = 360\,\text{m} \qquad\qquad T_{2D} = \frac{w_{2D}\, r_h^2\, T_{3D}}{h_c\, r_m^2} = 0.2\,\text{h} \tag{5.1}$$

Where:

r_m	Radius of monopile
r_h	Radius of hole
h_c	Height of crack
n	Numbers of holes
T_{2D}	Wave period in two-dimension
T_{3D}	Wave period in three-dimension

With the extended width of the chamber, any effect of the back wall greatly is reduces. The effect of the back wall is expected to have a large effect on the mixing inside the monopile. Therefore, the width is kept constant on 6 m. This results in a reduction of the wave period from 12 h to 12 min instead. The reduced wave period is dependent on the hole diameter, so is only 12 min, when a hole diameter of 0.1 m is used. The problem occurring from the reduced wave period is that as the velocity is unchanged, the distance the flow travels inside the monopile is reduced. As a result of this, expectantly the exchange rate will decrease, as a higher percentage of the sea water will be located at the inlet. It is therefore believed this method results in a underestimated exchange rate and a safe estimate of the effect on the pH-value. As the model is reduced to two-dimensions, the back wall is change from curved to a straight wall. When the flow in three-dimensions interacts with the curved back wall, the flow can both travel vertical or return back along the curve surface in the horizontal plane. In two-dimensions the flow can only travel vertical, resulting in a larger vertical flow, that easier can achieve a complete exchange.

The design of the monopile in two-dimensions is shown with one crack in Fig. 5.3. The model is with a crack height of 0.1 m, and the crack is located in the center of the allowed area. Based on the results found in Chap. 3 on page 17, the sea is reduced to a 1x1 m miniature sea outside the inlet, when calculating on the tidal condition. For the two other conditions the miniature sea is avoided, and only the inlet is modelled. The simplified water level is shown in Fig. 5.2, where the wave period is reduce to 12 min.

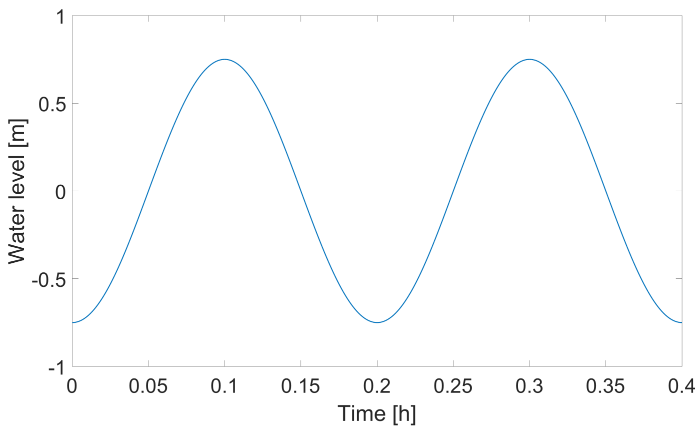

Fig. 5.2: External surface elevation for two-dimensional case.
Wave period reduced from 12 h to 12 min.

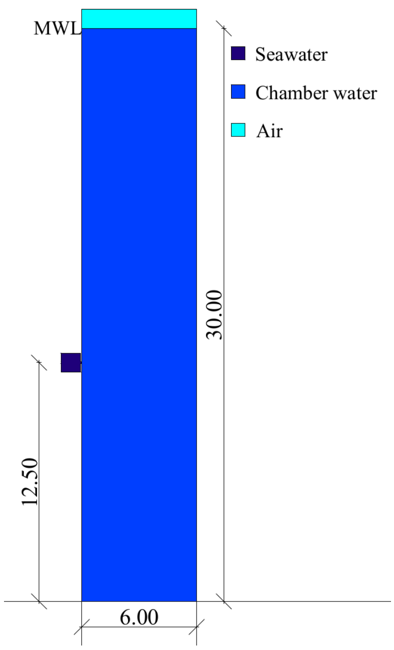

Fig. 5.3: The two-dimensional design of the monopile with one inlet.
Measurements are in m.

Based on the design of the monopile in two-dimensions, the exchange rate of the enclosed water is analysed. Initially an analysis of each of the three sea conditions are performed, These are performed with a constant water density of 1025 kg/m^3, the seasonal effects are first introduced in the optimisation and three-dimensions.

The boundary conditions is similar to the conditions discussed in Sec. 3.2 on page 19, and are shown on Draw. 01. The inlet flow is calculated as a mass flow from the energy equation. The Energy equation, at Eq. (3.1), calculates the velocity, and the mass flow is then calculated with Eq. (3.6). The velocity through the inlet is calculated and is shown in Fig. 5.4. The initial internal water level is equal to the external initial water level, and these are shown in Fig. 5.4.

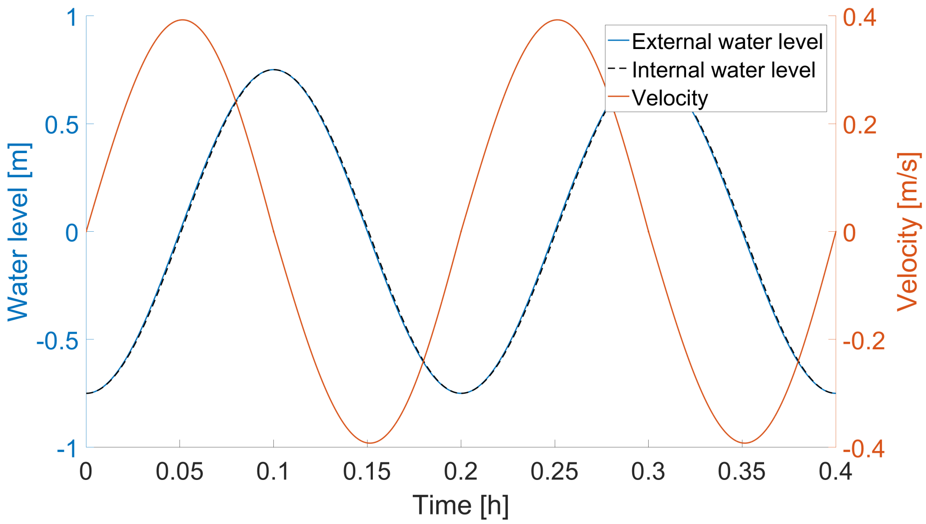

Fig. 5.4: Internal and external water level during the first 2 cycles relating to the left y-axis and the velocity through the inlet relating to the right y-axis.

Due to the long wave period the internal water level follows close to the external. The largest difference is found at mean water level, where the external surface elevation change is steepest, which also can be seen on the velocity as it is maximum at $t = T/4$ and $3\,T/4$. For the analysis of the exchange to be possible, the enclosed water and the sea water need to be individually identified from each other. The models uses the Eulerian multiphase model, which enable the identification of multiple phases in the same model independent of each other. The three main phases used are; sea water, chamber water and air. Further, the model is created as an unsteady state, as the flow vary over the tidal period, and the percentage of sea water inside the monopile changes as well over time. The turbulence in the flow is calculated with the $k-\varepsilon$ turbulence model, which is validated by experimental data in Chap. 8 on page 65.

As the model is designed, the calculation depends on the design and the fineness of the mesh. The mesh design and the fineness presented is in the following sections.

5.1 Mesh design

The design of a mesh is based on creating a fine-graded mesh at the location where large changes occur, and coarse-graded mesh, where only minor changes occur. The mesh design of the two-dimensional chamber with one crack is shown in Fig. 5.5. The mesh is constructed by Trimmed mesh elements.

The large changes is located at the inlet, as the velocity is largest in the inlet and streaming into a close to stationary water column. This is generating large velocity gradients. To achieve an accurate water level, the mesh is graded finer there as well. The extra fineness at the water surface is based on estimating the correct water level and the split between the water phases and the air phase. Therefore, the changes are primarily in the height. To reduce the element count the surface elements are anisotropic, so only reduced in the height as shown on Fig. 5.5. As the goal is the exchange of the enclosed water, it is important to identify the location of the chamber water and sea water independent of each other in the entirety of the chamber area. As the goal is to exchange the water of the entire water column, no part of the water column is without interest,

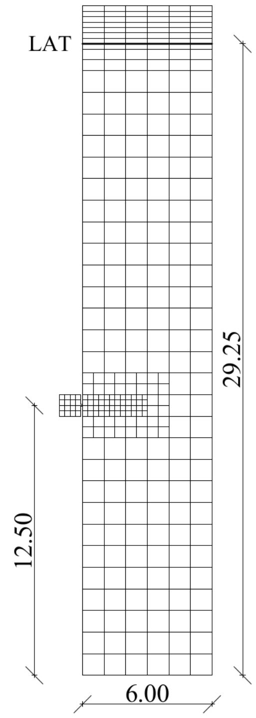

Fig. 5.5: mesh design for the two-dimensional models with fine-graded mesh around inlet and at water surface. Base size equal to 1 m.

5.2 Initial tidal exchange

An initial course model is simulated to determine the general flow and a method of determining the exchange rate of the enclosed water. Following this, a convergence analysis of the fineness of the mesh is created based on the exchange rate. The tides and waves are calculated with constant periods, therefore the flow of each period can be expected to be identical, independent of the amount of periods into the flow is measured. One way to determine the exchange is to simulate the model until all the enclosed water is exchanged, or at least no more is being exchanged. This would result in very long simulations, therefore it is preferable to fit a function to the exchange of a couple of periods, and thereby calculate the total time of the exchange. To be able to fit a function, the flow inside the monopile needs to be independent of which period is measured. To validate this, a model is created, where the location of the sea water from each period independently is compared. This model is created with seven phases. Of the seven phases, five of them are sea water and the remaining two are chamber water and air. The five phases of sea water is created to independently measure the results from each of the first five wave periods. The water flowing in through the inlet is therefore changes depending on the period. In the first period the phase entering the model, through the inlet, is sea water 1, and during the second period it is sea water 2 and so on. A surface plot of the flow inside the monopile for each of the five sea water phases is shown in Fig. 5.6. They are compared after each sea water phase has been inside the monopile for one period. This means the surface plot of sea water 1 is taken after the first period, sea water 2 is taken after the second period and so on. The model is created with a base size of the mesh of 0.08 m, which is the later converged fineness of the mesh size.

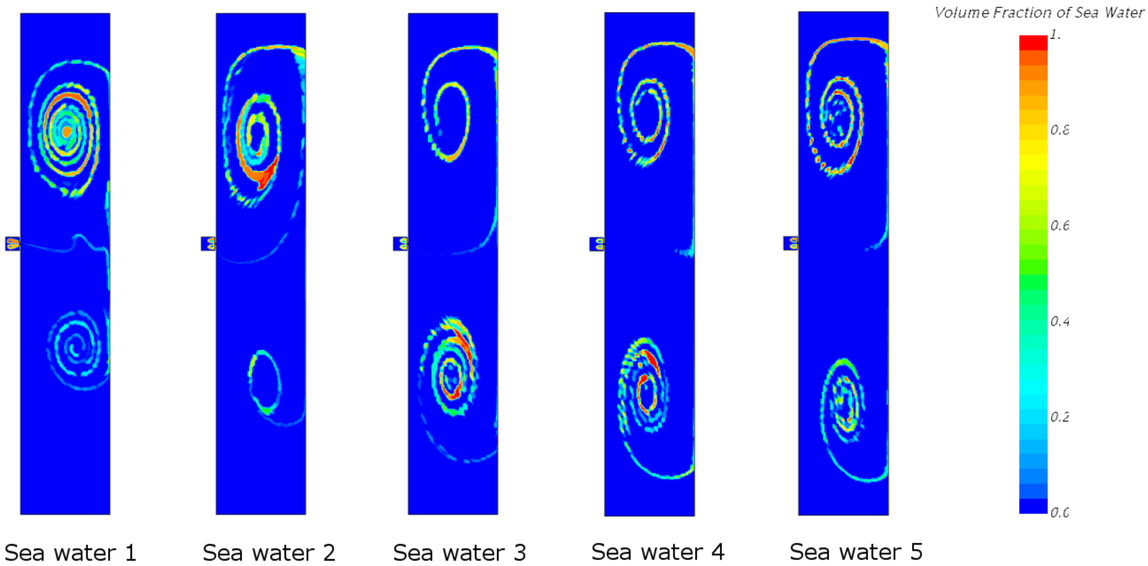

Fig. 5.6: Location of each sea water phase after it has been in the chamber for one period.

From Fig. 5.6 it is shown that they all have the same main flow, with splitting at the back wall and the larger part flows toward the surface, as it was also seen in the validation. The difference between sea water 1 to sea water 5 looks to be lowering the further into the number of periods the comparison is made. Therefore, difference is smaller between sea water 4 and 5, rather than between sea water 1 and 2. This is because sea water 1 travels into a completely stationary water column. The later periods are flowing in to a water column, where the velocity and turbulence is affected by the previous periods. The result therefore becomes more and more alike as the periods passes. Surface plots of the five sea water phases after two periods each are shown in App. D on Fig. D.1. These show similar results, that the first couple of periods are used to accelerate the flow inside the monopile. To shown the exchange of the water are independent on the periods, the percentage of the sea water 2 to 5 remaining inside the chamber are compared in Fig. 5.7. The percentage of the sea water phases are compared over 2 period, meaning for sea water 2's period 1 and 2 in the figure, are period 2 and 3 in model time, and for sea water 3 is used period 3 and 4 in model time. This gives a exact comparison between the phases. In the beginning of the period there are no increase. This is due to the miniature sea. As the inlet boundary is at the edge of the miniature sea and not at the chamber inlet, the sea water has up to a meter to travel before entering the monopile. The volume of the miniature sea is small compared the total exchanged, and is therefore accepted for the tide. For the wave this volume is significantly compared to the flow through the inlet during each period, and therefore is not included here.

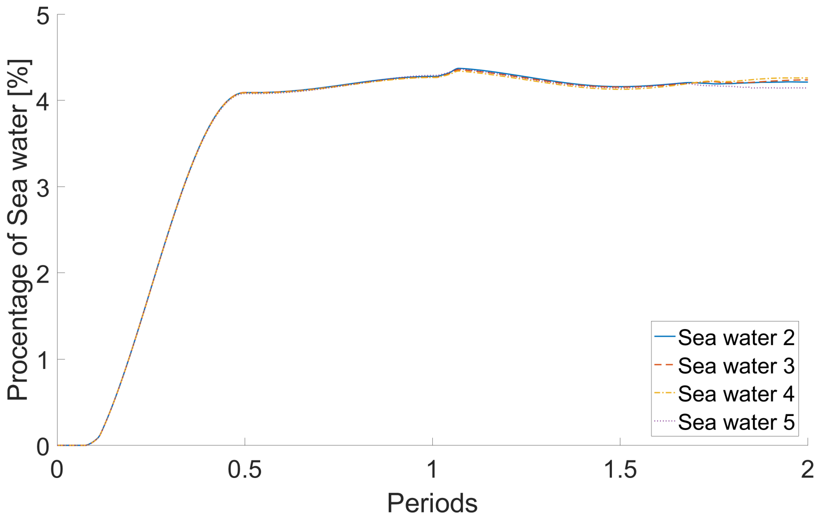

Fig. 5.7: Percent of the five phases remaining inside the monopile over their first two periods.

In Fig. 5.7 the percentage are equal over their first two periods, which support that the exchange is constant across each cycle. The small increase at the beginning of the second cycle is due to some sea water from the previous period remaining in the miniature sea.

The more phases included in the model the more calculations are needed in the simulation, and therefore the simulation time increases. To include a phase of sea water for each period simulated would require to much processing power or time, so instead only the three main phases are used. As there is only one sea water phase, there is no direct way of determining how much of the sea water that are from each period. As the pH-value of the water decreases over time, the amount of sea water from each period remaining inside the monopile needs to be known. Knowing that the flow of each period is alike, the amount remaining from each period can be determined. This can be determined based on the percentage remaining of enclosed water inside the monopile after each period. To determine this a new model is simulated, and the percentage of the enclosed water remaining in the chamber is measured. This model uses a base size of 1 m, and the water level and inlet mesh has a size of 25 % of the base size. The percentage of enclosed water remaining in the monopile depending on the numbers of periods is shown in Fig. 5.8. The remaining enclosed water percent is calculated based on the measured volume of sea water and chamber water inside the monopile:

$$mono = \frac{V_{F,chamber}}{V_{F,chamber} + V_{F,sea}} \tag{5.2}$$

Where:

$mono$	Percent of chamber/enclosed water remaining in the chamber
$V_{F,}$	Fraction of the phase present inside the chamber

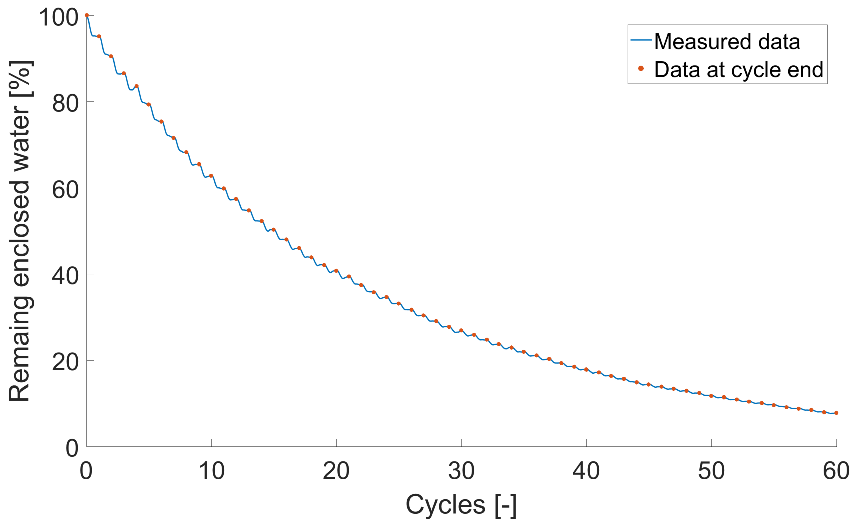

Fig. 5.8: Remaining enclosed water depending of numbers of cycles.

Fig. 5.8 show that the rate of change looks to be exponential decreasing. The exponential decrease is because more and more sea water, from the previous periods, exits the monopile instead of enclosed water. By estimating this decrease change, the amount of water from each period can be determined, and used for calculating the correct mean pH-value of the water. As well it can be seen that each cycle is divided into two parts, one flowing in and one flowing out of the monopile. This is seen as the first part has a drastic decrease in the enclosed water percentage and the second part has a linear or slight increase in the percent of enclosed water remaining. The percentage decreases in the first part as the flow in is pure sea water. At the second part the percentage remains stable if the flow out is purely enclosed water. It is constant because it equalises with the water level decreasing to low tide again. The percentage is measured based on the current surface elevation. The increase of the percentage is dependent on the amount of sea water returning out of the monopile again. To avoid simulating until the exchange is complete, two different functions are fitted to the measurements. The functions are fitted to the "Data at cycle end" on Fig. 5.9, where the surface elevation is at low tide. This result in an equivalent surface elevation at ever point. The fit is done to real values rather than percent. The fitted functions are compared base on the R-square value of the error.

The first equation is a exponential decreasing function. The equation fits well as it take the increasing amount of sea water inside the monopile into account. The exponential function is based on the Remaining coefficient, which describes the amount of the remaining enclosed water, which remains inside the monopile after a period.

$$mono = R^C \tag{5.3}$$

Where:

R	Remaining coefficient
C	Cycle number

Eq. (5.3) describes the amount of enclosed water remaining based on the numbers of cycles, that has passed. To describe it, then a remaining coefficient of 0.95 means that after one period 95 % of the enclosed water remains in the monopile, and after two periods 95 % of the remaining 95 % remains. Therefore 90.25 % remains. The 0.25 % less that were exchanged in the second period is sea water from the previous periods. By knowing 0.25 % sea water from the previous cycle left the monopile, the amount of sea water remaining from cycle 1 is known. Therefore the amount of sea water and the time it has been in the chamber can be used to determine, without including multiple extra phases to identify each period from each other. This is used in calculating the mean pH-value of the water in Eq. (5.6).

Eq. (5.3) estimates that a complete exchange of the monopile will occur. As this is not certainty, a factor for the amount of the enclosed water that is not being exchanged, is introduced. This factor tells if the enclosed water will be completely exchange, and the sea water reaches around in the entire chamber. Eq. (5.3) is with that, expanded to Eq. (5.4).

$$mono = (1 - A_e)\, R^C + A_e \tag{5.4}$$

Where:

A_e Amount of enclosed water not being exchanged

The fitted equation and R-square values are shown on Tab. 5.1 and the functions are shown in Fig. 5.9.

	Equation coefficients		R-square
Exponential function	R 9.567×10^{-1}		9.986×10^{-1}
Expanded exponential function	R 9.539×10^{-1}	A_e 2.732×10^{-2}	9.996×10^{-1}

Tab. 5.1: Equation coefficients and R-square for the two fitted equations.

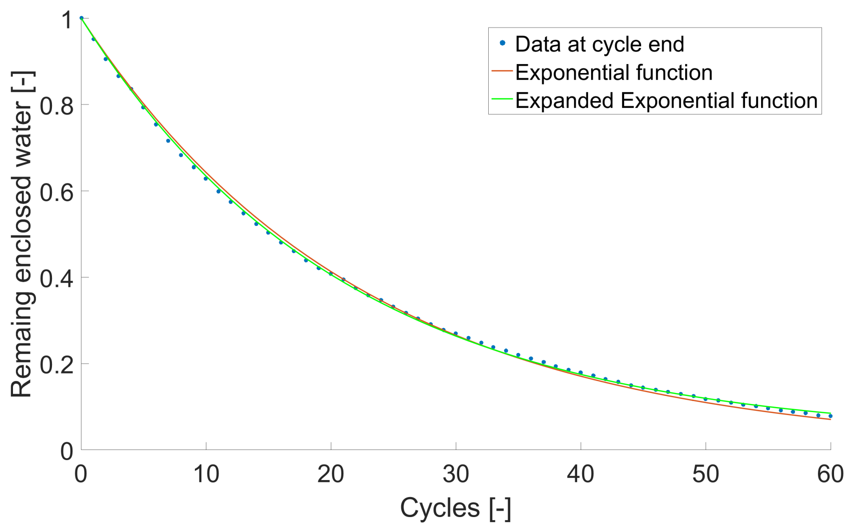

Fig. 5.9: The two equations fitted to the measured data.

Based on the fitting, the best is the "expanded exponential function", where the increase in sea water inside the monopile and the amount of enclosed water not being exchanged are included in the equation. The two exponential equations shows only little difference as roughly 98 % of the enclosed water is exchanged. To show that the sea water reaches around in the entire monopile in this model a surface plot from the simulation is shown in Fig. 5.10.

With the equation for the remaining enclosed water fitted, the exchange rate is estimated. If a stable state of the exchange rate is reach, the amount of each tide wave that remain inside the monopile is constant. This can be calculated with Eq. (5.5), with the equation coefficient fitted.

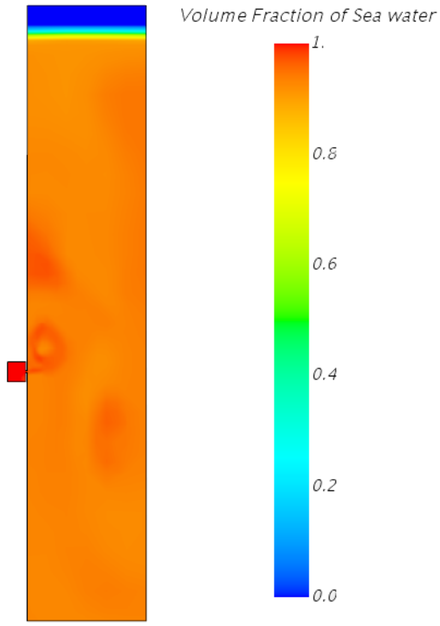

Fig. 5.10: Surface plot of the volume fraction of sea water inside the monopile after 60 cycles.

$$H_{s,in} = (1-R)\left((h+\eta)\left(1-A_e\right)\right) \tag{5.5}$$

Where:

$H_{s,in}$ Exchanged water height

As the measurement are fitted to wave trough, the value of $(h+\eta)$ is 29.25 m. The exchanged water height then result in 1.31 m, which is 87.7 % of the sea water that entered the monopile. The fit is based on 60 cycles. To avoid simulating 60 cycles the fit is performed depending on the numbers of cycles used, and the exchanged water height is shown in Fig. 5.11.

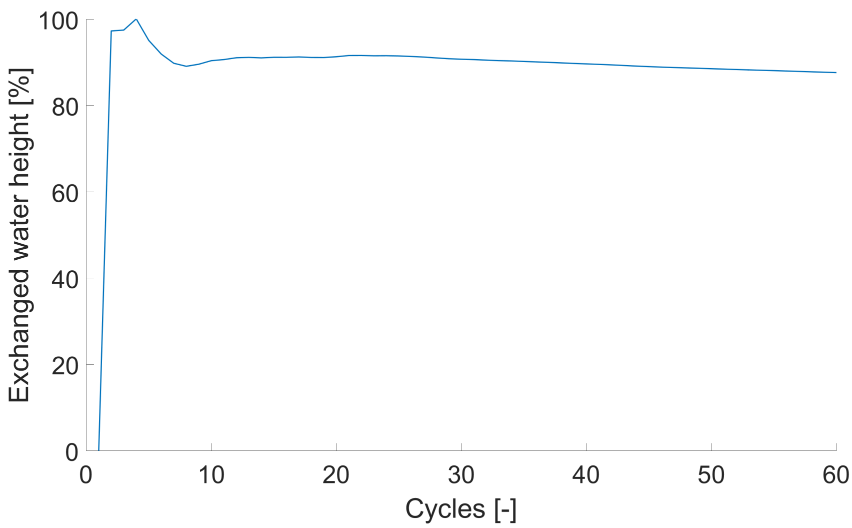

Fig. 5.11: Exchanged water percent of the internal water level variation.

As seen on Fig. 5.11, the value shows to stabilising after just around 10 cycles and varies below ± 0.5 %. The simulations can therefore be done for fewer periods to reduce simulation time and still gain accurate results. An acceptable error is determined to be that four consecutive cycles needs to have a difference of below ± 0.5 % of their mean value. With this criteria the exchange water stabilises on an exchange percent of 90 % after only 13 cycles. This gives a definitive way of calculating the exchange rate from the simulated data.

5.2.1 Mesh convergence

With the definitive way of determining the exchange rate, and convergence analysis toward a stable exchange rate can be performed to determine the mesh size. The base size of the mesh element and the relating numbers of elements is shown in Tab. 5.2. The mesh size at the water level and the inlet, is determined as a percentage of the base size, and the percentage is shown in Tab. 5.2.

Base size [m]	Water level mesh [%]	Inlet mesh [%]	Numbers of elements
1.00	25	25	661
0.50	25	25	1,494
0.25	25	25	4,234
0.15	25	25	10,928
0.10	25	25	24,143
0.08	25	25	37,140
0.04	25	25	145,482
0.03	25	25	257,022

Tab. 5.2: Numbers of element in the model based on the base size.

The convergence analyse results in the exchange water percentage shown in Fig. 5.12 dependent on the numbers of elements.

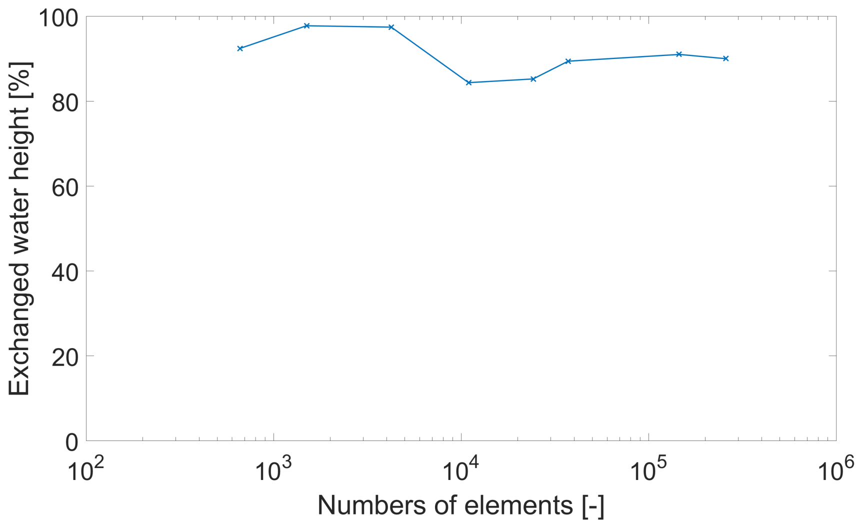

Fig. 5.12: Convergence analysis of the mesh grade based on the remaining enclosed water.

The convergence analysis shows it converge, and the mesh is accepted to at a base size of 0.08 m. The converged model results in 89.5 % of the sea water remains inside the monopile after each cycle, and is accepted as two larger models results in values of 90.0 % and 89.4 %, respectively. The A_e factor shows the exchange occur in the entire chamber. This fit well with a surface plot shown in Fig. 5.13 for the model with a base size of 0.08 m, after 17 periods.

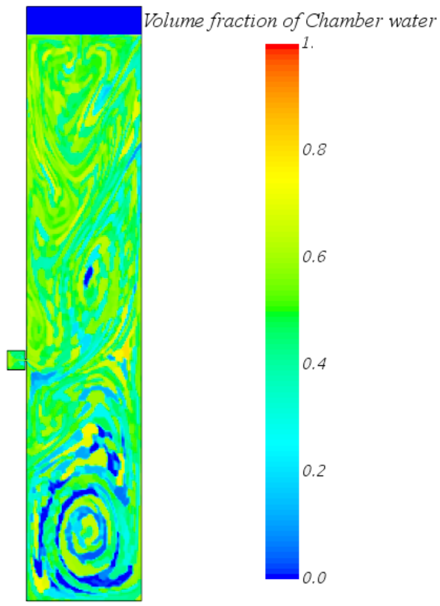

Fig. 5.13: Remaining chamber water inside the monopile after 17 cycles.

The main reason to estimate the exchange rate is to determine the mean pH-value inside the monopile. This value will go from a low pH-value of 4.3 for the enclosed water and reach a stable value, depending on the exchange rate. The mean pH-value is calculated with Eq. (5.6) and is shown in Fig. 5.14 depending on the numbers of cycles after the hole is drilled. The length of a cycles is 12 h, as here is simulated with the tidal conditions.

$$pH_{in}(C) = mono(C)\ pH(\infty) + \sum_{i=1}^{C} \left((mono(C_{i-1}) - mono(C_i))\ pH(C_i) \right) \tag{5.6}$$

Where:

pH_{in}	Mean pH value of the water inside depending on numbers of periods
$pH(t)$	pH-value of enclosed water, as estimated in Eq. (1.1)
$pH(\infty)$	pH-value of the water initially in the chamber, before exchange begins, meaning it has a pH-value of 4.3

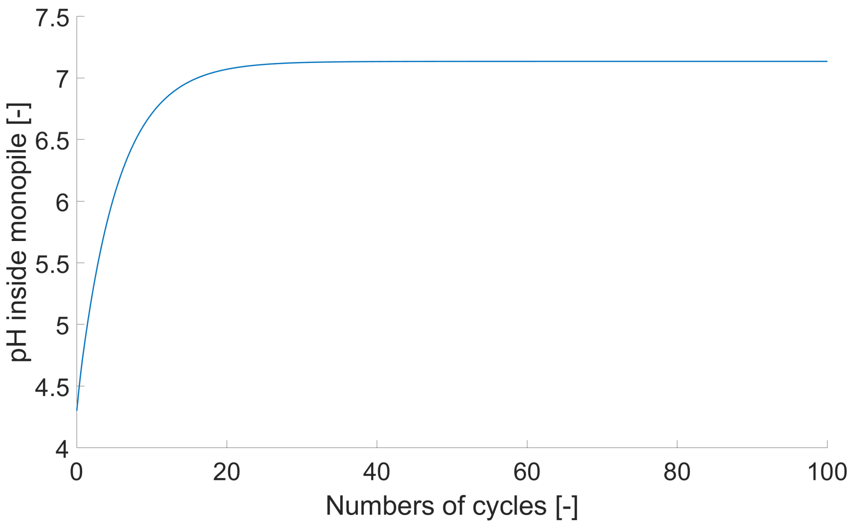

Fig. 5.14: Mean pH-value inside the monopile with the calculated exchange rate.

The pH-value calculation is based on the hole being drilled after the pH-value has decreased to 4.3. It will however stabilise on the same value for the case, where the hole is drilled before the monopile is submerged, and the water is enclosed, as it reaches an equilibrium state between the exchange rate and the decreasing pH-value. The pH-value shows to stabilise at a value of 7.13, which based on Fig. 1.4 on page 4 result in only 27.5 % anode material is needed, if a hole is drilled in the monopile, compared with a case without any exchange. This is based on the tide and without the density effects created by the seasons. The density effects on the exchange rate is evaluated later on, after an initial analysis of the wave and current is described.

5.3 Initial wave exchange

With a convergence of the mesh performed on the tide, the same mesh is used for the wave analysis. With waves compared to tide, the large difference is the wave period, as it is significantly smaller for the waves. This results in the pressure calculated in Sec. 4.2. With the changing pressure outside the chamber known, the velocity through the inlet can be calculated from the energy equation, the same way as for the tidal conditions. The model used for the initial investigation of the waves is similar to that used for tidal condition. The main difference is that the miniature sea is removed and a velocity inlet is used as the inlet condition, as shown on Draw. 02. The miniature sea is removed due the reduced wave period and the volume induced from each wave is 50 times smaller than the miniature sea volume. The model is again with one inlet located at a depth of -17.5 m at the front of the monopile. The wave period is reduced based on Eq. (5.1) from 13 s to 0.216 s. This reduction results in a very short period, which is also why the miniature sea is avoided. The error from simulating in two-dimensions are expected larger for the wave, than the tide, as here the flow practically wouldn't have time to distance itself from the inlet. Therefore, the waves are primarily focused in three-dimensions. The two-dimension wave is shown in Fig. 5.15. Calculated with the energy equation is the velocity through the inlet, and the internal water level determined, and these are as well shown in Fig. 5.15.

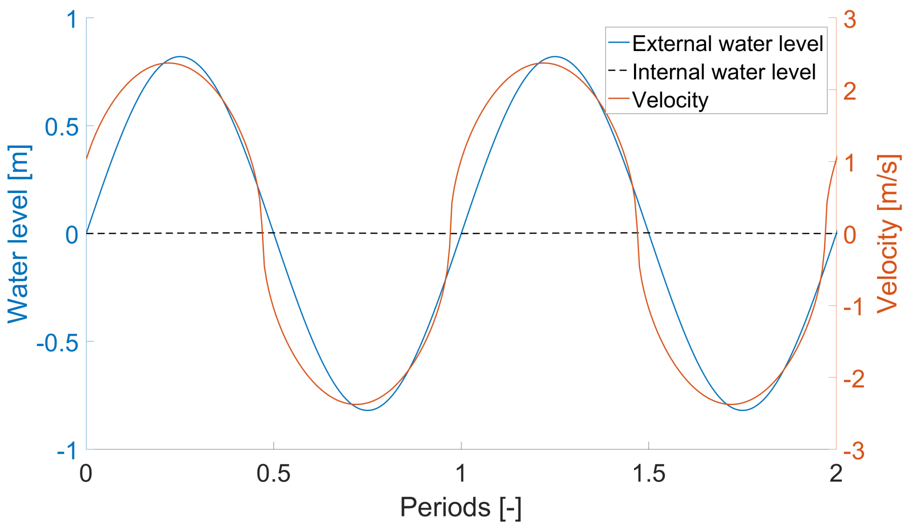

Fig. 5.15: Wave height at the front of the monopile over two wave periods and the internal water level relating to the left y-axis and the resulting mean velocity relating to the right y-axis.

The velocity from the waves are significantly larger that for tides, because the short period and small inlet result in very small change in the internal water level. As the internal an external water levels are equal at 0, doesn't result in a velocity through the inlet of0 m/s. This is due to the inertia induced pressure, which is maximum at mean water level, as the particle acceleration here is horizontal. Opposite to the tides, the max velocity is at wave crest and trough, as the internal water level doesn't change along with the external water level. The internal water level varies approximately 3.3 mm. The internal water level variates around the mean water level, with an amplitude of the surface elevation of 1.64×10^{-3} m. For the simulations and calculation the initial internal water level is therefore -1.64×10^{-3} m. Comparing the tides and waves, then there are 3323 waves per tidal period. If the percentage of the sea water remaining within the monopile from each period to that of the tides, then the internal water level change with the waves only needs to be:

$$\frac{1.5\,\mathrm{m}}{3323} = 5 \times 10^{-4}\,\mathrm{m} = 0.5\,\mathrm{mm}$$

The internal water level change from the waves is approximately 6 times as large with just one hole. Therefore, there is a great chance that the exchange from waves results in a far greater exchange of the enclosed water. By adding more holes for the wave the internal water level changes are raising significantly, where drilling more holes for the tidal conditions the internal water level wouldn't change, but the velocity will fall. With the velocity through the inlet defined, the simulation model is created.

The simulation of the waves in two-dimensions shows, as feared due to the reduced wave period, that the sea water doesn't stream very far into the chamber, but instead results in small impulses of the sea water at the inlet. The sea water is located just inside the inlet, but is being pressured further into the monopile by the continuing cycles. In Fig. 5.19 the length of the flow inside the monopile from each wave, can be seen to be very short. From the later simulations in three-dimension the sea water during one wave period travels approximately half way through the monopile, rather than 10 cm, as shown here. The exchange is therefore more effected by the inlet, than what truly will occur. Therefore the percentage of sea water remaining inside the monopile per cycle is expected larger in three-dimensions. Letting the simulation run further an exchange still occurs of the enclosed water. The exchange can be fitted to Eq. (5.4), to estimate the renewal of the enclosed water. The remaining coefficient result in a value very close to 1, because the internal water level change per cycle is small compared to the water depth in the monopile. The fits of the exchanged water height and amount of enclosed water not being exchanged, are shown in Fig. 5.16 and Fig. 5.17.

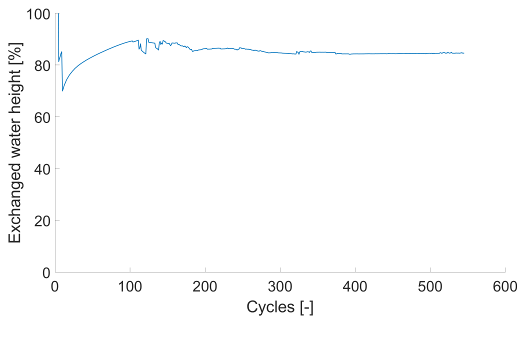

Fig. 5.16: Exchanged water height fitted to the simulated data from one hole with wave pressure.

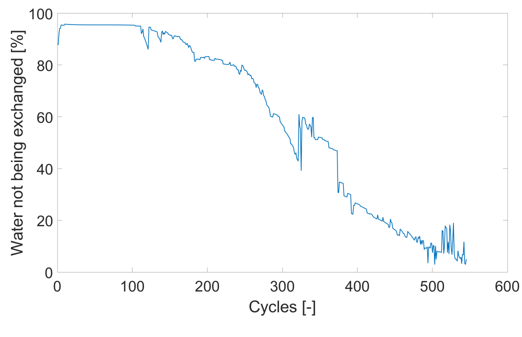

Fig. 5.17: Percentage of the enclosed water not being exchanged by the wave pressure.

The results in Fig. 5.17 seems stable during the first 100 cycles. This is because the sea water flow have not yet hit the back wall, therefore it has only flowed in a straight line from the inlet. This result in practically non of the enclosed water being exchanged. As it hits the back wall, the sea water start to flow around the entire monopile, and therefore more of the enclosed water begins to exchange. This results in the decrease of the A_e value toward 0. The flow after 500 periods is shown in Fig. 5.18. Looking close at the flow just inside the inlet, the impulses from each wave are still visible in Fig. 5.19.

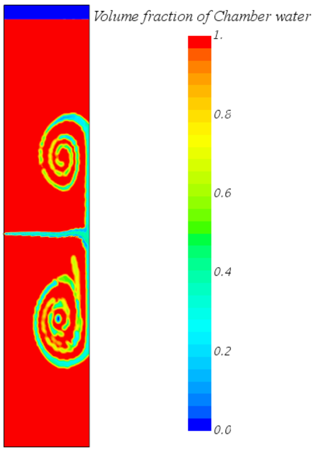

Fig. 5.18: The sea water in the monopile after 500 periods in the wave case.

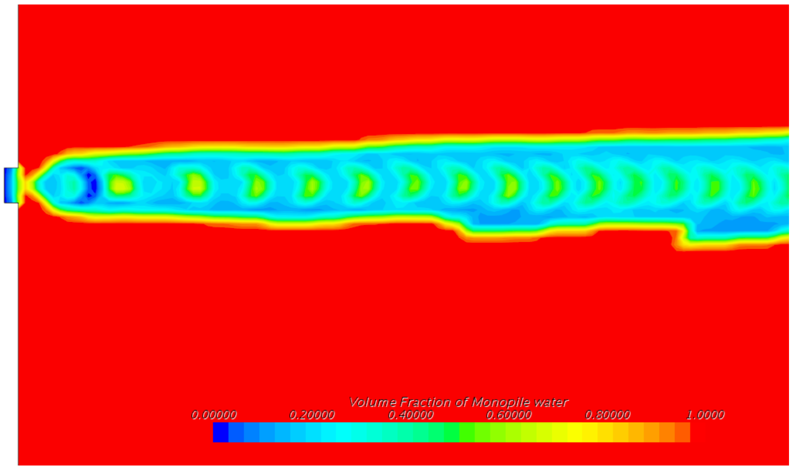

Fig. 5.19: A close look at the flow at the inlet after 500 periods.

Even as the model haven't stabilised yet, the model is ended. It is ended because the reduction of the period simply results in too large variation from a true flow. The flow in the monopile have a similarity to the flow from the tidal condition. As the results from the tidal case showed the entire monopile was exchanged, and Fig. 5.17 seems to reach toward that as well, it is expected that it is possible with waves as well. It is still tried to estimate the mean pH-value based on the end result here. The pH-value is calculated with Eq. (5.6), where it is important to remember that a wave period is 13 s compared to the 12 h a period is for the tides. The exchange show that the pH-value stabilise even higher than for the tides. The mean pH-value is shown on Fig. 5.20 where it stabilise at a pH-value of 7.73. This result in a reduction in the needed anode material to only 23.3 %.

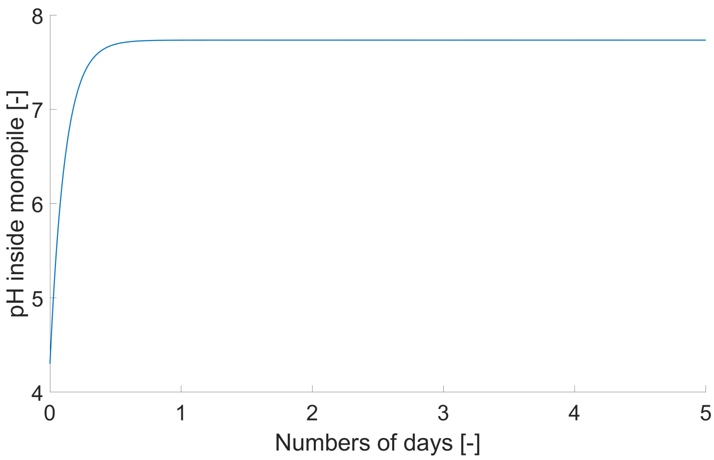

Fig. 5.20: The mean pH-value of the enclosed water with one hole in the monopile. The pH-value stabilise at 7.73.

Because the length of the wave period is reduced this much in two-dimension, the flow will not be further evaluated in two-dimension with respect to the seasonal effects. As the results show better exchange rate than the tide, the wave will later be evaluated in three-dimensions, where the seasonal effects are included in the simulation.

5.4 Initial current exchange

The current condition used in this project is calculated as a constant velocity, which is averaged over the daily variation. The results is a simplification, where the periodic effect isn't included. The sea water will not flow in and out of the same inlet, as the pressure is constant at the holes. The calculated pressure in Sec. 4.3, show an increase in the pressure on the front and a decrease on the rear side. The negative pressure is due to the wake development behind the monopile. As the pressure is constant, only one hole on the front will not result in any exchange. This is due to the pressure inside will raise until the pressure equalise, and then the flow through the inlet will stop. Therefore, to achieve any exchange there needs to be holes both on the front and rear side of the monopile. The outlet on the rear side will result in a flow out of the monopile, as the pressure is lower in the wake behind the monopile. A constant flow will therefore travel through the monopile, and an initial investigation will determine if the enclosed water can be exchanged by the current alone. As the pressure on the front and rear isn't mere opposites off each others, the current will result in a slight internal pressure change. This results in an initially higher flow velocity through the rear outlet, decreasing the internal pressure. This accelerates the flow into the monopile and decrease the flow out, until these are equal and a steady flow is achieved. The velocity through the flow is shown in Fig. 5.21. The calculation show the velocity stabilises at a value of 0.487 m/s.

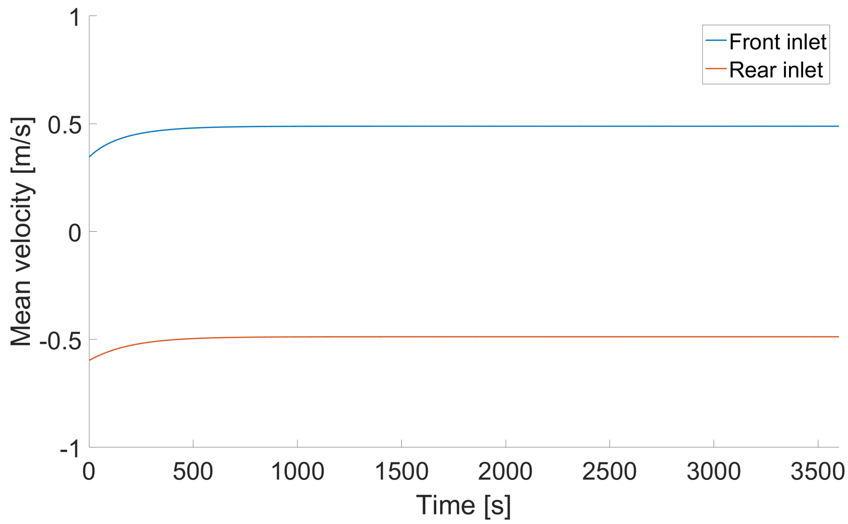

Fig. 5.21: Velocity through the front inlet and rear outlet with a current velocity of 0.5 m/s.

With the velocity through the inlets determined, a model is created. To try an achieve a flow around, inside the entire monopile, the inlets aren't just placed directly opposite each others, but instead at different depth. This is seen in Draw. 03. As the flow is constantly in or out of the inlet, the different depth guarantee a flow vertically across the monopile. The front inlet is placed at a depth of -23 m, and the rear inlet at a depth of -12 m. A continuous flow is simulated and a stable state is reach as all the water leaving the monopile at the rear inlet is sea water. The percentage of sea water across the rear inlet is measured, until the percentage reaches 100 %. The sea water percentage at the inlet over time is shown in Fig. 5.22.

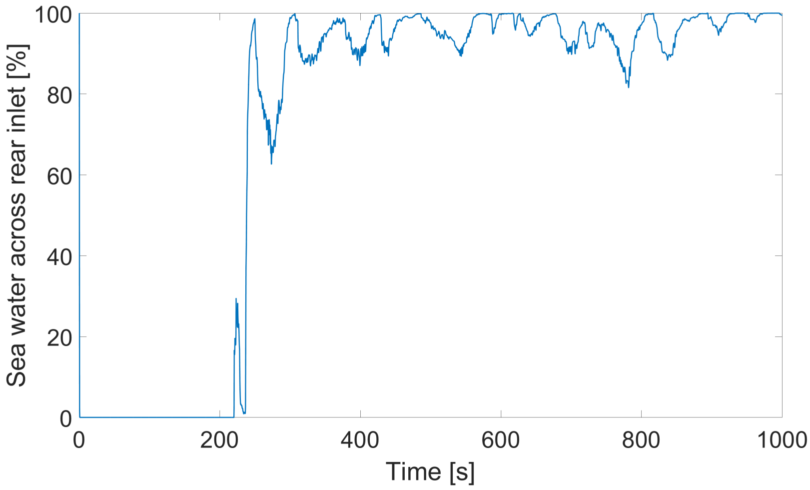

Fig. 5.22: Percentage of water leaving the rear inlet, which are sea water.

The percentage stabilises after only 1000 s, after this no more of the enclosed water is exchanged. During the first 200 s the value is 0, as the sea water travelling into the monopile has yet to reach the rear outlet. The percentage remaining of enclosed water are 90 %. The drop to 90 % was almost purely within the initial 200 s. As the amount of sea water leaving the chamber is equal to the amount entering, a constant stream between the front inlet and rear outlet is required. This stream is clearly shown in Fig. 5.23, which shows a surface plot of volume fraction of seater in the monopile.

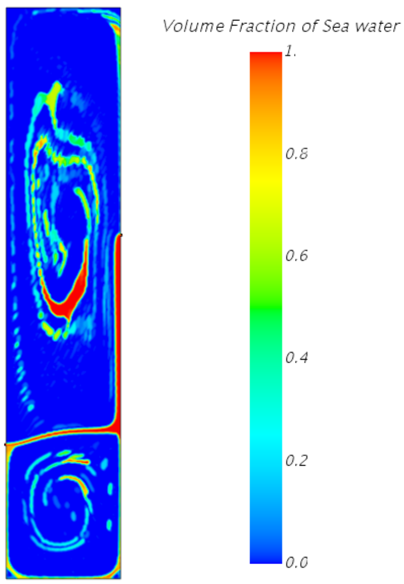

Fig. 5.23: Location of sea water inside the chamber. A clear stream going from front inlet to rear outlet.

With the current condition the flow will travel between the inlets, fairly direct, and therefore not generating a very large exchange of the enclosed water. Of cause by drilling more holes the flow can reach more of the monopile, but with the direct flow between the inlets, the enclosed water above the highest and below the deepest inlets will not be exchanged. Based on the location criteria stated in Sec. 2.2 on page 8, then around half of the enclosed water would not be exchanged, as it is located above or below the criteria. Due to these results the exchange by currents is eliminated, and no further investigation is performed.

6 2-D model optimisation of tidal condition

The initial evaluations showed that the current only exchanged a little part of the enclosed water, because the sea water traveled nearly directly between the front inlet to the rear outlet, without mixing a lot with the enclosed water. For the wave a fairly good exchange was achieved, but the effect of the reduction to two-dimension was drastic. Therefore, the wave condition is avoided to calculate further on in two-dimensions and limited to three-dimensions. In three-dimension the wave condition is investigated, including the seasonal effect of the density, plus the form and size of inlets and the monopile. With tides the reduced period is still long enough to reach around the monopile, and therefore achieves a more reliable result. It is therefore chosen only to investigate further in two-dimension with the tidal condition, and introduce the effect from the correct densities determined in Sec. 2.6 on page 11. Besides including the densities, a comparison of different designs of the location and numbers of holes is performed.

6.1 General models

The density of the water is dependent on the waters temperature and salinity at the specific location. Fig. 6.1 shows the three seasons, with the densities depending on the location in the chamber.

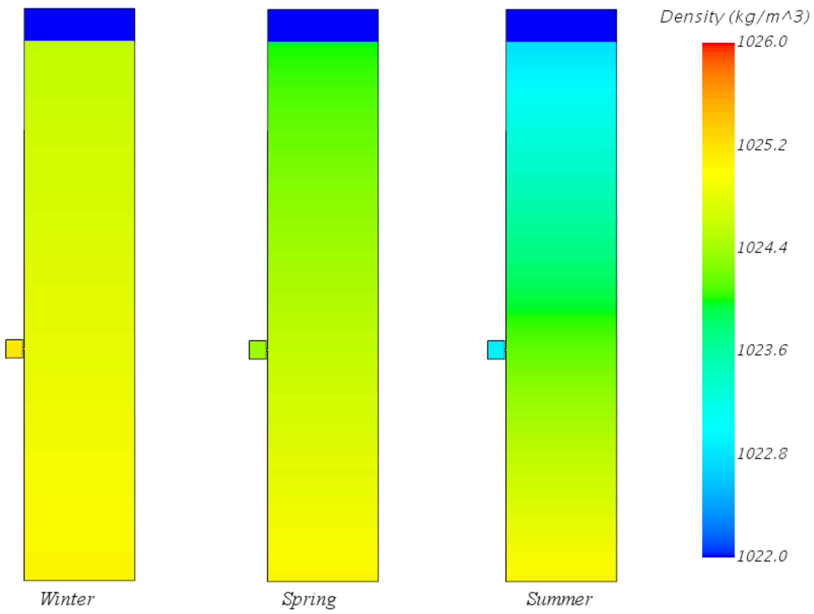

Fig. 6.1: The density of the water in- and outside the monopile depending on the season.

As also discussed previously, then the density of the sea water is higher outside during winter and lower during summer and spring. The flow will therefore naturally flow upward during summer and spring, and downwards during winter. The difference in density is greatest at the summer season, as the highest temperature difference occurs here. To evaluate the effect of the density on the internal flow, three models are created. The three models are created with one, two and three inlets, all located at the front side, but at different depths. The location of the inlets are shown in Tab. 6.1. The crack height of the inlets are all 0.1 m, and they are evenly distributed in the allowed area.

	Depth		
	Inlet 1	Inlet 2	Inlet 3
Model 1	−17.5 m		
Model 2	−12.5 m	−23.5 m	
Model 3	−12.5 m	−17.5 m	−23.5 m

Tab. 6.1: Depth of the inlets for the three models.

Following this criteria the hole in Model 1 is located 2.5 m deeper than half the water depth. An alternative could be to place the inlet in the middle of the water column, but it is expected to be more difficult to get the sea water to mix with the deep laying enclosed water, as it is during summer the largest density difference occurs.

As shown in the initial analysis the internal and external water levels are very similar with only one inlet due to the large tidal wave period, therefore when more inlets are added, the velocity is divided between them, resulting in even lower velocities at each inlet. The inclusion of more inlets have the advantage of the flow initially being spread over a larger area, as they are placed at different depths. but the lower velocity might result in smaller mixing between the phases. The volume fraction of sea water after five periods inside the chamber for Model 1 is shown for each season in Fig. 6.2. The sea water for Model 2 and Model 3 is shown in App. E, Fig. E.1 and Fig. E.2.

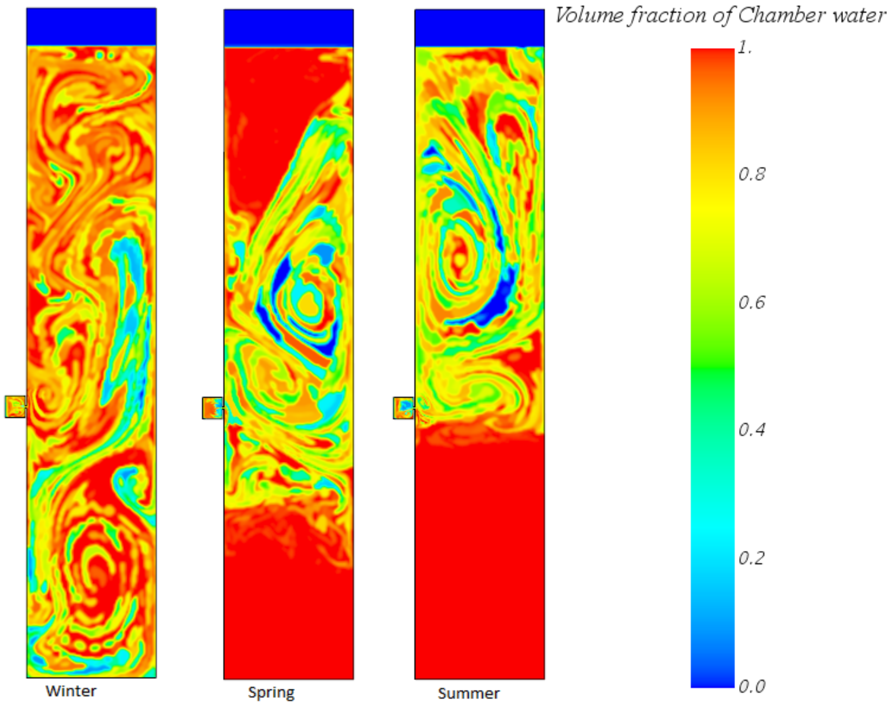

Fig. 6.2: The remaining chamber water with Model 1 after five periods for each season.

Based on the surface plots in Fig. 6.2 it is clear to see the effect of the density. For the winter season the sea water flows around in the entire chamber, but is dominated by an exchange in the lower half of the chamber. This was as expected as the density difference is low and it therefore looks more similar to the initial simulation, than the other seasons. The dominating exchange of the enclosed water was also expected to be the lower part of the monopile, due to the lower external temperature and higher density. At spring the exchange is dominating in the central part of the water column, but slight more in the upper part. This also fits the expected as the density of the sea water flowing into the chamber is somewhere between the density at the surface and at the seabed. For the summer season, the exchange is clearly dominated in the upper half of the monopile and has close to no exchange of the water below the inlet. In Model 2 and Model 3 the effects of the densities becomes more dominating as the inlet velocity decreases. This can be seen as the exchange below the deepest hole, becomes smaller for the spring and summer season as more inlets are introduced in Fig. E.1 and Fig. E.2. The percentage of the enclosed water that is not being exchanged and the percentage of the sea water remaining inside the monopile are calculated with Eq. (5.4) and Eq. (5.5). The results are shown in Tab. 6.2.

Model	Season	Percentage not exchanged, A_e	Percentage sea water $H_{s,in}$
Model 1	Winter	11.1 %	80.4 %
	Spring	18.2 %	74.3 %
	Summer	44.8 %	81.2 %
Model 2	Winter	17.5 %	80.5 %
	Spring	19.1 %	79.4 %
	Summer	18.6 %	76.6 %
Model 3	Winter	20.0 %	71.0 %
	Spring	20.9 %	74.4 %
	Summer	17.6 %	68.5 %

Tab. 6.2: Comparison of the percentage of the enclosed water that is not exchanged, A_e and the percentage of the sea water entering the monopile, which remains after a period, $H_{s,in}$. All depending on model and season.

The results shows that it is the summer season that is most affected by the density. This was as expected, as the largest difference occur here. During the summer season the exchange is completely limited by the lowest placed inlet. The temperature then result in all the above is exchanged. Looking on the results in winter and spring, the number of inlets effects the results more. During winter the best result is found with only one inlet placed in the middle, and as more inlets are drilled, the exchanged water percentage decreases. This is a result of more inlets decreases the velocity through the inlets, and more stratification occurs between the sea water and the chamber water. For a complete exchange one hole at the top could probably do it during the winter season, as the density helps to exchange the deeper water. Though with one hole at the top the exchange the rest of the year would just be very low. Especially during summer would only around 33.3 % be exchanged. Model 2 shows the highest general exchange across the seasons. This is due to the inlets are spread far from each other, and the velocity is still relatively large.

The main problem is to get the split at the back wall to dominate more than the density difference. This can be achieved by either moving the back wall closed to the inlet or by increasing the velocity of the flow through the inlets. As the monopile is a specific size, the distance to the back wall can't be reduced directly, instead focus will be on increasing the velocity of the flow.

The velocity is dependent on the pressure difference between the internal and external water pressure. The external water pressure is dominated by the tidal condition, and can't be affected. The internal pressure on the other hand is dependent on the internal water level, and that is dependent on the continuity equation. The value in the continuity equation that is decided by the design is the inlet area. By halving the inlet diameter, the flow velocity increases roughly four times. The increase in velocity is a result of the area of a circle is only one-fourth, if the diameter is halved. As the inlet area decreases the mass flow decreases, resulting in a larger pressure difference, and this increases the velocity. The increase in the velocity should create a more dominating jet from the inlet, and decrease the percentage water that are not being exchanged. To exchange the full monopile during the summer, an inlet located as low as possible would be preferable. For the winter season a high located inlet would achieve most optimal exchange. Considering this, a new model is created. This model has two inlets, one located at shallow depth, and one located deep in the monopile. The diameter of the inlets is reduced to the minimum allowed diameter, 0.05 m. The halving of the inlet diameter and creating two holes, result in approximately a double of the velocity through each inlet, compared to Model 1. The inlets velocity and the relating internal and external water levels are shows on Fig. 6.3. Due to the reduction function from three to two-dimensions, see Eq. (5.1), the period is reduced further to 0.1 h, as the diameter is changed.

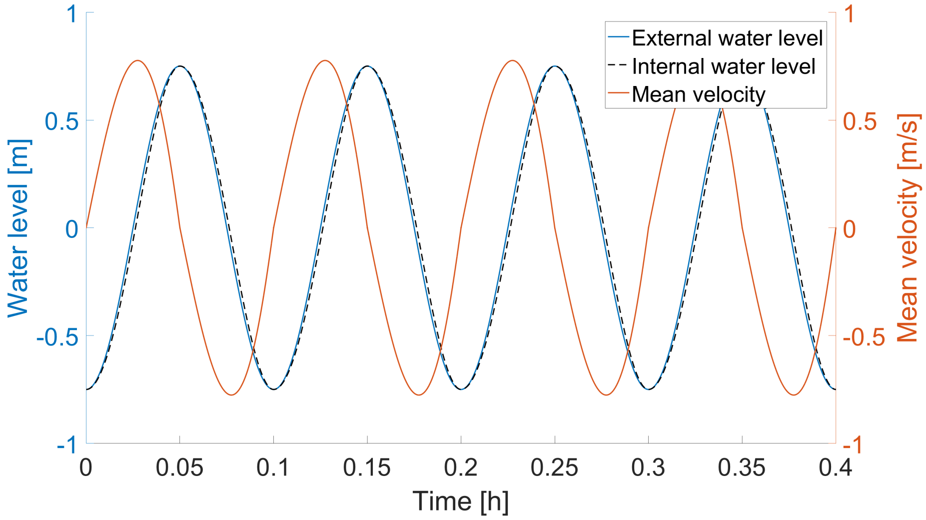

Fig. 6.3: The internal and external water level, relating to the left y-axis, and the mean velocity through each inlet, relating to the right y-axis.

As the period is reduce even further, the effect of the simplification to two-dimension is larger. With the period is reduced and the velocity kept, the sea water flows travelling distance inside the chamber is reduced as well. The reduction of the wave period could undermine some of the wished effect from increasing the velocity. As the velocity is doubled, but the period is halved, the flow distance is approximately unchanged. In a three-dimensional model the flow distance will double, as the period will remain unchanged, when the inlet size is changed. The jet will instead be with a smaller diameter, as in two-dimension the crack width can't be altered, as it is lacking the third dimension.

The two inlets are placed at opposite sides of the monopile, at the two different heights. The model is created for the summer season, as from the surface plots it is clear the summer season shows the most drastic stratification between chamber water and sea water. In Model 1 at winter season, the largest amount of the enclosed water was exchanged. With this model the velocity through the inlet is twice as high and an inlet is located at lower depth, so it should increase the amount exchanged during the winter season as well.

The result of this model, for the summer season after ten periods, is shown in Fig. 6.4.

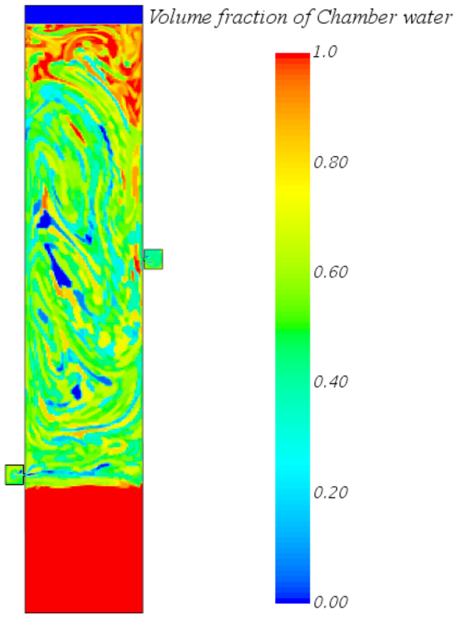

Fig. 6.4: Remaining chamber water after ten periods for the summer season. Created with two inlets, with crack heights of 0.05 m.

Based on Fig. 6.4 the flow looks similar to Model 2. It was expected that the larger part of the monopile would be exchange, but the exchanged water percentage only increases slightly to a value of 84.2 %. This shows the velocity increase doesn't change how much of a vertical flow that occur. This is opposite the expected, as an increase of the velocity should be less affected by the stratification. The main reason for the lack of change is expected to be found in the simplification to two-dimensions. As the inlet diameter is smaller, then so is the two-dimension period. The decrease in wave period therefore counteracts the increase in velocity. As the period correctly will stay constant in three-dimension, the velocity will result in a larger exchange. This determines that the simplification results in some significant problems, and the seasonal effects truly can be expected to be less.

6.2 2-D conclusion

The most significant problem for the two-dimensional models are the simplification from three to two-dimensions. This is due to the geometry of the monopile and the holes. The simplification results in a drastic decrease in the wave period, and due to this it is expected that the exchange rate is a underestimation. The simulations shows that the largest problem for the tidal condition is to achieve a high velocity, which is needed to avoid stratification between the sea and chamber water. An increase in the flow velocity shows little added exchanges, but this is expected to be due to the decreased wave period. This emphasised the chance for a complete exchange with the use of the wave conditions. The simulation has shown that the exchange is probably possible, and can result in large saving on the needed anode material.

In the following, the simulation model is validated against some experiments, and further, the exchange for a correct three-dimensional model is simulated.

Part III

Experimental

In this part CFD-models are validated against experimental test, which are performed in the laboratory. This validates the used of the $k - \varepsilon$ turbulence models in the simulations.

7 | Experimental model

The experiments are used to validate, if the $k-\varepsilon$ model is a fair turbulence model for modelling the turbulence and the general sea water flow in this project. This is done by taping videos of the flow and the mixing between the sea water and enclosed water, plus measuring the water level change and velocity from the experiments. This is compared to simulated data from CFD-models of the same conditions. The compared videos of both the experiments and simulations are placed on the digital appendix in App. A.2.

The comparisons are done between the experimental results and numerical simulations. The simulation model is created with the same geometry as the experiment.

7.1 Experimental geometry

The experiment is constructed as a scaled model of the monopile and the ocean around it. The experimental model can be seen on Fig. 7.1. The tecnical design of the experimental model is found on Draw. 04.

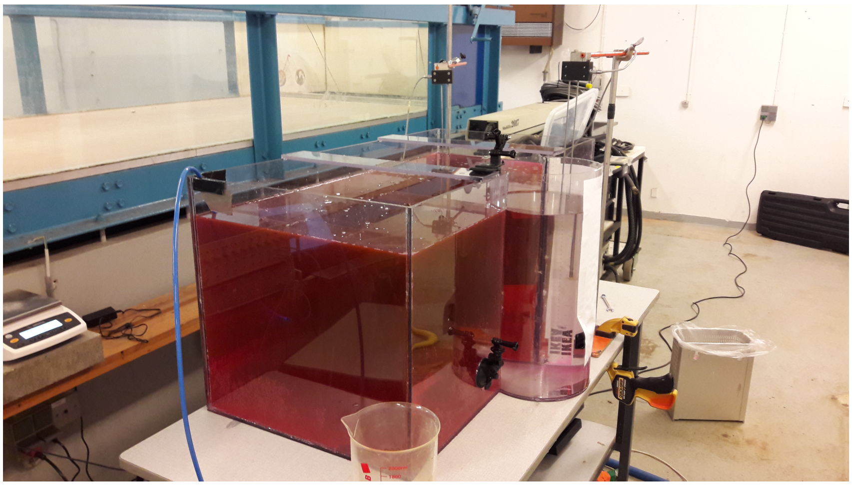

Fig. 7.1: Model of the experiment.

The experiment is build up by a basin to model the ocean outside the monopile, and a cylinder located at the edge, to model the monopile. The monopile is at the edge of the basin to enable a view of the flow from the sides, as well as from above. These views are used for the comparison to the simulations. The experimental model is created with one inlet into the monopile, which allows a flow between the two chambers. The inlet is closed with a ballofix valve to isolate the sea water in the basin from the enclosed water in the monopile, until the experiments are started. For the videos of the experiments to identify the sea water from the enclosed water, the sea water is coloured red with Rhodamine and the enclosed water remains clear. The sea water is coloured, as the interest is within the monopile and therefore the sea water flow can be seen through the clear water. The ballofix will effect as an element not present in nature, but is chosen for simpler repetitions of the experiments. The ballofix is included in the numerical simulations as well, to achieve the best comparable results. Besides the ballofix another possibility for a blockade between the two chambers was discussed. Here a piece of tape blocks the inlet during the preparation, and then is removed to start the experiment. The problem in using the tape is in the preparation and start of the experiment. For the use of the tape the water level needed to be lowered below the inlet for repetition of the experiment, as a new piece of tape needs to be applied, before the initial states can be prepared. This will include problems applying the tape on the wet surface of the monopile. For the experiment to start the tape is needed removed, which will cause turbulence right at the inlet and therefore influence the flow through the inlet at the beginning of the experiment. The use of a ballofix will move the turbulence from the opening of the inlet, a little further away from the inlet. The ballofix instead reduces the accessibility to the inlet from around, which is why the ballofix is included in the numerical simulations. The ballofix also create a little amount of enclosed water in the sea in the volume between the lock and the monopile wall. This volume of enclosed water is expected not to influence, as it is of an insignificant size compared, to the flow during the experiments.

7.2 Scaling

As the model is not in full size, but only a model of nature, a scaling is needed and this causes inevitable scaling effects. Scaling law is used to ensure geometric, kinematic and dynamic similitude, with as small scale effects as possible for the considered problem. As the flow is dominated by the gravitational and inertia forces, due to the free surface in the model, the scaling is created based on Froude's model law. The shear force is only effecting through the inlet, which is of a low size compared to the complete model. The basis for the scaling is given in App. F.

7.2.1 Scaling of the model

The scaling factor primarily used for the model is:

$$\lambda_L = 25$$

Where:

λ_L Length scaling factor

The scaling factor is chosen depending on the materials used for the construction of the monopile in the experimental model. The monopile is constructed from a cylinder with an outer/inner diameter of 250/244 mm, resulting in the given scaling factor. The modelled monopile is with a thickness of 3 mm, slightly thinner than the real scale monopile. As the effects of the friction through the inlet has limited effect, due to the inlet length, the change is acceptable. The effect is instead dominated by the diameter of the inlet, which is scaled with 25 to 4 mm. As the experiments are used for evaluation of the flow tendencies and validation the use of the $k-\varepsilon$ turbulence model, the interesting area is focused around the inlet. The height of the monopile is therefore created with a larger scaling factor to reduce the size of the experimental model and simplifying working with it.

$$\lambda_{L,h} = 66.6$$

Where:

$\lambda_{L,h}$ Length scale for the height

This results in a mean water depth of 0.45 m in the model, contra the 30 m in nature. The flow is primarily in the center of the monopile and therefore doesn't reach the surface or seabed. If this occur, the height is of little to no influence as, the flow is not affected by the seabed or surface. If the flow is effected by the seabed or surface, then it would result in little to no effect, as the numerical model is created with a hight scaled equally.

The scaling of the water levels changes will remain with a scaling factor of 25. This results in a more larger change and therefore easier to measure, compared to a scale of 66.6.

7.3 Experimental setup

Two different experiments are performed to evaluate the flow in the monopile and validate the use of the $k-\varepsilon$ turbulence model. These experiment are explained here.

7.3.1 Experiment 1

The first experiment will evaluate how the flow acts with high velocity, by having an initial water level difference between the two chambers. The setup will be as shown in Fig. 7.2, and the initial water level difference is 20 mm. The initial 20 mm water level difference, giving 500 mm difference in nature, is chosen to use the same water level difference, as in the two-dimension validation, Chap. 3.

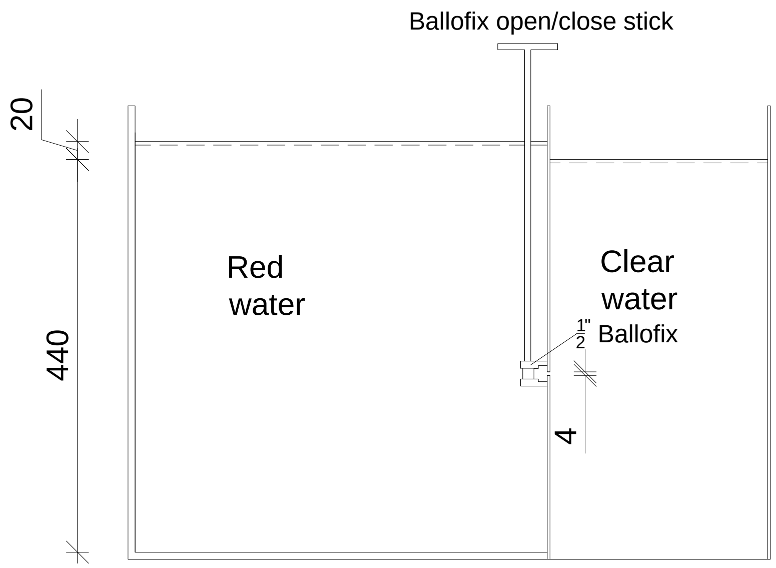

Fig. 7.2: Initial conditions for experiment 1. All measurements in mm.

The experiment will show the tendencies of the flow, until the water levels have stabilised at the same depths. The flow is taped by cameras around the monopile, as shown on Draw. 04. The water levels will be measured by wave gages, located in the monopile and in the basin. Their locations are shown on Draw. 04. By measurements of the water levels, the average velocity through the inlet is determined as:

$$V_{avg}(t) = \frac{A_{monopile}\ |(h(t+\Delta t) - h(t-\Delta t))|}{2\ \Delta t\ A_h} \tag{7.1}$$

$A_{monopile}$	Monopile cross area
h	Water depth
A_h	Hole area
t	Time
Δt	Time between measurements

The results from Experiment 1 are compared with a simulation created with the same initial conditions. They are compared on the flow and the velocity at the inlet.

7.3.2 Experiment 2

Experiment 2 will evaluate the tendencies at low velocities through the inlet. This is done by initially having the same water level in the monopile, as the basin. Then during the experiment, raising the water level in the basin to simulate the raising of the tide. The tidal height is 1.5 m in nature, resulting in a modelled height of 60 mm. The period for the tide is in nature 12 h for a full period, giving 6 h for the raising tide period, which is only included in this experiment. It is limited to only the raising tide in the experiment, as the flow out will not be visible, due to the colouration. From the time scale calculated by Froude scale, the model period is 1 h and 12 min. The volume flow rate created by the tide is simplified to be constant, and the volume flow rate is calculated to:

$$Q_M = \frac{A_{c,M}\, h_{t,M}}{T_{p,M}} = 0.027\,\mathrm{m^3/h} = 0.45\,\mathrm{l/min}$$

$A_{c,M}$	Area of cross section of model
$h_{t,M}$	Tide height in model
$T_{p,M}$	Tide period for raising tide in model

The volume flow rate is kept constant to use a pump to add water for the raising tide. By keeping the volume flow rate constant, compared to the cosine curve, it results in a steeper change in the water level at the beginning and the end, and a less steep change in the center, as shown on Fig. 7.3. This will result in a faster change of velocity in the beginning and then reach a constant water level difference, and constant velocity, until the experiment ends. This will give a larger water level difference at the end, as it does not level out slowly, as for the cosine function. The maximum velocity is lower, due to the less steep change at the center of the period. The initial conditions for Experiment 2, with the same initial water levels are shown in Fig. 7.4.

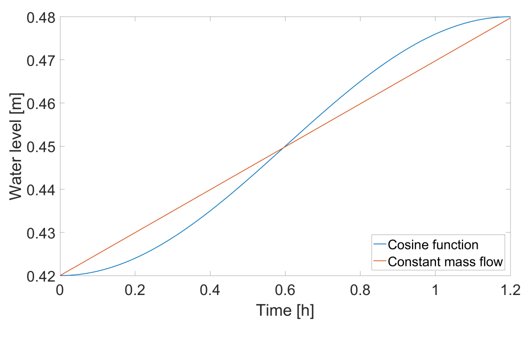

Fig. 7.3: Raising water level with cosine function and constant volume flow rate.

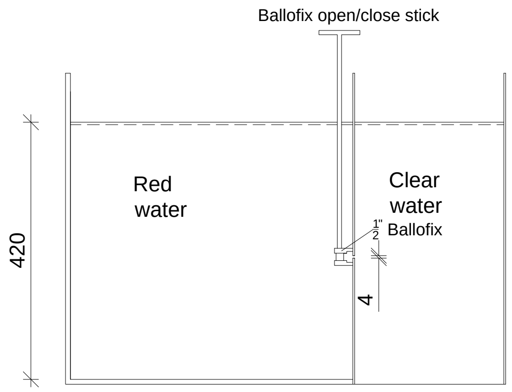

Fig. 7.4: Initial conditions for Experiment 2. All measurements in mm.

Experiment 2 evaluate how the flow acts for small acceleration and velocity of the inlet flow. Here the jet into the flow will be less dominating, as the water levels are expected to be close to equal during the period of the experiment. Experiment 2 will be tested with some different temperatures between the sea water and the enclosed water, to determine the accuracy of the different densities modelled in the simulations. The temperatures in the experiment are measured with an analogue thermometer. The experimental flow is compared with the simulated flow to validate the flow inside of the monopile, and the $k-\varepsilon$ turbulence model.

8 | Experimental validation

The experiments are divided in two experiment, where both focus on validating the turbulence model. The turbulence model used in the simulations are the $k-\varepsilon$ turbulence model. The turbulence is used to create some diffusion between the sea water and the enclosed water. The $k-\varepsilon$ turbulence model is the most commonly used turbulence models in CFD simulations. The model describes the turbulence with two transport equations. The two equation describes:

1 The turbulent kinematic energy in the flow, shortened to k
2 The turbulent dissipation in the flow, shortened to ε

The turbulence model thereby describes the amount of turbulent kinetic energy in flow and its rate of dissipation.

8.1 Experiment 1 results

The first compared between Experiment 1 and the simulated model, is the water level change. In Experiment 1 the external water level is 20 mm above the internal water level. No water is added to the ocean to keep the water level constant during the experiments duration, resulting in the ocean water level decreases slightly. As the ocean has a roughly eight times greater surface area than the monopile, the domination water level change is within the monopile. The external water level decreases just over 2 mm and the internal water increases with just below 18 mm. The measurements of the water level in the experiment are averaged over 10 measurements, to reduce the fluctuation. The water level change is as well calculated with the energy equation to compare with the experiment and the simulation. These three are compared in Fig. 8.1. The energy equation is calculated with a total loss coefficient of 2.1, determined in Sec. 3.2, as the inlet is scaled from a hole diameter of 100 mm.

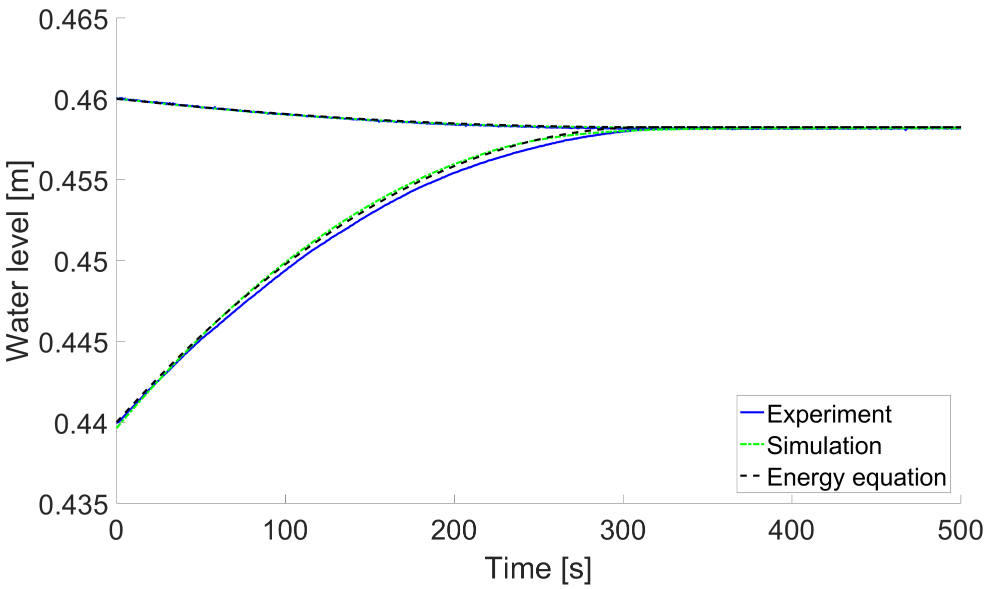

Fig. 8.1: Internal and external water level for experiment, simulation and energy equation. Internal water level initiates from 0.44 m and external initiates from 0.46 m.

As it is seen on Fig. 8.1, the water level stabilises at the same value, 0.458 m, which is also an necessary, as the surface areas of all three are equal. The interesting part to compare is therefore the time it takes to reach a stable water level. Here is shows an equal result between the simulation and the energy equation, but the experiment is slightly slower. The time at which the water level stabilises for the three estimates is shown in Tab. 8.1.

	Time
Experiment	319 s
Simulation	316 s
Energy equation	314 s

Tab. 8.1: Time before stable water level is reached for the three estimates.

They all stabilise within just above five seconds. The difference in their velocity is very small, with a mean velocity of 0.059 m/s and a variation within $\pm$0.007 m/s between the three. The difference to the experiment is expected to be due to imprecision in the initial water levels of the experiment. As the initial water levels are measured with a ruler, the precision is only within half a millimetre for both water level. This results in up to $\pm$1 mm in the initial water level difference before the experiment is stated. Calculating this variation with the energy equation, the time is within a span from 306 s to 321 s. This variation includes both the simulation and experimental result. Experiment 1 is performed seven times to estimate the variation in the time before stabilising. The seven experiments shows the stable water level is reach after an average time of 318 s, and the time variates with a standard deviation of 10.7 s. The results show that the result of the simulation and energy equation is slightly below the experiment, but well within expected the error margin from the initial state. The energy equation shows that the total loss coefficient has not changed after the inlet has changed from a crack to a hole.

As it is seen the velocity is equal in the experiment and simulation. The second to compare is the flow of the sea water within the monopile. Experiment 1 is only performed with the same water temperature inside as outside the monopile, therefore there is no difference in the density between the enclosed water and the sea water. In Fig. 8.2 and Fig. 8.3 are shown the sea water flow in the experiment and simulation, respectively, just as the flow breaks at the back wall of the cylinder. The seawater from the simulations are showed as green to identify it from the experimental, when they are compared. the In the figure of the simulated flow, the monopile water is made transparent to view only the sea water. The dark red seen in the left side of figures is the sea, and it is darker due to the higher concentration. The flow directly at the inlet isn't visible due to only two thirds is extended beyond the modelled ocean.

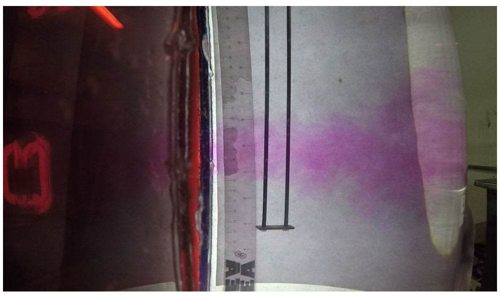

Fig. 8.2: Experimental flow breaking at the back wall of the cylinder after 6 s.

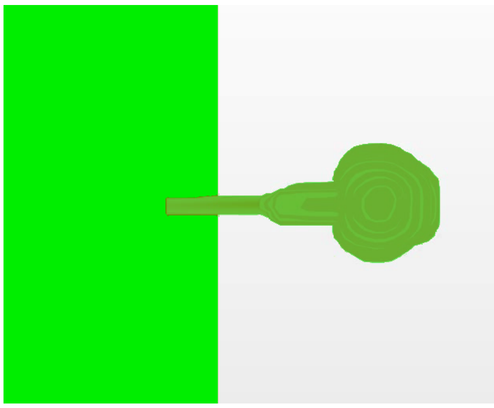

Fig. 8.3: Simulated three-dimensional flow breaking at the back wall of the cylinder after 6 s.

The break at the back wall occurs 6 s after the flow is initiated. To compare the difference between the two flow, the simulated stream is placed on top of the experimental image, and is shown in Fig. 8.4.

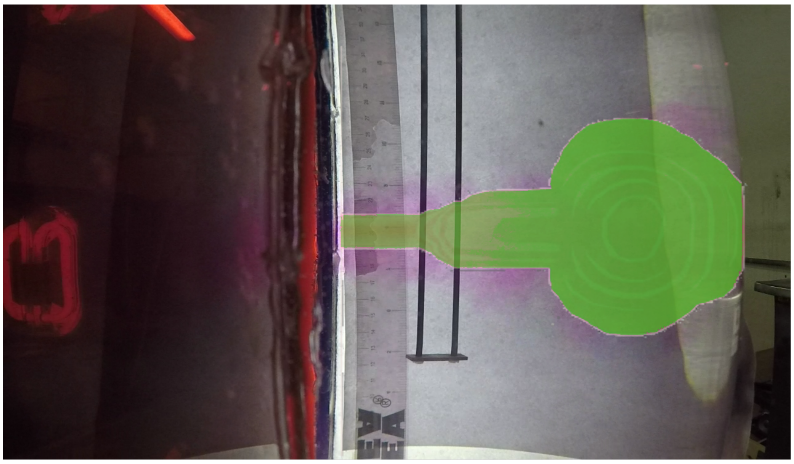

Fig. 8.4: Comparison between the experimental flow and the simulated flow, 6 s after the experiment is initiated.

In both the experiment and simulation, they break at the back wall at the same time. The flow is straight into the cylinder, but widen itself the further into the cylinder is looked. The expanding is due to the decreasing velocity and turbulence around the streams surface. The sea water stream in the experiment is a little wider that what the simulation shows. The extra width in the experiment is not necessarily due to extra turbulence, but could be due to diffusion of the red colour, Rhodamine. The Rhodamine spread from the high concentration in the sea water to the clear monopile water. As the turbulence is smaller in the $k-\varepsilon$ turbulence model than the experiment, the mixing between the two phases is underestimated. As the point of this project is to achieve a complete mixing of the phases, this will resolve in a safe estimate of percentage mixed and a safe result of the enclosed water exchanged.

At the back wall the flow breaks and flows along the cylinder surface. As the back wall is curved in the horizontal plane, the flow runs back along the surface toward the inlet. This results in a fast exchange of the water along the surface, and thereby covers what can be seen with the cameras.

Seen in the two-dimensional simulations, the flow has a tendency to flow upwards at low velocities, even with no difference in the density. The same occurs in the experiment, and is shown in Fig. 8.5. The figure shows the flow after 4 min, and the flow from the inlet is just visible as a slightly darker red, due to the higher concentration of Rhodamine.

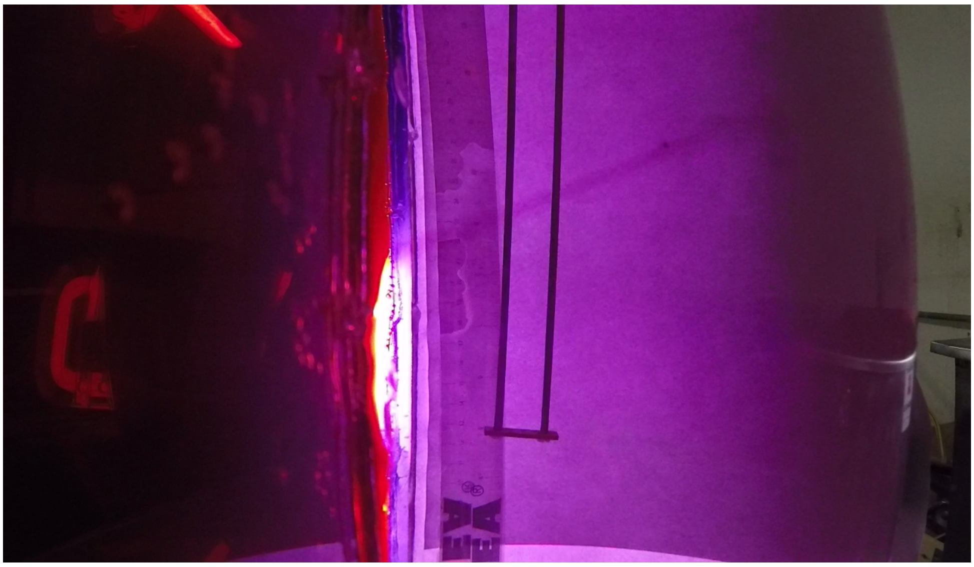

Fig. 8.5: Sea water flow after 4 min, which show an upwards flowing sea water stream.

The same upwards flow is seen in the simulation. The experimental and simulated flow is compared on Fig. 8.6, here the simulated flow is shown in a vertical cut plane taken at the centre of the cylinder. The experimental flow only show the last two-thirds of the cylinder width, where the vertical cut plane show the flow through the whole cylinder width. The slope of the flows in the figures are measured to 25 ° and 24 ° respectively, from horizontal. The difference in the slope can be seen in Fig. 8.6 as the simulated flow is a little below the experimental flow.

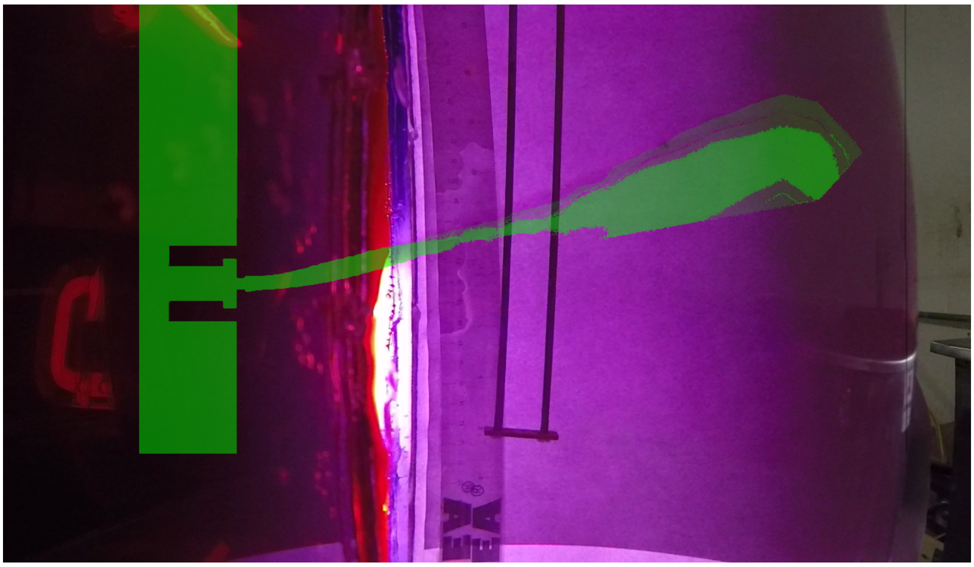

Fig. 8.6: Comparison between simulated and experimental sea water flow after 4 min, which show an upwards flowing sea water stream.

With only a one degree slope difference between the experimental and simulated flow after 4 min, the difference is acceptable.

8.2 Experiment 2 results

In Experiment 2 the external water level raises during the experiment, generating a flow from the ocean into the cylinder, which then increases the internal water level. Initially the two water levels are equal. Experiment 2 stabilise to a constant velocity through the inlet, opposite Experiment 1 where the velocity is decreasing, as the water level difference goes towards zero. A constant velocity is reached, because the water level change is simplified to be constant during the experiment, as shown in Fig. 7.3. The constant velocity through the inlet is 0.052 m/s, and is reached within the first 300 s of the experiment being initiated. To compare the experiment with the simulation and the energy equation would be on the difference between the two water levels. The difference in the water levels is below one millimetre, and therefore below the fluctuation of the measurements from the wave gauges. With this limited difference the comparison is limited to only being a comparison between the flow in the experiment and the simulation. Experiment 2 is performed in two variations:

- Equal density between sea water and enclosed water
- Low density sea water, high density enclosed water

The different densities are varied by changing the temperature of the water.

8.2.1 Equal density

Experiment 2 with equal density is performed with a water temperature of 16 °C for both the sea water and enclosed water. The equal temperature is achieved by setting up the experiment a minimum of 12 hours before the experiment is performed. The temperature is determined by multiple random samples taken at both the surface and bottom of the model. The water is fresh water, and the temperature results in a density of 998.9 kg/m^3. In Fig. 8.7 the experimental flow is shown after one minute and thirty seconds, when it encounter the back wall.

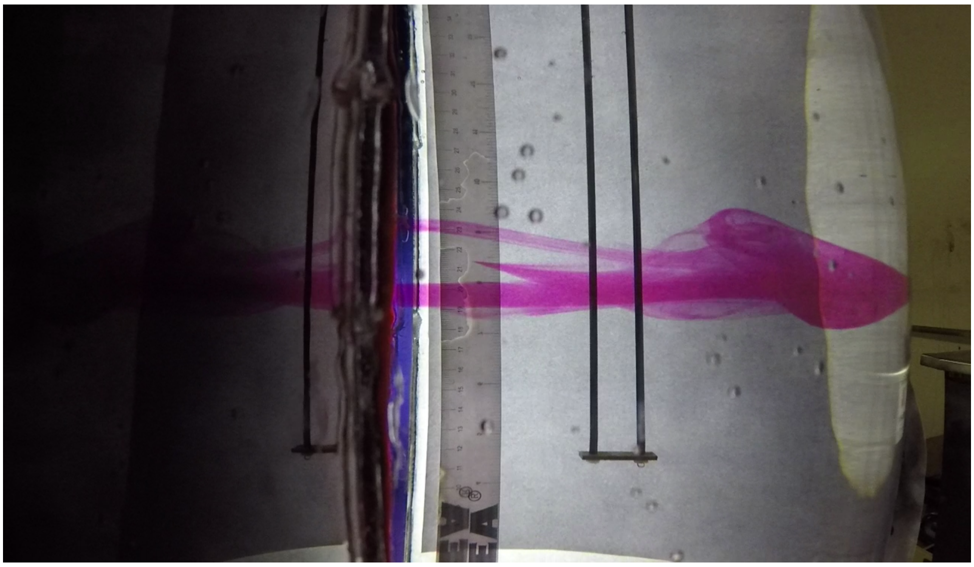

Fig. 8.7: Flow in Experiment 2 after 1 min and 30 s, with the same density of the sea water and enclosed water.

The experiment show a close to completely levelled flow into the cylinder, but a little extra above, than below. This flow is compared with a simulation with a similar equal density, and the two flows are shown in Fig. 8.8.

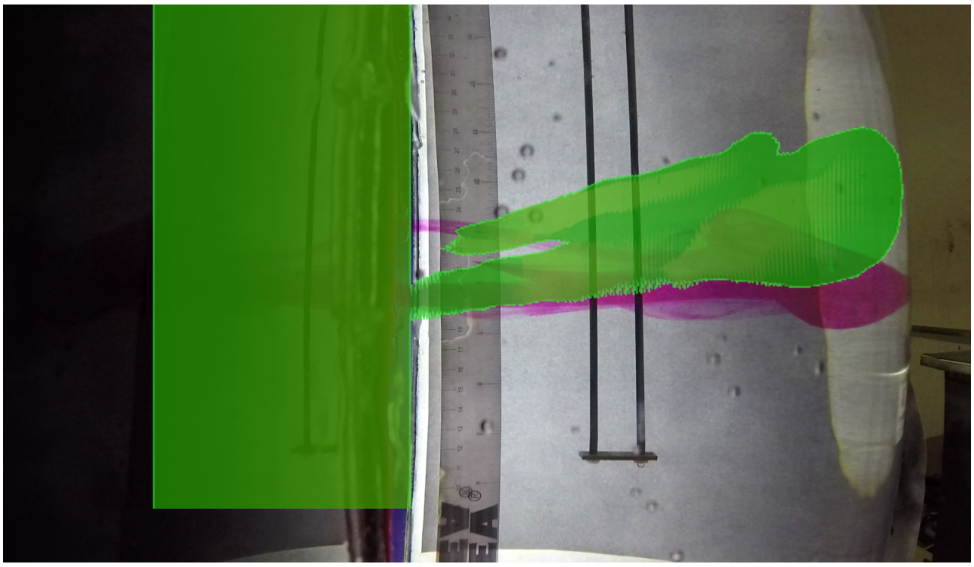

Fig. 8.8: Flow in Experiment 2 and simulation after 1 min and 30 s, with the same density of the sea water and the enclosed water.

Comparing these two flows show that the turbulence around the flow is similar, but the direction varies. Both flows have a secondary stream above and a widened tip of the flow. The simulated flow has a direction slightly toward the surface, as also occur in Experiment 1 and the related simulation at low velocity. The precise reason for the difference is unknown, but could be due to a lower temperature in the sea water, resulting in a slightly higher density. The reason for a lower sea water temperature than the measured, could be found in the measurement method. For the measurements in the sea water, the temperature was unable to be read of the thermometer while it was submerged in the water, because of the colouration of the sea water. This resulted in the thermometer needed to be lifted above the water, and the temperature documented, before a change occur from the changed surrounding. For the enclosed water the temperature was measured with the thermometer submerged, as the temperature can be read through the clear water. Measurements of the enclosed water, both submerged and lifted showed no visible difference, therefore this measurement method was accepted and the effect was expected insignificant. Based on these results a larger effect could occur, which could be the reason for the difference.

As the experiment continuous, the sea water flows along the monopile surface, as was seen in Experiment 1. At the end of the experiment the sea and enclosed water seems to have mixed completely, as shown in Fig. 8.9.

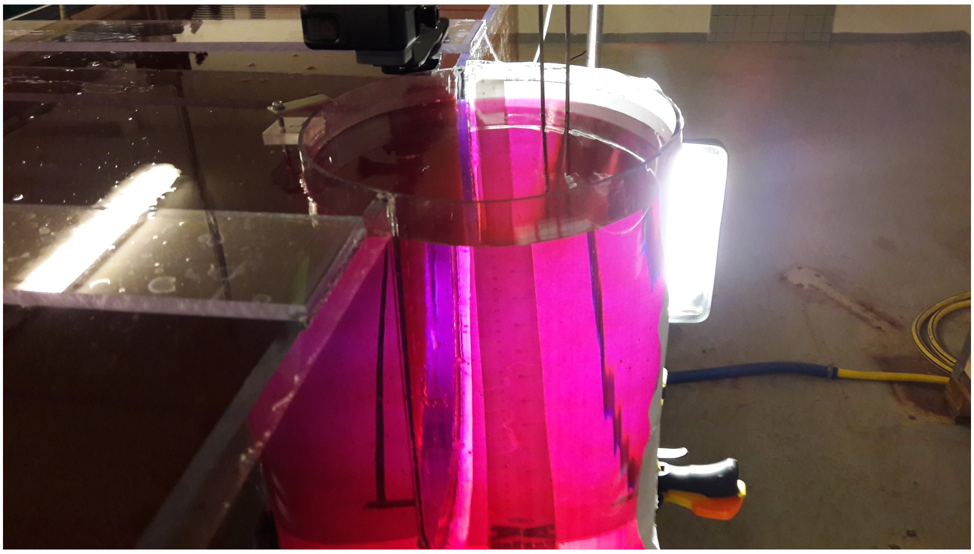

Fig. 8.9: Complete mixing between the sea water and enclosed water at the end of Experiment 2.

8.2.2 Low density sea water

To test the effect of different densities between the sea water and enclosed water, Experiment 2 was performed with a low density of the sea water and a higher density of the enclosed water. This is used to determine how drastic the difference in temperature, thereby density, affects the flow. As well, a comparison with the simulated model, shows how well the simulation reacts with two phases interacting with two different temperatures. The experiment is performed with the temperature of the sea water on 14°C and of the enclosed water on 9°C. These temperatures results in a density difference on 0.75 kg/m^3. This is a difference below 1 %, but the experiment shows this is enough to highly influence the flow, especially with as low a velocity as occur in this experiment. The sea water flow in Experiment 2 after 1 min and 30 s, is shown in Fig. 8.10.

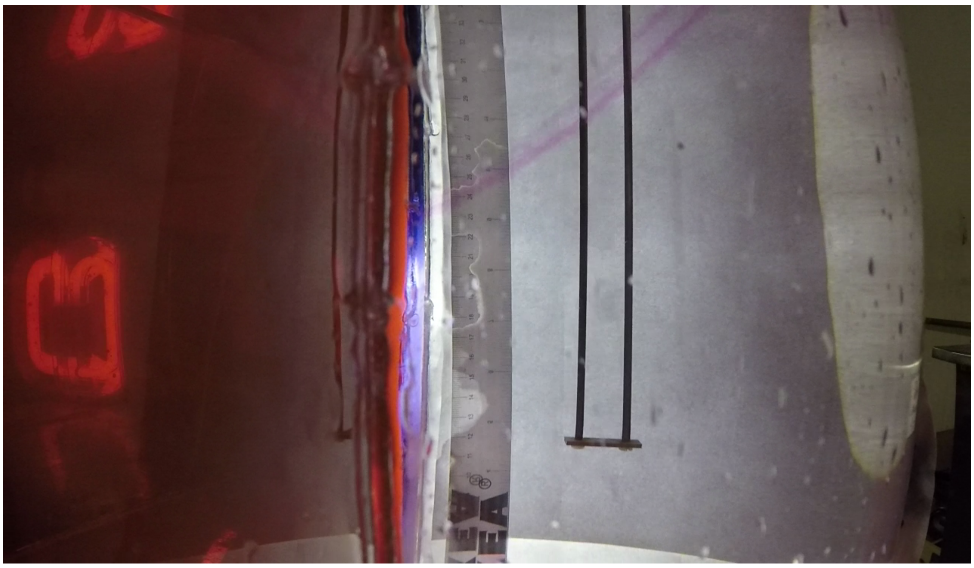

Fig. 8.10: The experimental flow inside the cylinder after 1 min and 30 s with low density sea water.

A clear steep slope occur here due to the density difference, as it was expected. This results in the mixing between the sea and enclosed water is dominated in the upper half of the monopile. A comparison of the flow in this experiment with the simulated flow, is shown in Fig. 8.11.

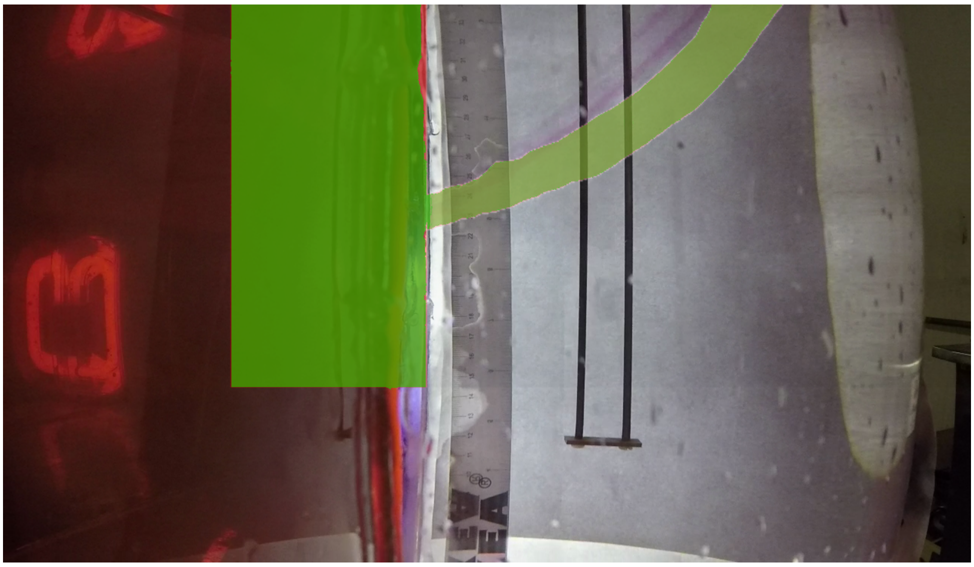

Fig. 8.11: The experimental and simulated flow inside the cylinder after 1 min and 30 s with low density sea water.

The flows here shows to be very similar with an even steep slope. This show that the temperature and turbulence effects in the simulation performs good, compared to the experiment.

8.3 Experimental conclusion

The comparison between the experimental and simulated results show some minor difference in form of the slope and the width of the flow. Part of the increased width seen in Experiment 1 is due to diffusion of the Rhodamine and some small turbulence at the flow surface. The increase in turbulence at the flow surface would only benefit the mixing of the two phases, and therefore the simulation is acceptable as a safe estimate with the use of the $k-\varepsilon$ turbulence model. Experiment 2 show the temperature effects are estimated good in the simulations. As a result of these experiments, the $k-\varepsilon$ turbulence model is accepted as an accurate model for the simulations performed both in two and three-dimensions.

Part IV

3-D

In this part the three-dimension models are analysed. The analysis of the model is based on the results gain from the two-dimension models.

9 | 3-D analysis

For the three-dimensional analysis, only the wave conditions is simulated. This is because the two-dimensional results showed that a high velocity is critical to getting the flow around in the entire model. The velocity with the wave condition results in a significantly higher velocity, because of the short wave period, that result in a large pressure differences. As well a combination of the waves with the tides would result in an insignificantly small change, due to the long period of the tide, and the wave and tidal height are similar.

9.1 3-D design

The three-dimensional design is similar to the two-dimensional design, with the major changes being the chamber is now a cylinder, and the inlets are holes, rather than cracks. These changes results in the wave period is no longer simplified, and the monopile wall is curved. The simulation models are simulated with the same boundary conditions. This meaning a pressure outlet at the top of the model, and velocity inlet at the inlets. It is velocity inlets at the inlets, and without the miniature sea, as the three-dimensional simulations are limited to the wave condition.

9.2 One inlet

The first model which is analysed, is with one hole with a diameter of 0.1 m. The hole is located at the center of the monopile, see Draw. 05. The inlet is at the front of the monopile. The simulation is created with the summer season for the densities of the sea water and enclosed water. The summer season is simulated, as it has the largest density difference. With one hole the inlet velocity is calculated with the energy equation, where the total loss coefficient is kept at 2.1. It is kept at a value of 2.1, because the results from Experiment 1 showed this loss coefficient still fitted after it was reduced to a hole, rather than a crack. Since the hole in the experiments are a scaled version of the 0.1 m diameter hole, the same result is used here. The velocity through the inlet and the internal and external water level are shown in Fig. 9.1. The internal water level only changes with ± 1.7mm around a mean water level at datum 0 m.

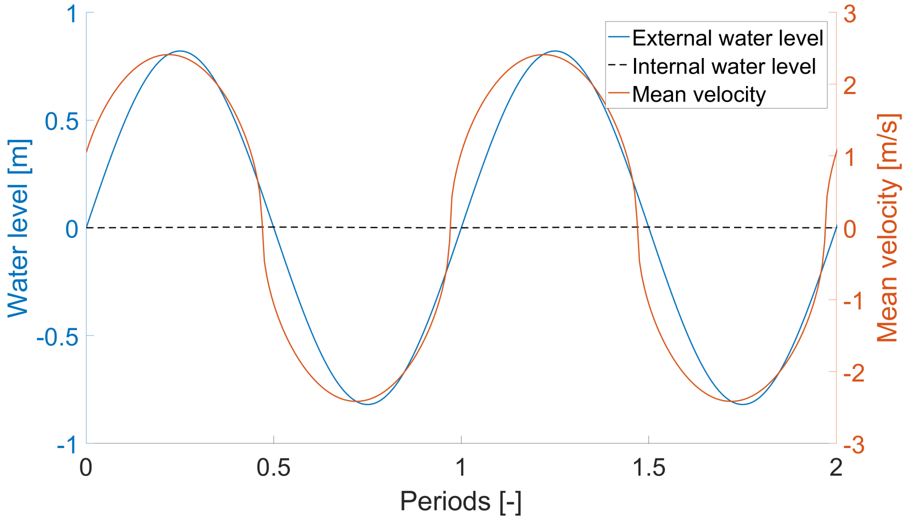

Fig. 9.1: The internal and external water level, relating to the left y-axis, and the velocity, relating to the right y-axis, for two wave periods.

With this small change in the internal water level, many waves are needed for the complete exchange to occur. The two-dimensional analysis of the waves, in Sec. 5.3, showed the sea water only travelled around 0.1 m into the monopile at each period, due to the reduction of the wave period. In Fig. 9.2 is showed the flow of sea water in the monopile, after the first half period, during which the water streams into the monopile. Here the flow reached approximately halfway through the monopile.

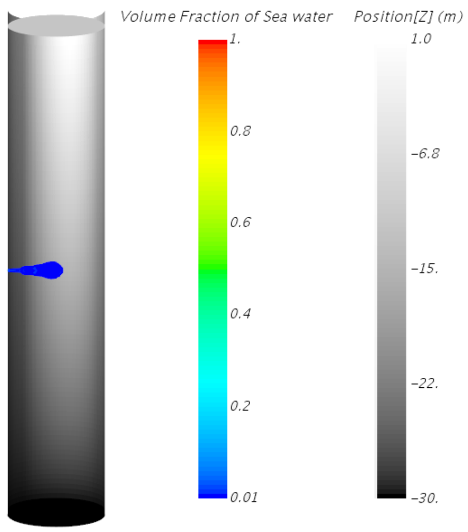

Fig. 9.2: The sea water flow in the monopile after the first half period. Has a flow length just above half the monopile diameter.

The reason the longer flow at each period is due to the inlet is a hole and only a small part of the surface, rather than the entire front as it is in two-dimensions. This difference is seen on Fig. 5.1. As a result, the flow is free of the surfaces. Thus is it the same percentage of sea water that is inside the monopile after a period, but is just a longer jet, rather than a wide jet that occur.

The simulation is continued for 70 periods, to determine the continuous flow, and the exchange of the enclosed water. The exchange measured over the first 70 periods show a linear tendency, as seen on Fig. 9.3. The reason for the linear exchange, rather than the exponential exchange, seen in two-dimension, is because only one percentage of the enclosed water has been exchanged yet. During these 70 periods the sea water is only mixing with the enclosed water, and has not reached a stable state, where it begins to flow out of the monopile again. Compared with the tide, the volume of sea water from each period is far greater, therefore reaching this stable state only in a few periods.

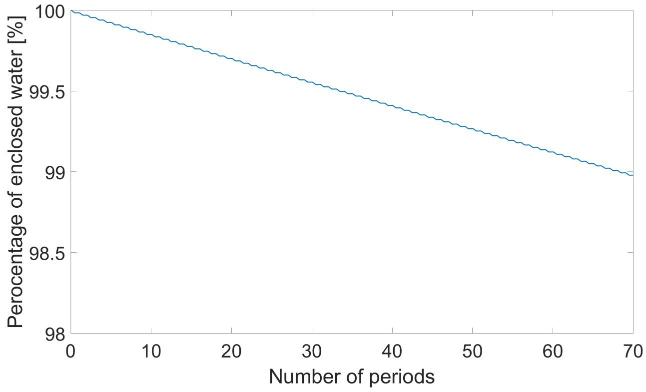

Fig. 9.3: Remaining enclosed water inside the monopile depending on numbers of periods.

Knowing that increasing the number of periods simulated, the percentage of enclosed water will decrease and eventually reach an exponential decaying function. Before reaching this visible exponential function, an exchange of minimum 10 to 15 % would be expected, based on the result from two-dimension. To achieve such an exchange the amount of period simulated needed to reach a minimum of 700 to 1000 periods. This results in to large simulation time for this thesis. Even without a stable exchange, some results can still be obtained. As it is not exponential decaying the rate of exchange, R, and the percentage of enclosed water not being exchanged, A_e, can't be obtained. However, as it is linear the amount of sea water from each period, which remains inside the monopile after its first period, $H_{s,in}$, can be estimated. Besides based on the exchanged flow, the amount expected to be exchanged is discussed. As it is linear, the flow of sea water is yet returned to the hole, therefore the only sea water exiting the monopile, as it flows out. is from the current period. The percentage of sea water from each period that remains is then estimated to 95 %, giving a $H_{s,in}$ of 3.2×10^{-3} m.

For an estimate of the percentage of the enclosed water, that is not being exchanged, a three-dimensional plot of the sea water in the monopile is compared after 10, 40 and 70 periods. These will show how fast the sea water extend up and down inside the monopile. The sea water after 10, 40 and 70 periods is shown in Fig. 9.4.

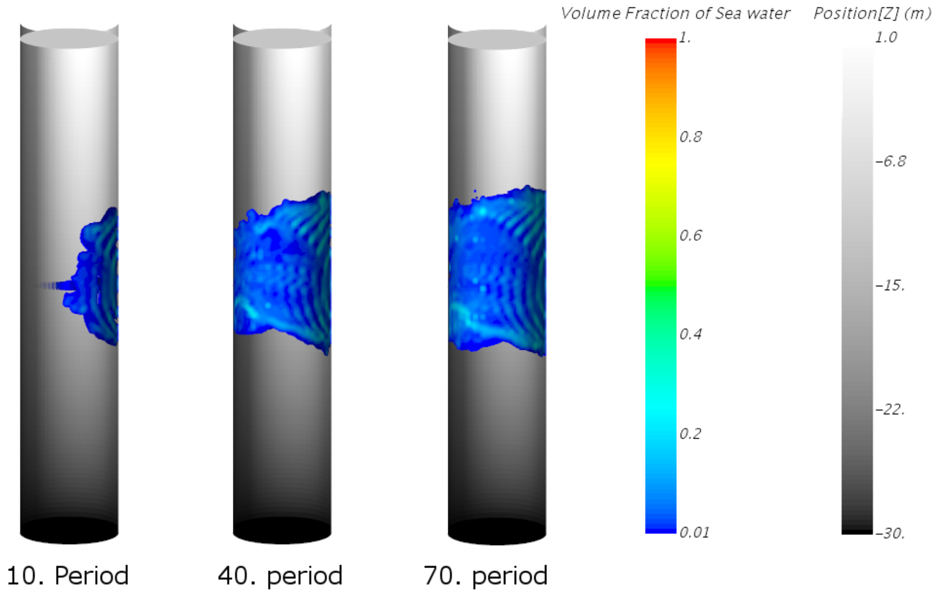

Fig. 9.4: The flow of sea water after respectively 10, 40 and 70 periods.

From these three plots, the extend in the z-direction is clearly mainly occurring in the beginning due to the flow splitting at the back wall. Afterwards the sea water flow travels along the monopile surface back towards the inlet. The flow is still expanding toward the surface, which is mainly because the simulation is performed with the summer conditions, and the sea water is slightly lighter than the enclosed water. It is visible that the temperature difference is of less effect here than in the tide simulations. This was also expected as the velocity is far greater here. From these plots it looks as the exchange is larger that only the one percent measured. This is because the flow is dominated along the surface, which is the visible flow here, and the flow is also mainly around one percent sea water and 99 % enclosed water. Based on these plots there are an exchange in around one-third of the monopile, thus giving an A_e value of 0.66.

With an estimate of $H_{s,in}$ and A_e and knowing the low internal water level, Eq. (5.5) can be rearranged to calculate the remaining coefficient, R. The remaining coefficient results in a value very close to one due to the small volume of sea water at each period, but can't be equal to one, as that would mean no exchange at all. The exact value is used, together with A_e value, to estimate the mean pH-value of the water, with Eq. (5.6), and is shown in Fig. 9.5.

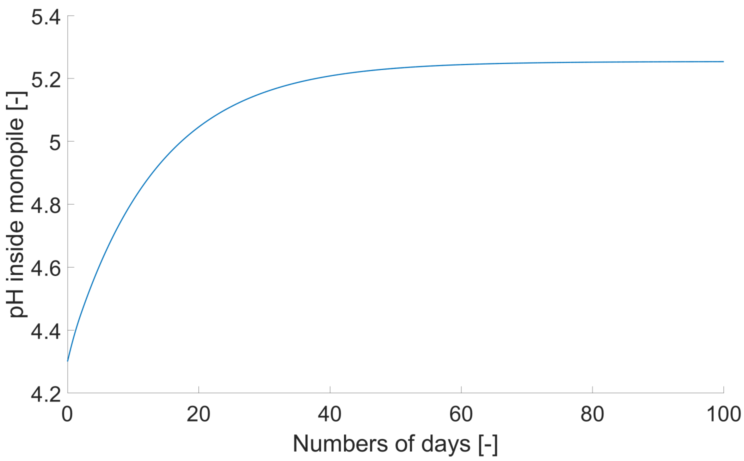

Fig. 9.5: The mean pH-value of the water inside the monopile with one hole. The pH-value stabilises on a value of 5.25.

The pH-value result in 62.8 % anode material is needed, compared with a monopile without the hole. The mean pH-value is a mean for the entire monopile, as the exchange is only of the 33 %, the remaining 66 % has a constant pH-value of 4.3. This would mean the anode should be located mainly near the seabed and surface, instead of equally divided over the depth.

Even without a stable model, the exchange seems to be limited to only around the inlets depth and not the entire monopile. To try and reach an exchange of the entire monopile more holes is needed, at different depth to spread out. Therefore a new model is created.

9.3 Eight inlets

Due to the high simulation time and the flow tendency seen the previous model, a monopile with eight holes are simulated. The inlet diameter is as well increased to 0.2 m. The drastic increase in holes and size is to achieve a larger internal water level change, and therefore be able to reach a stable state of the flow. The holes are located in two rings of four around the monopile, at depth of -10 m and -25 m. The monopile design is shown in Draw. 06. In the previous model the flow reached halfway through the monopile during one period. This is the reason for the hole being located at two depth, rather than eight different depths. By applying the holes opposite each other, the jets collide at the center of the monopile and the split occurs with a higher velocity. This is expected to reach a greater par of the monopile, and make it less affected by the different temperatures. With the eight hole the external and internal water levels variate as seen on Fig. 9.6.

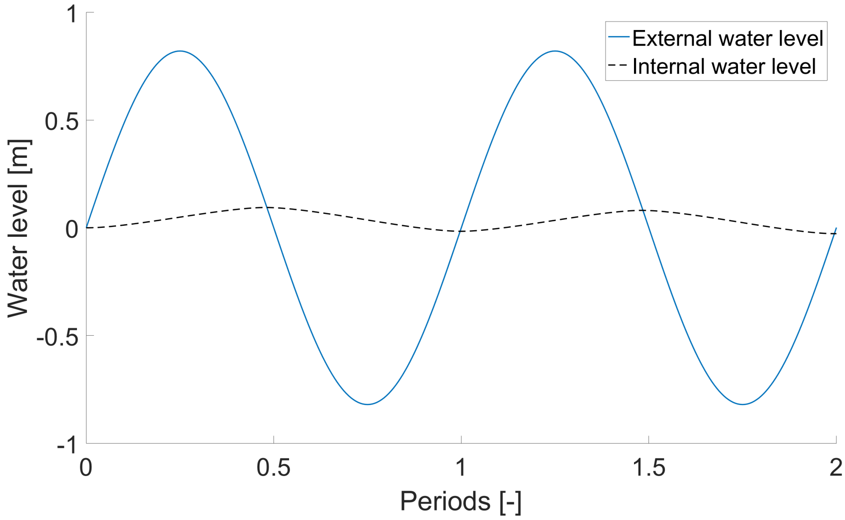

Fig. 9.6: External and internal water level for the two periods with eight holes.

The internal water level has an amplitude of 5.2×10^{-2} m. As the flow is generated by the waves, the velocity through the inlets variates a little depending on the depth and location. The velocity for the four inlets at datum -10 m is shown in Fig. 9.7, and the four inlets at datum -25 m in Fig. 9.8.

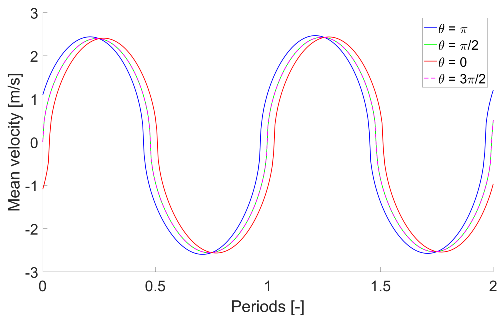

Fig. 9.7: Velocity for the four inlets at datum -10 m.

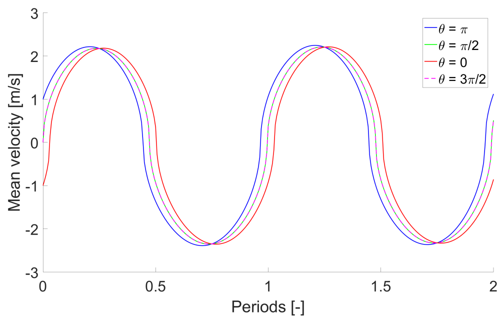

Fig. 9.8: Velocity for the four inlets at datum -25 m.

The velocity is higher at shallower depth, as the particles are more influenced by the wave.

The model is performed for the summer condition, and the end of the first, second and third period is shown in Fig. 9.9.

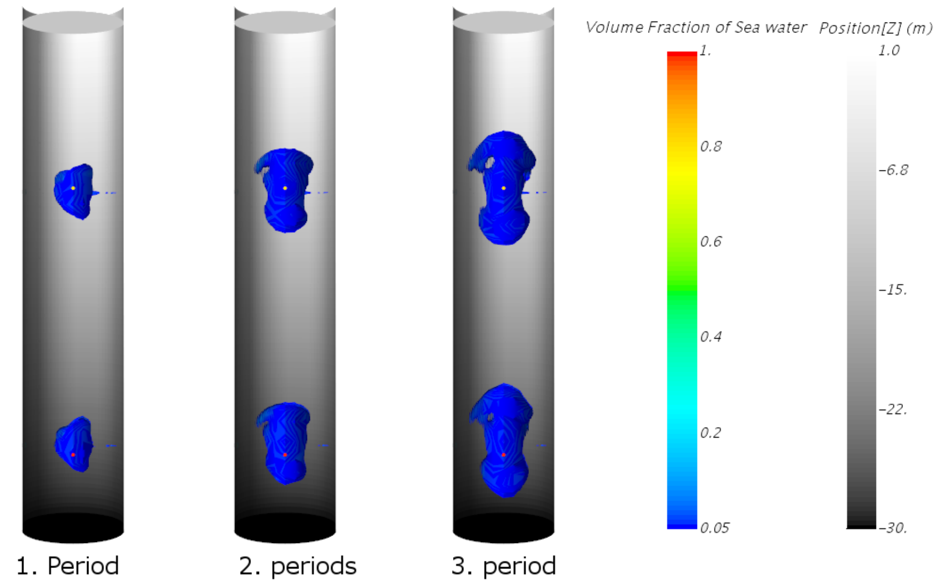

Fig. 9.9: The flow of sea water from the 8 holes after 1, 2 and 3 periods.

As the holes are located opposite each other, a vertical flow now occurs as well. This results in an easier exchange of the whole monopile. This model is as well continued for 70 periods, and sea water flow after 10, 40 and 70 periods are shown in Fig. 9.10.

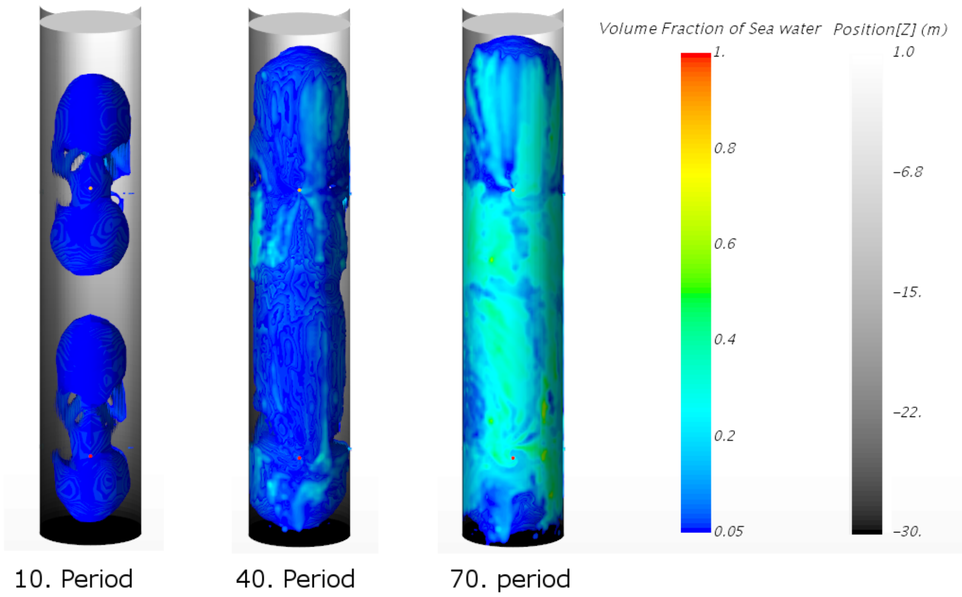

Fig. 9.10: The flow of sea water from the 8 holes after 10, 40 and 70 periods.

It is clear that the flow here comes around in the entire monopile, because of the this vertical directed stream. Due to the increased amount of holes and the increased size, the amount of enclosed water exchanged after 70 periods is significantly larger than with one hole. The calculated remaining enclosed water inside the monopile, at the end of each period, is shown in Fig. 9.11. Eq. (5.4) is fitted to the 70 period.

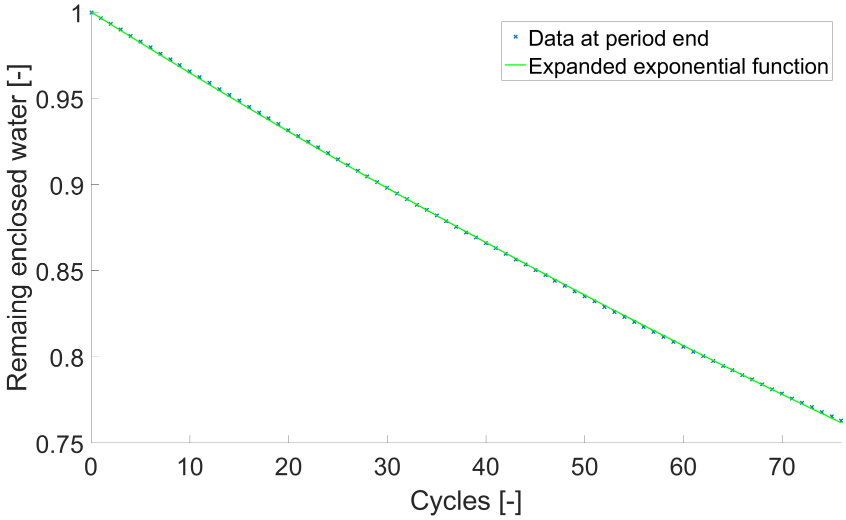

Fig. 9.11: Remaining enclosed water inside the monopile depending on numbers of periods.

Here a large enough amount of enclosed water has been exchanged for the tendency of the exponential decayingfunctionto be visible, and the values for R and A_e are fitted. The remaining coefficient is shown in Fig. 9.12 and the amount of enclosed water not exchange is shown in Fig. 9.13.

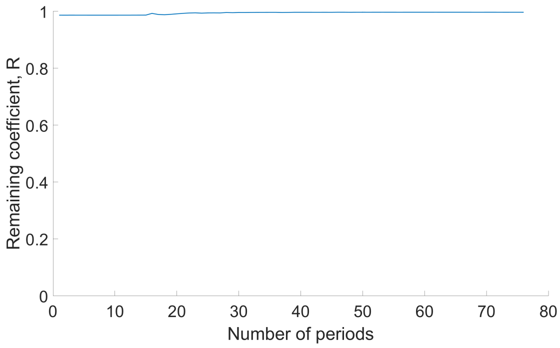

Fig. 9.12: Remaining coefficient, R, depending on number of periods fitted to. Stabilised at a value of 0.9964.

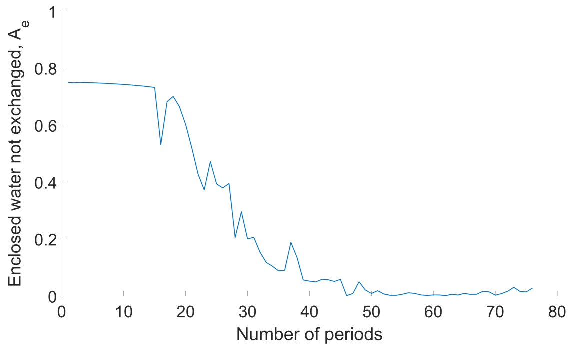

Fig. 9.13: Amount of enclosed water not being exchanged, A_e, depending on number of periods fitted to.

Fig. 9.13 show that the exchange occur in the entire monopile, which is the primary goal for this thesis. Due to the location of the holes and the high velocity of the flow, the density difference between the sea water and the enclosed water seems to have little effect. As all the enclosed water is exchanged over time, the anodes can be evenly distributed inside the monopile, and the amount of needed anode material is reduced to 21.6 %. This is a result of the pH-value stabilises at a value of 7.98, as is shown in Fig. 9.14.

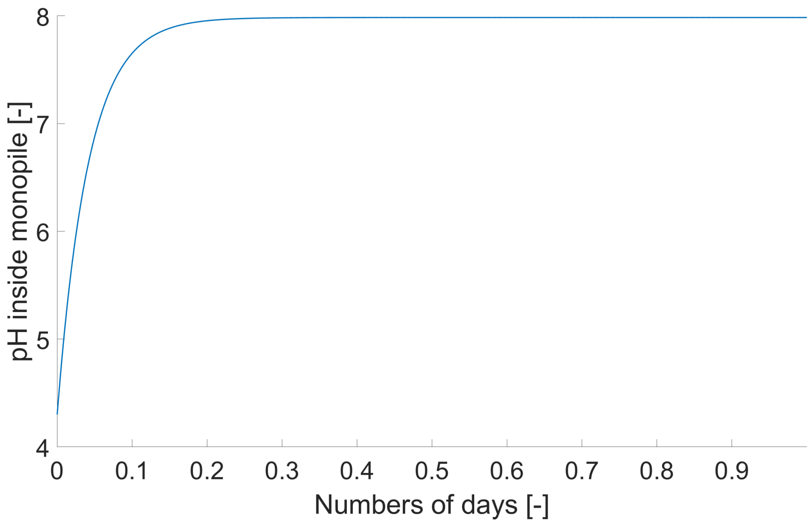

Fig. 9.14: The stabilised mean pH-value with eight hole for the summer season. The mean pH-value stabilises at a value of 7.98.

The exchange result in a very rapid exchange, and therefore it result in an almost optimal pH-value. Fig. 9.14 show the pH-value stabilises within one day, thus the exchange is rapid enough to have an effect with the use of aluminium anodes as well.

To be curtain the effect of the density aren't an issue to achieve a complete exchange, the model is simulated for the winter season as well. The model is simulated 70 periods and the sea water in the monopile is shown in Fig. 9.15, where it is compared with the flow in during the summer after 70 periods.

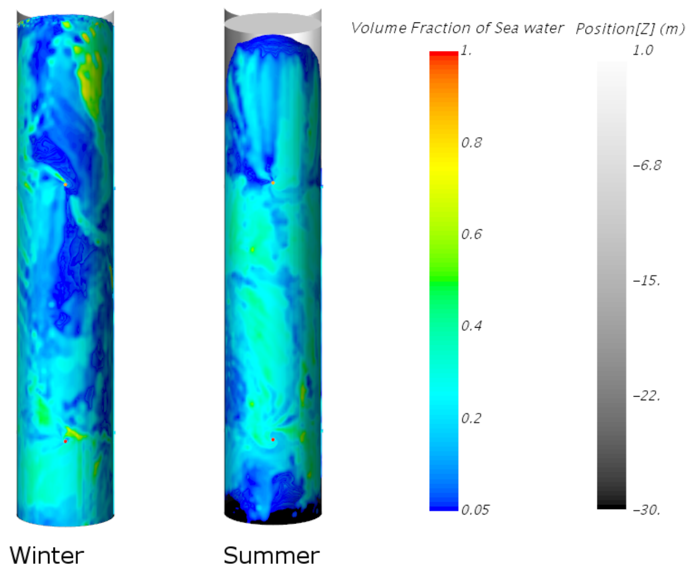

Fig. 9.15: Sea water inside the monopile after 70 periods for summer and winter.

Fig. 9.15 show the sea water reaches around the entire monopile. Fitting the 70 periods in the winter season, results in equal results as for the summer season, meaning there is an exchange in the entire monopile and the remaining coefficient is 0.9964. Based on the plots in Fig. 9.15 there is a difference, but it is only insignificantly small. Thus is the simulation not really affected by the density differences, when they are as small as the case is here.

9.4 3-D conclusion

The simulation in three-dimensions generally show the exchange is possible, but the period of a wave is too short to spilt at the back wall and create enough vertical flow to exchange in the entire monopile. Thus is it advisable to place holes opposite each other to half the length before the flow splits and travels vertically around inside the monopile. The simulations here show an easy and fast exchange of all the enclosed water, and the pH-value is practically unchanged from the pH-value of the sea of 8.

To get the entire monopile exchanged is primarily dominated by the period and the velocity, and therefore a total exchange would still occur if the diameter of the holes were reduced. By reducing the holes the exchange would take longer as the internal water level change is lower, but the velocity would increase slightly, due to a larger pressure difference, and the wave period would remain the same. Thus by reducing the holes, a complete exchange is expected to still be reach, and the effect on the structural capacity of the monopile would be reduced.

As the wave condition is calculated for a 50 % wave, this exchange is only achieved half the time. The remaining time the waves are smaller, thereby the velocity is decreases and the exchange can't be guarantee. The simulation is calculated with only the wave conditions. For a true case all sea conditions occur simultaneously, and adding the tidal condition to the wave conditions, the velocity amplitude will increase, especially with small wave heights. As the tidal conditions in two-dimensions resulted in close to complete exchange, then a complete exchange is very possible with a combination, even for a smaller wave condition.

Part V

Conclusion

10 | Conclusion

The performance of a passive exchange system on a monopile is analysed in this thesis. The exchange system increases the pH-value of the internal water and thereby decreases the corrosion of the structure. The system is based on exchanging the internal water with the external sea water, which has a higher pH-value. The exchange occur with a flow through holes drilled in the monopile surface. To achieve a passive system, the flow through the holes is generated by the sea conditions, here divided into three sea conditions; the tides, waves and currents. The passive exchange system is analysed with numerical CFD models for both two-dimensional and three-dimensional models. These analyses are performed to determine the exchange rate of the enclosed water, so the increase in the internal pH-value can be determined.

Before the exchange system is analysed, the models are simplified. The simplification is made in order to save computational time. The main simplification is that only a small part of the ocean is included, as the large ocean area is without interest in the thesis. This simplification shows that the flow at the inlets can be determined correctly with the energy equation. Thereby the model can be reduced to only include the monopile, where the interest of the exchange is focused.

The two-dimensional analysis is divided into; firstly an initial evaluation of the three different sea conditions, and secondly an optimisation of the tidal conditions in the two-dimensional models. To perform the two-dimensional analyses, the model is simplified to two-dimensions. This is problematic as the monopile is a cylinder with one or more holes. In two-dimensions it becomes a chamber with one or more cracks. The main challenges is to achieve the same flow and induced the same sea water percentage per period. The method chosen is to reduce the two-dimensional wave period, to compensate for the larger percentage of inlet, that the crack results in. The decrease in the wave period result in a shorter flow distance during each period, and expected a smaller exchange per period. The initial evaluation results in the largest exchange occurred with the wave condition, but it is highly affected by the reduced period, due to its already short period. The current condition shows that no complete exchange of the enclosed water occurs, as a steady flow between inlet and outlet is created. The tidal conditions show to be least affected by the reduction of the wave period, and still achieving a proper flow distance. The tidal conditions also shows a good exchange rate of almost the all the water inside the monopile.

Because of the wave condition being largely affected by the reduction to two-dimensions, only the tidal condition is optimised in for the two-dimensional models. In these analyses the different water temperatures occurring during the year are included. This induces an effect of different densities between the sea water and the enclosed water. The tidal case results in low velocity of the flow, and with the different densities introduced, the flow is highly effected. This results in clear stratification between the sea water and enclosed water, especially during summer, where the largest density difference between the sea water and enclosed water occur. The amount of enclosed water exchange during the summer shows to be determined by the deepest located hole. With more holes in the monopile, the velocity decreases due to a smaller pressure difference, and the stratification becomes more drastic. Therefore a higher velocity is needed to compensate for the difference in density. The correct wave period could increase the exchange some, but it is unlikely it will be enough without an increase in velocity.

Before the three-dimensional models are analysed, the internal flow is validated through experiments. The experiments are used to validate the modelled turbulence and density in the simulation models. The flow is validated by comparing the experimental flow with an equal CFD model. The comparison shows that the $k-\varepsilon$ turbulence model results in a good approximation of the sea water flow inside the monopile. Thus is the use of this turbulence model in the simulations validated. The density effect is validated by comparison of the slope of the sea water flow, which shows good results with different densities between the sea water and the enclosed water as well. With the flow validated by the experiments, the three-dimensional simulations are performed.

The simulation in three-dimensions is performed for the wave condition. The wave conditions is used as the velocity is significant larger than for tides. A model with one hole shows that the wave period is too short for the flow to split at the back wall and generate a large enough flow vertically in the monopile to exchange all the enclosed water. To increase the vertical flow, eight holes are studied. These are located opposite each other to reduce the length before splitting to the center of the monopile, where the jets interact, rather than the back wall. This results in a high vertical flow, and an exchange of the water in the entire monopile. This is simulated for both winter and summer season, to guarantee the exchange occur all year. As a result of the exchange rate the corrosion is reduced, so only 21.6 % anode material is needed compared with a monopile without any holes.

Over all the simulations has shown that the exchange is possible and result in a large reduction in the anode material needed for the corrosion.

Bibliography

Assosiation, 2017. American Galvanizers Assosiation. *In Chemical Solutions*. URL: http://www.galvanizeit.org/hot-dip-galvanizing/how-long-does-hdg-last/in-chemical-solutions, 2017. Downloaded: 10-01-2017.

Briskeby et al., 2015. Stein T. Briskeby, Linda Børvik and Sven M. Hesjevik. *Cathodic protection in closed compartments - PH effect and preformance of anode materials*. NACE international Corrosion 2015, 2015.

Brorsen and Larsen, 2009. Michael Brorsen and Torben Larsen. *Lærebog i HYDRAULIK*. Aalborg universitetsforlag, 2009.

DMI, 2017. DMI. *Tidal tabels*. URL: https://www.dmi.dk/en/hav/maalinger/tidal-tables/, 2017. Downloaded: 25-01-2017.

DNV, 2007. DNV. *DNV-RP-C205: ENVIRONMENTAL CONDITIONS AND ENVIRONMENTAL LOADS*, Det Norske Veritas, 2007.

Energinet, 2016. Energinet. *Dansk vindstrøm slår igen rekord – 42 procent*. URL: http://energinet.dk/DA/El/Nyheder/Sider/Dansk-vindstroem-slaar-igen-rekord-42-procent.aspx, 2016. Downloaded: 17-11-2016.

Hilbert et al., 2011. L. R. Hilbert, A. R. Black, F. Andersen and T. Mathiesen. *Inspection and monitoring of corrosion inside monopile foundations for offshore wind turbines*. FORCE Technology, 2011.

Mathiesen et al., 2016. Troels Mathiesen, Anders Black and Frits Grønvold. *Monitering and inspection options for evaluating corrosion in offshore wind foundations*, Force Technology, 2016.

Millero and Poissont, 1981. Frank J. Millero and Alain Poissont. *International one-atmosphere equation of state of seawater*, Pergamon Press Ltd., 1981.

Nielsen, 2000. Mads Hvid Nielsen. *Dynamisk beskrivelse og hydrografisk klassifikation af Den Jyske Kyststrøm*, PDANISH METEOROLOGICAL INSTITUTE, 2000.

Ramboll, 2016. Ramboll. *MONOPILES TO REMAIN DOMINANT OFFSHORE FOUNDATION IN EUROPE*. URL: http://www.ramboll.com/megatrend/feature-articles/monopiles-to-remain-dominant-offshore-foundation-in-europe, 2016. Downloaded: 17-11-2016.

Skjoldal, 2007. Hein Rune Skjoldal. *North Sea conditions - 2nd quater 2007*, Havforskningsinstituttet, 2007.

Vindmølleforening, 2016. Danmarks Vindmølleforening. *Vindmøller på havet*. URL: http://www.dkvind.dk/html/nogletal/pdf/havet_jul16.pdf, 2016. Downloaded: 17-11-2016.

zinc association, 2017. Internatioal zinc association. *Zinc for Corrosion Protection*. URL: http://www.galvinfo.com/Thermal_Spraying/zinc_for_corrosion_protection.html, 2017. Downloaded: 09-01-2017.

A | Overview of Digital appendix

1. CFD models
    a) Two-dimensions
        i. 2D_1_hole_mid_summer.sim
    b) Experiment
        i. exp_2_temp_14_out_9_in.sim
    c) Three-dimensions
        i. 2x4_holes.sim
2. Video Files
    a) Experiment 1
        i. Experiment 1 Simulation.avi
        ii. Experiment 1.avi
    b) Experiment 2 - Equal density
        i. Experiment 2 - Equal density Simulation.avi
        ii. Experiment 2 - Equal density.avi
    c) Experiment 2 - Low density sea water
        i. Experiment 2 - Low density Simulation.avi
        ii. Experiment 2 - Low density.avi
3. Drawings
    a) Drawing 01 - 2-D model, Tides.pdf
    b) Drawing 02 - 2-D model, Waves.pdf
    c) Drawing 03 - 2-D model, Currents.pdf
    d) Drawing 04 - Experiment design.pdf
    e) Drawing 05 - 3-D monopile one hole.pdf
    f) Drawing 06 - 3-D monopile eight hole.pdf

B | Overview of drawings

01 Initial evaluation - 2-D monopile model, Tide
02 Initial evaluation - 2-D monopile model, Wave
03 Initial evaluation - 2-D monopile model, Current
04 Experiment - Experimental model, Wave gauge and current location
05 3-D evaluation - 3-D monopile model, One hole
06 3-D evaluation - 3-D monopile model, Eight hole

C | Wave and current verification

The complete velocity potential are a sum of the undisturbed and disturbed potential, resulting in:

$$\varphi = \varphi_0 + \varphi_d = g_0 \cos(\omega t - k x) + \frac{R^2}{r^2} g_0 \left(\cos(\omega t - k x) - \cos(\omega t)\right) \tag{C.1}$$

To simplify this, the wave length are compared with the monopile diameter to identify the monopile as small cylinder. This would result in low influence on the wave movement. A small cylinder is defined by the relationship between wave length and monopile diameter is:

$$\frac{D}{L} < \frac{1}{5}$$

Where:

D Monopile Diameter
L Wave length

For this case the wave length is calculated iterative based on the wave period and mean water height.

$$L = \frac{g T}{2 \pi} \tanh\left(\frac{2 \pi h}{L}\right) \Rightarrow L = 196.4\,\mathrm{m} \tag{C.2}$$

The relationship is well below the criteria for a small cylinder, as it result in:

$$\frac{D}{L} = 0.03$$

As the interesting part is the pressure on the monopile surface, the x-value can be limited to:

$$x_{max} = \frac{D}{2}$$

With the given criteria, some approximations can be made and the x-value recalculated to polar coordinates:

$$\cos(k x) \approx 1 \tag{C.3}$$

$$\sin(k x) \approx k x = k r \cos(\theta) \tag{C.4}$$

Based on the rules for $\cos(a-b)$, $\cos(\omega t - k x)$ can be rewritten to:

$$\cos(\omega t - k x) = \cos(\omega t) \cos(k x) + \sin(\omega t) \sin(k x)$$

Using this rewriting and the approximations, the velocity potential can be rewritten and reduced to:

$$\varphi = g_0 \left(\cos(\omega t) + \sin(\omega t)\, k r \cos(\theta)\right) + \frac{R^2}{r^2} \left(g_0 \left(\cos(\omega t) + \sin(\omega t)\, k r \cos(\theta)\right) - g_0 \cos(\omega t)\right)$$

$$\varphi = g_0 \left(\cos(\omega t) + \sin(\omega t)\, k r \cos(\theta) \left(1 + \frac{R^2}{r^2}\right)\right) \tag{C.5}$$

In both the wave and current, the velocity potential needs to verify the Laplace equation. The Laplace equation in polar coordinates are as followed:

$$\frac{1}{r} \frac{\partial}{\partial r} \left(r \frac{\partial \varphi}{\partial r}\right) + \frac{1}{r^2} \frac{\partial^2 \varphi}{\partial \theta^2} + \frac{\partial^2 \varphi}{\partial z^2} = 0 \tag{C.6}$$

Beside the Laplace equation, both cases needs as well to verify the boundary conditions which are:

- φ(r=∞) = φ_0, as no disturbance from the cylinder occur far from it.
- u_θ(r=R) = 0, as no flow can penetrate the cylinder.

C.1 Wave

For the wave the velocity potential is given as:

$$\varphi = g_0 \left(\cos(\omega\, t) + \sin(\omega\, t)\, k\, r\, \cos(\theta) \left(1 + \frac{R^2}{r^2}\right)\right) \tag{C.7}$$

The Laplace equation can be verified if g_0 are made independent of z. Stating this the last part equals 0. The other parts are as follows:

$$\frac{\partial\, \varphi}{\partial\, r} = g_0\, \frac{k\, \cos(\theta)\, \left(r^2 + R^2\right)\, \sin(\omega\, t)}{r^2}$$
$$\frac{1}{r}\, \frac{\partial}{\partial\, r}\left(r\, \frac{\partial\, \varphi}{\partial\, r}\right) = g_0\, \frac{k\, \cos(\theta)\, \left(r^2 + R^2\right)\, \sin(\omega\, t)}{r^3}$$

$$\frac{\partial\, \varphi}{\partial\, \theta} = -g_0\, \frac{k\, \sin(\theta)\, \left(r^2 + R^2\right)\, \sin(\omega\, t)}{r}$$
$$\frac{1}{r^2}\, \frac{\partial^2\, \varphi}{\partial\, \theta^2} = -g_0\, \frac{k\, \cos(\theta)\, \left(r^2 + R^2\right)\, \sin(\omega\, t)}{r^3}$$

The Laplace equation is then verified as it equals 0. The boundary conditions stated can then be verified. First that no disturbance occurs far from the monopile:

$$\varphi = \varphi_0 \qquad \text{for } r \rightarrow \infty$$
$$\left(1 + R^2/r^2\right) \Rightarrow 1$$
$$\varphi(r = \infty) = g_0\, \left(\cos(\omega\, t) + \sin(\omega\, t)\, k\, r\, \cos(\theta)\right) = \varphi_0$$

The second conditions states no flow through the monopile waves. This is stated as for u_r at r=R is 0.

$$u_r(r = R) = \frac{\partial\, \varphi}{\partial\, r}(r = R) = g_0\, \sin(\omega\, t)\, k\, r \cos(\theta) \left(1 - \frac{R^2}{R^2}\right) = 0$$

C.2 Current

The velocity potential for the current are given as:

$$\varphi = U\, \cos(\theta)\, \left(r + \frac{R^2}{r}\right) \tag{C.8}$$

First the velocity potential can verify the Laplace equation.

$$\frac{\partial\, \varphi}{\partial\, r} = U\, \cos(\theta)\, \left(1 - \frac{R^2}{r^2}\right)$$
$$\frac{1}{r}\, \frac{\partial}{\partial\, r}\left(r\, \frac{\partial\, \varphi}{\partial\, r}\right) = \frac{U}{r}\, \cos(\theta)\, \left(1 + \frac{R^2}{r^2}\right)$$

$$
\begin{aligned}
\frac{\partial\ \varphi}{\partial\ \theta} &= -U\ \sin(\theta)\ \left(1+\frac{R^2}{r}\right) \\
\frac{1}{r^2}\ \frac{\partial^2\ \varphi}{\partial\ \theta^2} &= -\frac{U}{r}\ \cos(\theta)\ \left(1+\frac{R^2}{r^2}\right)
\end{aligned}
$$

$$
\frac{\partial^2\ \varphi}{\partial\ z^2} = 0
$$

The Laplace equation is thereby verified for the current flow. The boundary conditions are the same as for the waves, and the first state no disturbance far from the monopile.

$$
\begin{aligned}
\varphi &= \varphi_0 && \text{for } r \rightarrow \infty \\
\left(r+R^2/r^2\right) &\Rightarrow r \\
\varphi(r=\infty) &= U\ r\ \cos(\theta) = \varphi_0
\end{aligned}
$$

The second states no flow through the monopile:

$$
u_r(r=R) = \frac{\partial\ \varphi}{\partial\ r}(r=R) = U\ \cos(\theta)\ \left(1-\frac{R^2}{R^2}\right) = 0
$$

The velocity potential for wave and current are thereby verified.

D | Multiple phase comparison

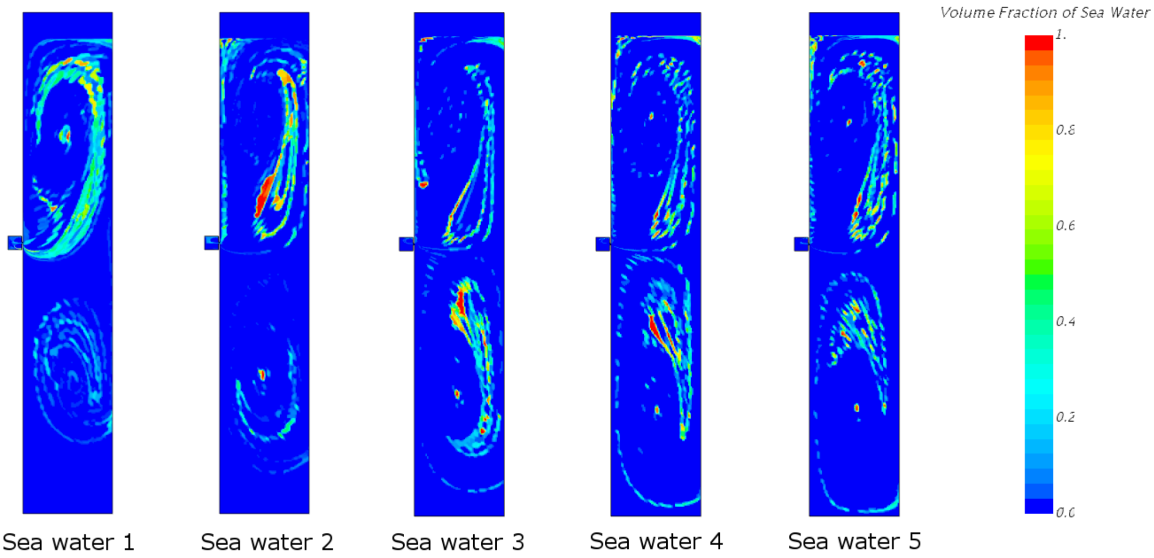

Fig. D.1: Location of each sea water phase it have floated for two cycle.

E Surface plots with density effect 2-D

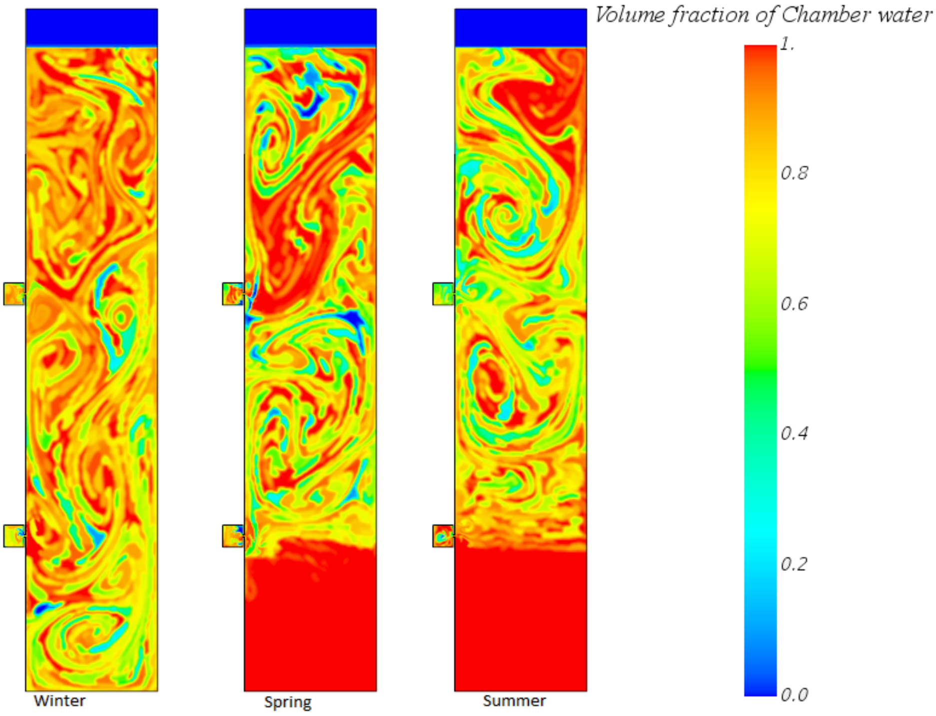

Fig. E.1: The remaining monopile water with model 2 after five periods and for each season.

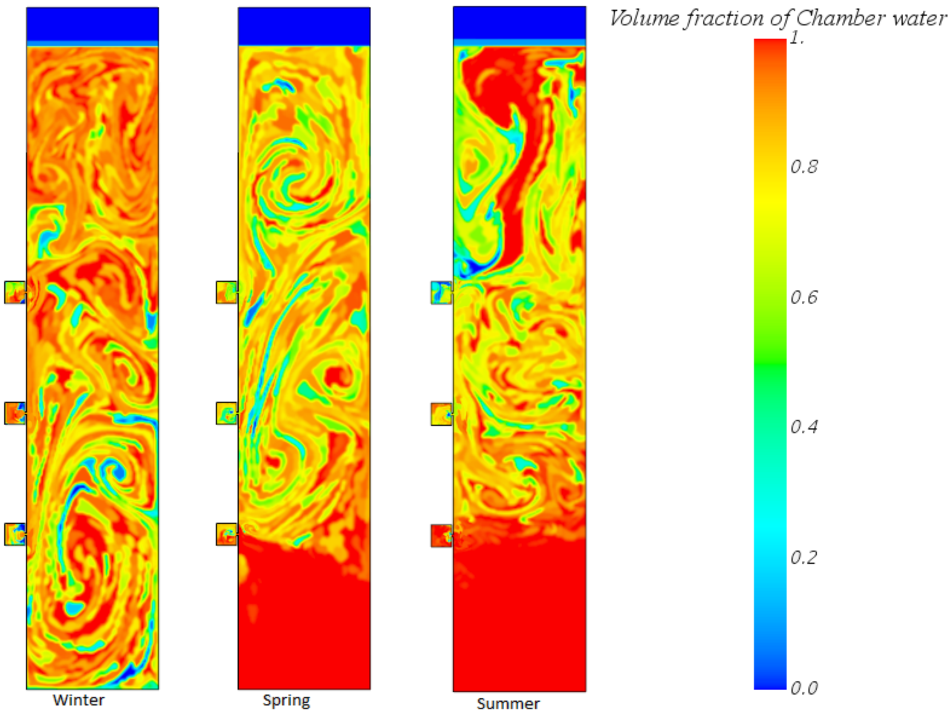

Fig. E.2: The remaining monopile water with model 3 after five periods and for each season.

F | Scaling

The model is scaled to achieve geometric, kinematic and dynamic similitude and the theory is based on Brorsen and Larsen [2009].

F.1 Geometric scaling

The scaling is based on the length scale, stated by the relationship between the geometrics in nature and the geometrics in the model, as seen in Eq. (F.1).

$$\frac{l_{1,N}}{l_{2,N}} = \frac{l_{1,M}}{l_{2,M}} \qquad \Leftrightarrow \qquad \frac{l_{1,M}}{l_{1,N}} = \frac{l_{2,M}}{l_{2,N}} = \lambda_L \tag{F.1}$$

Where:

$l_{i,N}$ Length i in nature
$l_{i,M}$ Length i in model

F.2 Kinematic scaling

Beside the scaling of the geometry, a scaling of the kinematic and dynamic similitude is needed. To achieve kinematic similitude all the particles in the nature have a scaled velocity vector at the same time as the scaled particles in the model. This principle is shown in Fig. F.1, which compare a nature and model setup.

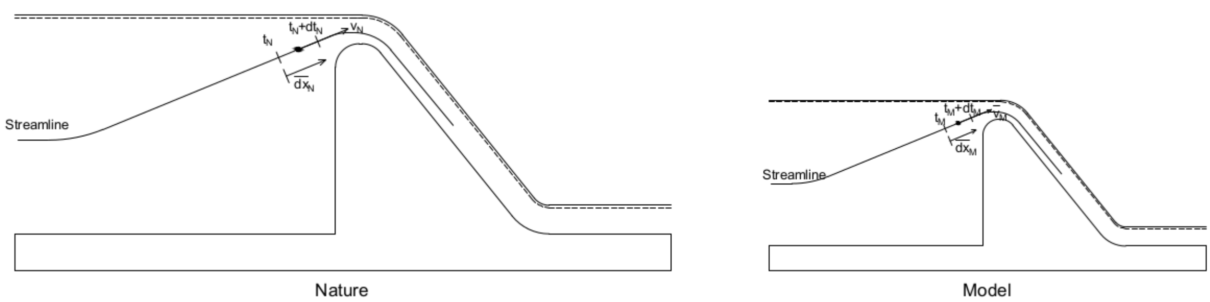

Fig. F.1: Principle of kinematic scaling between nature and model.

For the particles to move in accordance to the kinematic similitude it is required that:

$$\overrightarrow{v_N} = \lambda_V \overrightarrow{v_M}$$

Where:

$\overrightarrow{v_N}$ Length i in nature
$\overrightarrow{v_M}$ Length i in model

The velocity scaling factor is therefore stated as:

$$\lambda_V = \frac{\overrightarrow{v_N}}{\overrightarrow{v_M}} \tag{F.2}$$

In order to achieve kinematic similitude, the time scale is dependent upon the length and velocity scale. For the relationship to be found the particle velocity definition is used, which is defined as:

$$\vec{v} = \frac{d\vec{x}}{dt}$$

The relationship between velocity, length and time results in the scaling factor for the time as shown in Eq. (F.3).

$$\lambda_t = \frac{\lambda_L}{\lambda_V} \tag{F.3}$$

F.3 Dynamic scaling

To achieve dynamic similitude, the forces acting on the fluid particles are scaled alike. The fluid particles are effected by three main forces:

1. Gravitational force
2. Shear force
3. Pressure force

The force created by the gravity, is determined by the mass of the particle and the gravitational acceleration.

The shear force is divided between a part created by the viscosity of the fluid and friction along the walls, and a part created by the size and strength of the eddies. The shear force is created based on the density of the fluid, its kinematic and turbulence viscosity, and the mean velocity along the streamlines.

$$\tau = A\,\rho\,\nu\,\frac{\partial U_1}{\partial x_2} + A\,\rho\,\nu_{turb}\,\frac{\partial U_1}{\partial x_2}$$

The gravitational and shear forces are thus determined by either the gravitational pull or the friction created by the movement of the particle. This results in difficulties creating a unique scaling factor.

The pressure force is formed by the other two forces to give the total force, thereby equalising the total forces with Newtons second law of motion. The pressure force determines the fluids ability to flow freely.

For scaling of a fully dynamic similitude, it requires a scaling of either the gravitational acceleration, or the viscosity of the fluid, as seen in Eq. (F.4).

$$\lambda_\nu = \lambda_L^{3/2}\,\lambda_g^{1/2} \tag{F.4}$$

Scaling the gravity, is only possible in a centrifuge and therefore not possible for this experiment. A scaling of the viscosity requires a model fluid with a lower viscosity, which is difficult to accommodate as the natural fluid is water. Instead of a fully dynamic similitude, the scaling is made with an approximated dynamic similitude. This is done by scaling depending on the dominating force in the flow. The experiments are created with free surfaces, and the flow is dominated by the different water levels, thereby the pressure difference in the two chambers. The shear force is only effecting through the inlet, which is of a low size compared to the complete model. As a result the dominating force is the gravitational force, and therefore the Froude's model law are use for scaling of the experiments.

F.4 Froude scaling

Froude scaling is used as gravity is the dominating force. The Froude scaling is based on using the same force scale for gravitational force, as for the resulting force. The scaling is then based on having the same Froude number in nature as in the model. The Froude number is defined as:

$$Fr = \frac{V}{\sqrt{g\,L}}$$

The deviation of the velocity scale based on the Froude scaling is shown in Eq. (F.5).

$$\begin{aligned} (\lambda_F)_R &= (\lambda_F)_G \qquad \Leftrightarrow \qquad \lambda_\rho\,\lambda_L^2\,\lambda_V^2 = \lambda_\rho\,\lambda_L^3\,\lambda_g \qquad \Leftrightarrow \\ \lambda_V &= \lambda_L^{1/2}\,\lambda_g^{1/2} \end{aligned} \tag{F.5}$$

As the gravity was unable to scale so $g_N = g_M$, then λ_g is equal to 1, reducing the velocity scale to:

$$\lambda_V = \lambda_L^{1/2}$$

Based on the velocity and length scale, the time scale can be found to:

$$\lambda_t = \lambda_L^{1/2}$$